

DISSERTATION

INVESTIGATION OF THE MOLECULAR MECHANISMS AND THERAPEUTIC
POTENTIAL OF ONCOGENE-INDUCED KINETOCHORE-MICROTUBULE DEFECTS

Submitted by

Jacob A. Herman

Department of Biochemistry and Molecular Biology

In partial fulfillment of the requirements

For the Degree of Doctor of Philosophy

Colorado State University

Fort Collins, Colorado

Spring 2015

Doctoral Committee:

Advisor: Jennifer G. DeLuca

James Bamberg
Laurie Stargell
Jac Nickoloff

Copyright by Jacob A. Herman 2015

All Rights Reserved

ABSTRACT

INVESTIGATION OF THE MOLECULAR MECHANISMS AND THERAPEUTIC POTENTIAL OF ONCOGENE-INDUCED KINETOCHORE-MICROTUBULE DEFECTS

Kinetochores, large protein structures assembled on centromeric DNA during mitosis, bind to microtubules of the mitotic spindle to orchestrate and power chromosome movements. Deregulation of kinetochore–microtubule (kinetochore–MT) attachments has been implicated in driving chromosome instability and cancer evolution; however, the nature and source of kinetochore–MT attachment defects in cancer cells remain largely unknown. Here, we identify kinetochore-MT attachments, and their regulation by Aurora B kinase (ABK) as key targets for selective therapeutic intervention in glioblastoma and other cancers. We observe that accessory regulators of ABK and kinetochore-microtubule attachment stability are compromised in some cancers and fundamentally alter kinetochore signaling. First we identify RAS/MAPK oncogenic transformation as sufficient to induce these defects through an enzymatic cascade targeting the kinetochore. We then identify BUBR1 kinetochore recruitment and kinetochore-associated PP2A activity as cancer-essential activities, which are required for some cancers to form robust physical interactions between kinetochores and MTs. We also verify previous findings that many cancers are characterized by chromosome segregation errors arising from merotelic kinetochore-microtubule attachments (a single kinetochore bound to microtubules emanating from both spindle poles). We attribute the cause of these errors to be a decrease in MT dynamics independent of the physical

attachments status. Finally we characterize a novel kinetochore component, BUGZ, which serves as a molecular chaperone for BUB3 and thus indirectly stimulates ABK activity. We find that BUGZ binds to BUB3 through a conserved GLEBS domain, and this interaction is required for BUB3 kinetochore localization. BUGZ depletion decreases ABK activity resulting in lethal chromosome alignment defects in glioblastoma cells and genetically transformed cells. Together these findings further elucidate the molecular mechanism by which kinetochore-MT attachments are regulated and importantly, how this mechanism is perturbed upon transformation. These results will make the design and application of novel anti-cancer drugs with reduced side effects possible because they specifically target cancer populations.

ACKNOWLEDGMENTS

Looking back on the last five years I feel incredibly lucky to have my career shaped by such amazing people. First and foremost, I must thank my advisor Jennifer DeLuca who allowed me to dive into such a crazy project. From Jennifer I learned how to ground my excitement for science, about the successes and pitfalls of collaboration, new ways to mentor researchers, and that I am an expert. The rest of the DeLuca lab will forever be in my debt, they are the only reason I did not leave this program in my first year and why I was able to complete this work – thank you Lynsie, Jeanne, Eric, and Gina. Keith DeLuca showed me that science is absolutely unforgiving, and the only thing we can do is keep trying. His ability to balance a family, research, lab management, and social life was always and will continue to be an inspiration.

Patrick Paddison served as a de-facto co-advisor and complemented my education perfectly. He taught me to look for translational applications in my work, and brought a near-infinite amount of excitement and humor to the scientific process. From our first meeting he challenged me, while also treating me like a peer. My student advisory committee, Laurie Stargell, Jim Bamburg and Jac Nickoloff, was always excited about this work, and truly contributed to my growth as a scientific speaker and writer. I am also grateful to Laurie Stargell for mentoring my development as an educator. Jeff Hansen, Susan Bailey, and Steven Markus all boosted my career through amazing collaborations. I cannot begin to list all of the other amazing members of the biochemistry department that served as a family away from home during my time here.

I was fortunate to have the best cheerleaders in the world during this process. It is difficult to fail when a dozen people are encouraging you and eager to hear about your work. My parents Greg and Cindy made my life easier whenever they could and were the best role models I can imagine for working hard. They will never admit it, but I accomplished this only through their hard work for the last 20 years.

One of my biggest debts is owed to Will who tolerated every single selfish moment this work demanded – all the late nights, constant tardiness, and weekends spent at work. He was my support and caretaker through this entire process and I will never be able to repay those kindnesses.

TABLE OF CONTENTS

ABSTRACT	ii
ACKNOWLEDGEMENTS.....	iv
TABLE OF CONTENTS	vi
CHAPTER 1: INTRODUCTION.....	1
1.1 The Human Mitotic Process and Kinetochores.....	1
1.2 Signaling Kinetochores-Microtubule Attachment State	5
1.3 Forming Kinetochores-Microtubule Attachments.....	5
1.4 Phosphoregulation of Kinetochores-Microtubule Attachment Affinity.....	7
1.5 Generating and Preventing Kinetochores-Microtubule Attachment Errors.....	9
1.6 Kinetochores-Microtubule Attachment Errors in Glioblastoma and Other Cancers.....	12
CHAPTER 2: DOCUMENTING CANCER-SPECIFIC KINETOCHORE-MICROTUBULE ATTACHMENT DEFECTS IN GLIOBLASTOMA PATIENT ISOLATES.....	16
2.1 Introduction	16
2.2 Results.....	17
2.3 Discussion	29
2.4 Methods.....	31
CHAPTER 3: ONCOGENIC RAS/MAPK SIGNALING HYPERACTIVATES AURORA B KINASE AND WEAKENS KINETOCHORE-MICROTUBULE ATTACHMENTS.....	35
3.1 Introduction	35
3.2 Results.....	37
3.3 Discussion	62
3.4 Methods.....	65

CHAPTER 4: BUGZ IS REQUIRED FOR BUB3 STABILITY, BUB1 KINETOCHORE FUNCTION, AND CHROMOSOME ALIGNMENT	73
4.1 Introduction	73
4.2 Results.....	75
4.3 Discussion	98
4.4 Methods.....	102
CHAPTER 5: CONCLUSIONS AND FUTURE PERSPECTIVES	111
5.1 Summary	111
5.2 Repurposing currently FDA approved therapies.....	112
REFERENCES.....	117

CHAPTER 1

INTRODUCTION¹

1.1 The Human Mitotic Process and Kinetochores

Growth, development, and reproduction in all organisms require duplication and segregation of genetic material, which in eukaryotes is accomplished by mitosis. The mitotic process is absolutely essential and largely conserved from yeast to humans, yet molecular details can be surprisingly divergent through evolution (1). Mitosis in humans requires the duplication of a diploid genome and centrosomes during S phase. Upon mitotic entry, duplicated centrosomes nucleate separate to opposing sides of the dividing cell, where they nucleate the mitotic spindle and are termed spindle poles. At the same time, another mitotic apparatus is assembled on centromeric DNA – the kinetochore. During mitosis this massive molecular machine binds to microtubules of the mitotic spindle to orchestrate and power chromosome movements. In humans, prior to nuclear envelope breakdown, during prophase, kinetochore-microtubule (kinetochore-MT) attachment is precluded; however, upon entering prometaphase the nuclear membrane is fragmented and chromosomes spill into the cytoplasm with no

¹ Chapter One, an introduction to this dissertation, was published in part as a review article, “Molecular Pathways: Targeting Kinetochore-Microtubule Attachments in Cancer” in August 2014. Parts have been omitted or expanded where appropriate.

P.J.P. and I conceived the content and co-wrote this manuscript with input from J.G.D and J.M.O.

Herman JA, Toledo CM, Olson JM, DeLuca JG, Paddison PJ. Molecular Pathways: Regulation and Targeting of Kinetochore-Microtubule Attachment in Cancer. Clin Cancer Res. 2014;233–9.

organization. Once kinetochore-MT attachments are formed, concerted activity between motors, non-motor microtubule binding proteins, and microtubules congresses the chromosomes to the spindle equator where every single sister chromatid pair of a mitotic chromosome becomes properly bioriented – meaning each sister kinetochore is bound to microtubules emanating from opposing spindle poles. Prior to this stage, known as metaphase, a diffusible, inhibitory signal is generated to prevent anaphase onset until every single kinetochore is properly attached to a microtubule bundle consisting of 20-25 microtubules. This “anaphase wait” signal is then silenced and the mitotic cell progresses into anaphase where two complete diploid genomes are equally segregated to the spindle poles (Figure 1.1) (2).

The mitotic program requires a complete reorganization of cellular components and processes – chromatin factors are stripped or silenced, transcription and translation are significantly decreased, the cytoskeleton is completely remodeled, and membrane bound organelles are displaced or reorganized. During these massive changes the kinetochore is assembled on centromeric chromatin to serve as a master regulator of mitosis (Figure 1.2) (3,4). The first role of the kinetochore is signaling the attachment state of kinetochores.

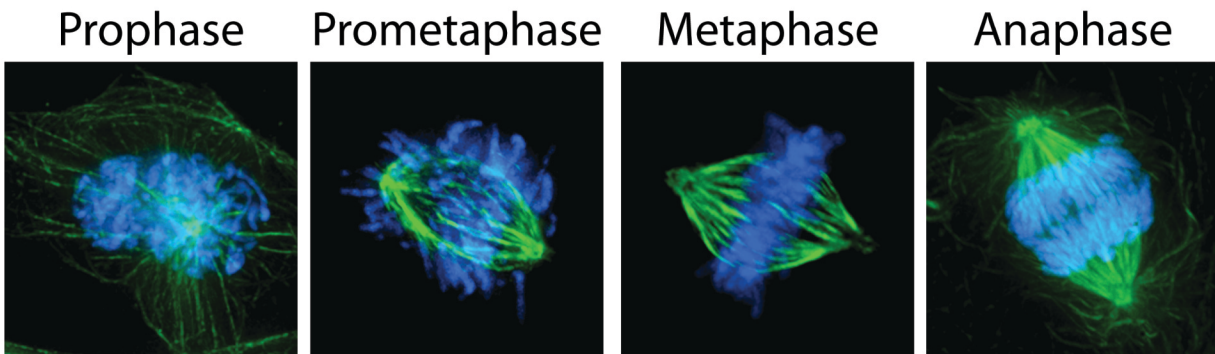


Figure 1.1. Mitotic phases in non-transformed cells.

Four unique phases of mitosis in human cells are categorized as follows: prophase, the nuclear envelope is still intact, chromosomes are fully condensed, outer kinetochore components are present, and spindle poles have duplicated; prometaphase, nuclear envelope has broken down, spindle poles separate to opposing ends of the cell and form the spindle, kinetochore-microtubule interactions are labile; metaphase, chromosomes are congressed to the spindle equator, stable kinetochore-microtubule attachments are generated; anaphase, kinetochore-bound microtubules depolymerize equally segregating sister chromatids to opposing ends of the cell.

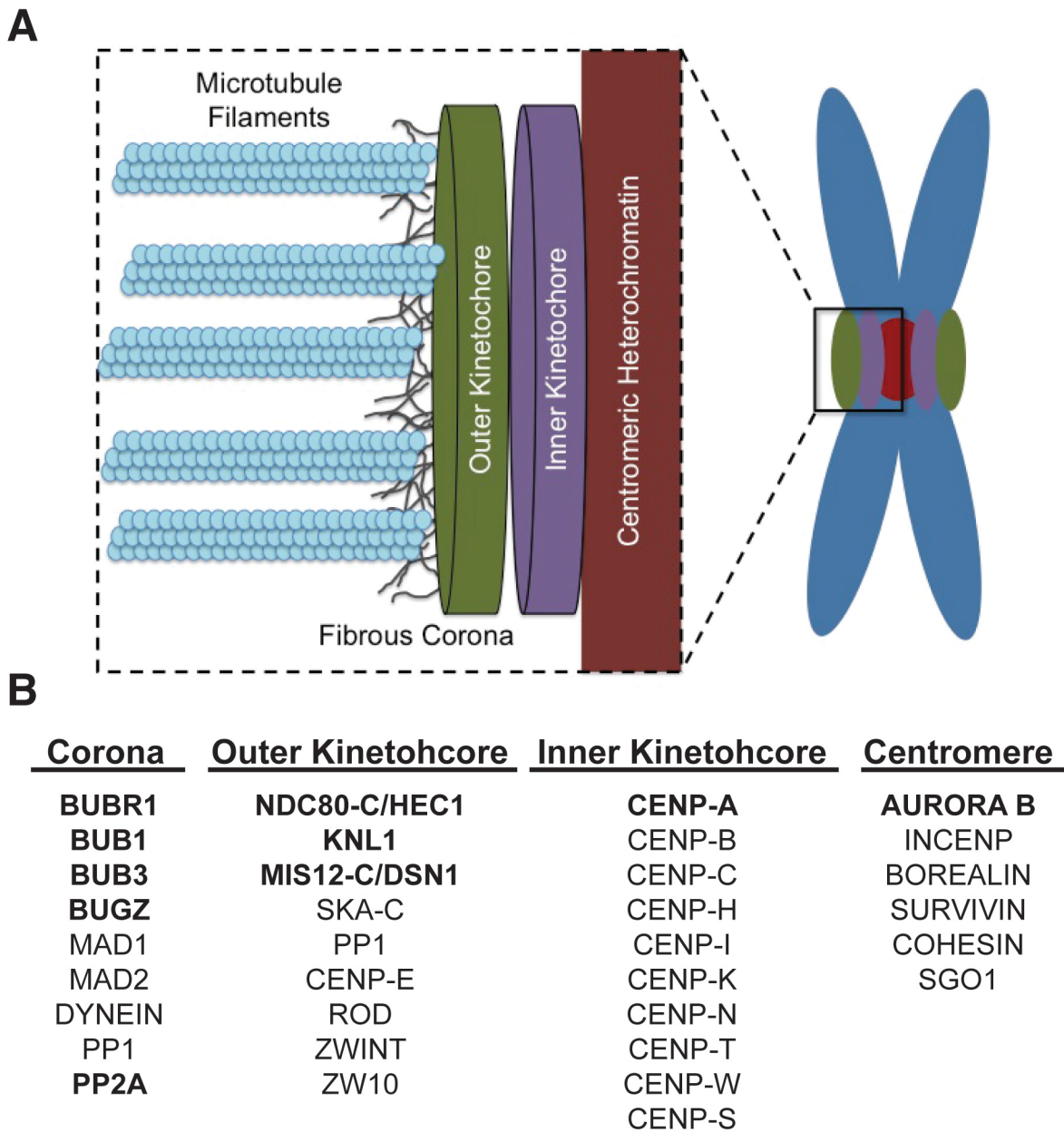


Figure 1.2. Structure and select molecular components of the human kinetochore.

(A) Kinetochores are built off the centromeric heterochromatin denoted as kinetochores by the epigenetic marker and histone H3 variant, CENP-A. Centromeric proteins bind directly to chromatin and regulate both sister chromatid cohesion and kinetochore function. Inner kinetochore components are constitutively associated with the centromere and serve as an architectural scaffold, which recruits more transiently, associated components. The outer kinetochore is the site of direct microtubule binding and spindle assembly checkpoint signaling. The corona is composed of spindle assembly checkpoint proteins with low residency time, and is largely absent after microtubule attachments form. (B) Select molecular components are loosely categorized into these regions; proteins described below are bolded.

1.2 Signaling Kinetochores-Microtubule Attachment State

To prevent mitotic exit until proper kinetochore–MT attachments have formed, the cell employs a surveillance mechanism known as the spindle assembly checkpoint (SAC). The core SAC proteins, MAD1, MAD2, BUBR1, BUB1, BUB3, and MPS1, accumulate at unattached kinetochores and generate a diffusible “wait anaphase” signal, which inhibits the anaphase promoting complex/cyclosome (APC/C) and prevents mitotic exit (5,6). The APC/C is an E3-ubiquitin ligase, which specifically targets the mitotic proteins Cyclin B and Securin for proteasome dependent degradation. Loss of these proteins promotes sister chromatid separation and biochemical exit from mitosis.

Through this mechanism the kinetochore serves as an enzymatic scaffold, and even a single kinetochore pair that is not bound to microtubules emanating from opposing spindle poles can prevent anaphase onset (7). Thus maintain a robust SAC is one feature in preventing errors in chromosome segregation and ensuring genetic fidelity. The intricacies of activating, maintaining, and silencing the SAC fill many reviews (1,3–5); this dissertation instead is focused on the role of the kinetochore in physically binding dynamic spindle microtubules because this interface is an exciting target for cancer intervention, which is discussed in more detail below.

1.3 Forming Kinetochores-Microtubule Attachments

To properly segregate chromosomes during mitosis, kinetochores must attach to the dynamic plus-ends of mitotic spindle microtubules (3). Microtubules are a unique

polymer because they are both polar filaments and exhibit dynamic instability. The polarity of microtubules arises from the ordered assembly such that the plus-end has an exposed β -tubulin monomer. Moreover, as the site of addition, the plus end has a GTP-cap containing tubulin dimers that have yet to hydrolyze their bound GTP. The loss and rescue of the GTP-cap gives rise to dynamic instability, the cycle of rapid polymerization and depolymerization of the plus-end (8). These cycles do not prevent net growth or shrinkage of the microtubule, but do result in an incredibly dynamic structure. Binding and processively tracking such a dynamic molecular assembly requires a host of kinetochore proteins. Although many of the >100 proteins that comprise the vertebrate kinetochore contribute to the generation of kinetochore–MT attachments, the core attachment factor is the “KMN network,” comprised of KNL1, the MIS12 complex, and the NDC80 complex (Figure 1.2) (3,9).

The NDC80 complex is a heterotetrameric complex containing one member, HEC1, which makes direct physical contact with spindle microtubules. In humans, a disordered N-terminal tail, and a calponin homology (CH) domain within HEC1 contribute to microtubule attachments (10,11). The ordered CH domain makes direct contact to a single tubulin dimer within the microtubule protofilament. In humans, the tail domain is not sufficient, but necessary for kinetochore-MT attachments. The prevailing model is the positively charged HEC1 tail contributes to binding through a tunable electrostatic interaction. This tail is phospho-regulated during mitosis, whereby a high phosphorylation state creates a repulsive interaction with the negatively charged α and

β tubulin c-terminal tails; conversely, a low phosphorylation state supports kinetochore–MT binding (Fig 1.3) (12–14)

1.4 Phosphoregulation of Kinetochore-Microtubule Attachment Affinity

Aurora B kinase (ABK) is primarily responsible for HEC1 phosphorylation (12,15). Through this mechanism ABK can alter the stability of physical attachments between HEC1 and microtubules. In general, ABK activity at kinetochores is highest immediately upon nuclear envelope breakdown, and decreases as a cell enters metaphase. This results in weak kinetochore-MT binding affinity in early mitosis and is stabilized attachments in later mitosis at metaphase (14,15).

While multiple mechanisms are suggested for silencing ABK activity during metaphase (16,17) it was only recently that the phosphatases involved in regulating kinetochore–MT attachments were identified. One of the first proteins demonstrated to counteract ABK activity at kinetochores was surprisingly a SAC protein, BUBR1. Independent of its well-defined SAC activity, BUBR1 depletion was shown to destabilize kinetochore-MT attachments in an ABK-dependent manner (18,19). Later it was discovered that B56-PP2A was recruited to kinetochores and similarly, depletion of the B56 targeting subunit destabilized kinetochore–MT attachments (20). Finally, these data were linked to demonstrate that B56-PP2A is recruited to kinetochores through a direct interaction with BUBR1 (21–23). These competing kinase and phosphatase activities directly or indirectly serve to tune HEC1 phosphorylation during mitosis to prevent errors in kinetochore–MT attachments (Figures 1.3).

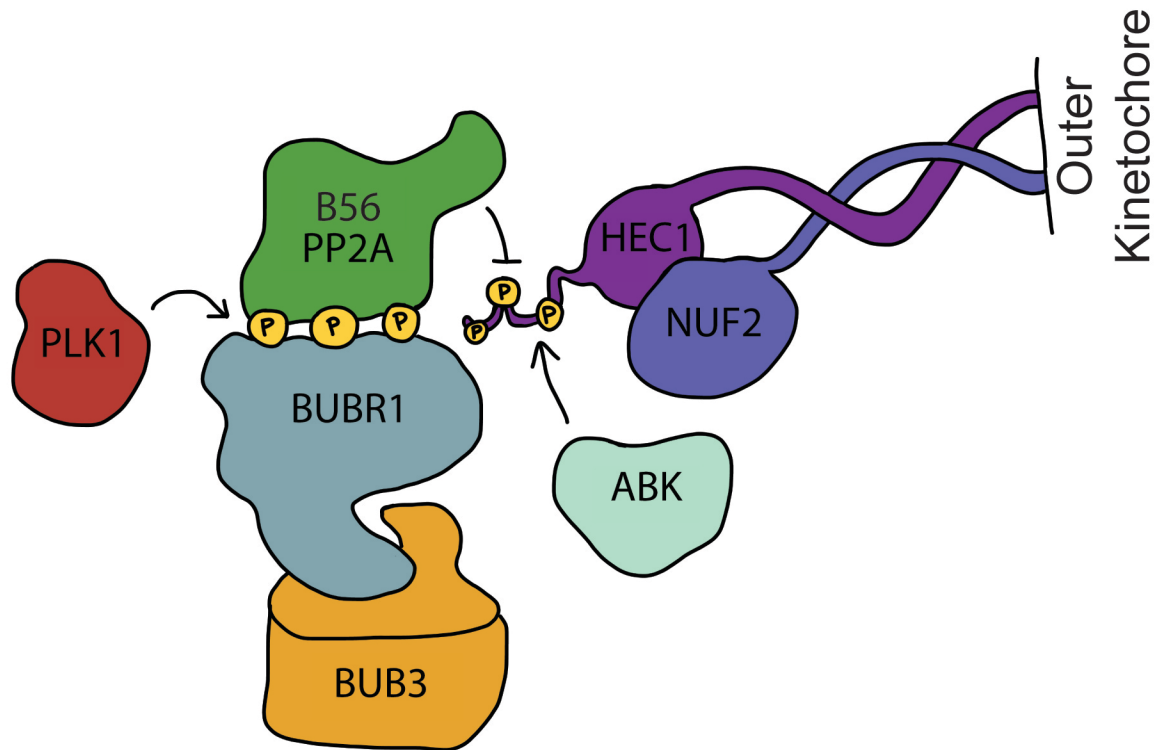


Figure 1.3. BUBR1 antagonizes Aurora B kinase activity at kinetochores and stabilizes attachment to microtubules.

BUBR1 is a key receptor of B56-PP2A at human kinetochores. In order to recruit the PP2A complex containing the targeting subunit B56 to kinetochores BUBR1 must bind BUB3 and be phosphorylated by PLK1. In this fashion BUBR1 antagonizes Aurora B kinase activity at the outer kinetochore. Currently, only KNL1 has been demonstrated as a PP2A substrate; however, it is likely PP2A also counteracts Aurora B kinase mediated HEC1 phosphorylation directly or indirectly. This activity would stabilize kinetochore-microtubule attachments.

1.5 Generating and Preventing Kinetochores-Microtubule Attachment Errors

Early in mitosis attachments are unstable and labile allowing improperly connected microtubules to be released. This prevents premature stabilization of commonly generated erroneous attachments, which leads to chromosome mis-segregation errors (3,24). Conversely, in late mitosis, kinetochore–MT attachments are stabilized to generate forces required for chromosome movements and to silence the SAC.

As discussed previously, regulation of kinetochore–MT attachments relies on ABK and likely PP2A (12,15,21,22) Upon nuclear envelope breakdown kinetochores lack spatial organization and bind microtubules indiscriminately. Thus, early in mitosis it is common for sister kinetochore pairs to attach to microtubules emanating from the same pole (syntelic attachment) or for a single kinetochore to attach to microtubules from both poles (merotelic attachment; Figures 1.4A,B) (3). To prevent the accumulation of such attachment errors, ABK phosphorylates multiple kinetochore proteins, primarily HEC1, to prevent premature stabilization of erroneous attachments (9,24–26). As mitosis progresses, kinase activity decreases and phosphatase activity dominates, resulting in low levels of ABK-dependent kinetochore phosphorylation. Decreased HEC1 phosphorylation increases its microtubule-binding activity, resulting in stabilized kinetochore–MT attachments (15).

This ABK mechanism is only one of the cell's 'error correction' pathways. Aside from destabilizing physical kinetochore-MT attachments, another approach to turning over erroneous attachments is to employ microtubule depolymerases. KIF2B, and

KIF2C/MCAK are known to depolymerize microtubules involved in erroneous attachments (27–29); however the mechanism is still unclear (28,30,31). In particular, MCAK mediated depolymerization of kinetochore bound microtubules has been indicated as the key mechanism for destabilizing merotelic attachments that persist into metaphase (27). These attachments are not detected by the SAC as sister kinetochores are bioriented, yet one kinetochore of the sister pair is attached to both poles (Figure 1.4). MCAK based depolymerization is required to completely correct, or reduce the number of incorrectly bound microtubules. If a merotelic attachment does persist into anaphase, the correctly oriented microtubule bundle typically (but not always) will be larger and exert a greater pulling force, maintaining genetic fidelity (32,33).

Defects in either the ABK regulatory system or depolymerase activity can result in erroneous kinetochore–MT attachments, which often lead to chromosome segregation errors and chromosome instability observed in many cancers (30,34).

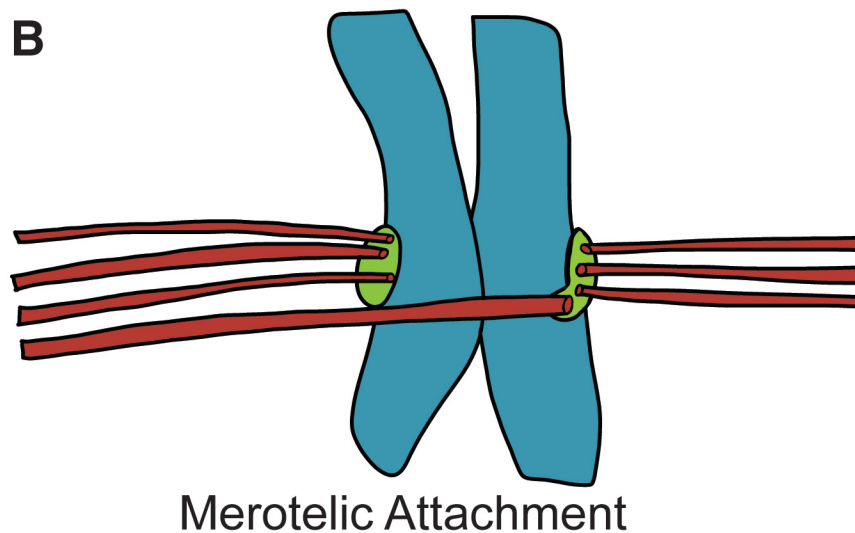
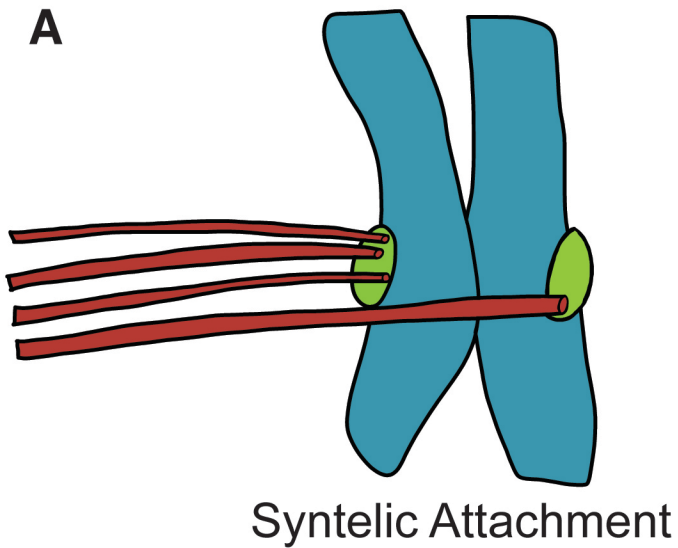


Figure 1.4. Description of erroneous kinetochore-microtubule attachments.

(A) Syntelic attachments occur when microtubules emanating from a single spindle pole bind to both sister kinetochores. These attachments fail to generate pulling forces normally seen upon proper biorientation (B) Merotelic attachments occur when one of sister kinetochores bind microtubules emanating from both spindle poles. These erroneous attachments often persist into metaphase and anaphase as they still build kinetochore-fibers and generate robust tension between sister kinetochores.

1.6 Kinetochore-Microtubule Attachment Errors in Glioblastoma and Other Cancers

Glioblastoma multiforme (GBM) is the common form of brain cancer in adults and is also considered highly aggressive due to its rapid onset and metastatic nature (35). Current standard of care therapy for GBM including surgery, radiation, and chemotherapy, is largely ineffective as nearly 90% of patients die within 2 years of diagnosis (36). Both adult and pediatric brain tumors are composed of cancer cell populations along all stages of differentiation, suggestive of a cancer stem cell origin (37–40). Consistently, glioblastoma stem cells (GSC) have recently been isolated that retain specific genetic markers and developmental potential found in patient tumors (37,38,41,42). When implanted in brain xenograft models, GSCs give rise to glioblastoma-like tumors with appropriate patient-specific molecular signatures and histologic features (39–42). Due to a cancer stem cell origin, and the malignant nature of this cancer, inter-patient and intra-tumor heterogeneity have challenged the efficacy of current therapies.

Cytological analysis of most late-stage solid tumors such as GBM reveals dramatic numerical and structural chromosome alterations (43) and intratumoral genomic heterogeneity (43–46). All of these features can promote tumor cell evolution, invasiveness, therapy resistance, and recurrence (47–50). Such chromosomal alterations often arise from aberrant mitoses (e.g., lagging chromosomes, anaphase bridges), consistent with increases in chromosome instability during tumor progression (47,51,52). Loss of SAC function is a common explanation proffered for increased chromosome instability and aneuploidy in cancers (53–55). This notion that loss of SAC

activity promotes tumorigenesis has found support in studies of certain cancers (53,54) and model systems, e.g., mouse knockouts of certain SAC genes (51,56). However, loss-of function mutations in SAC genes are rarely observed in cancers (55); furthermore many late-stage cancers exhibit high SAC gene expression (57,58), suggesting hyperactivity (Figure 1.5) (58,59).

As discussed above, the SAC protein BUBR1 plays an additional role in kinetochore–MT attachment regulation. Surprisingly, yet another SAC member regulates kinetochore-MT attachments: BUB1 has been shown to destabilize attachments independent of its role in the SAC (17,60–62). Thus, paradoxically, instead of loss of SAC activity causing chromosome instability and complex karyotypes observed in high-grade glioma and ductal carcinomas, it is likely that SAC proteins become increasingly required to support mitotic defects in kinetochore–MT attachments as low-grade tumors transition to aggressive malignancies such as GBM.

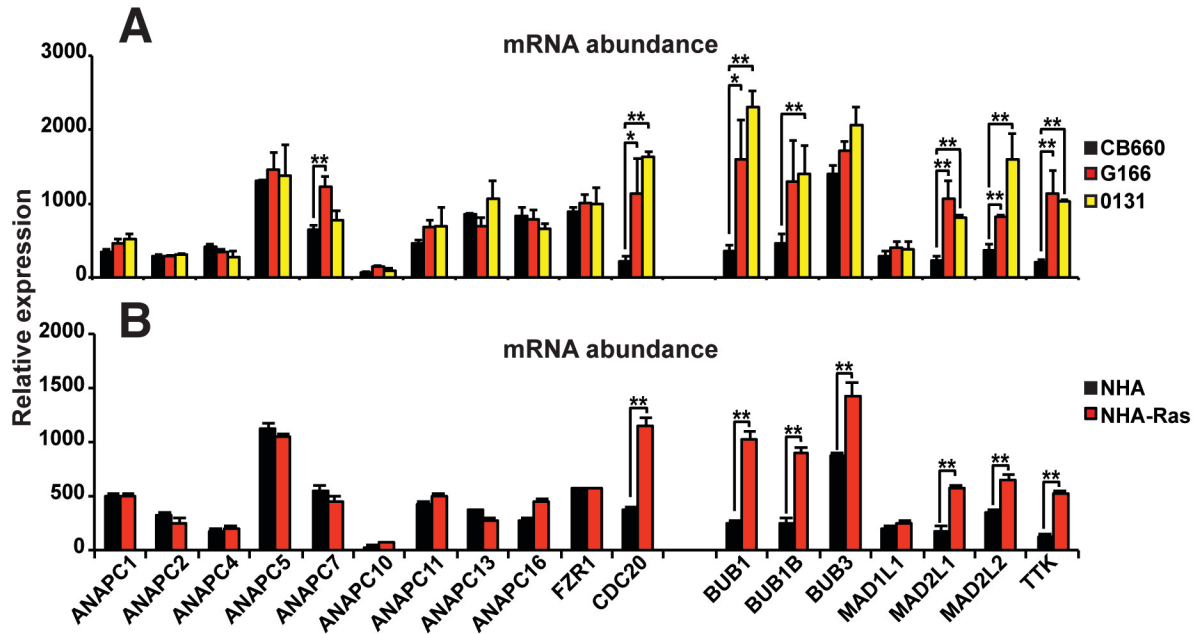


Figure 1.5. Spindle assembly checkpoint proteins are transcriptionally amplified in many cancers.

(A) mRNA abundance of mitotic checkpoint genes and components of the anaphase promoting complex in neural stem cells (black) and glioblastoma patient isolates (red and yellow). (B) Many spindle assembly checkpoint genes have increased mRNA abundance after normal human astrocytes (NHA) are genetically transformed with the RAS oncogene.

One hypothesis is that oncogenic signaling fundamentally alters regulation of kinetochore–MT attachments in some cancers resulting in a compensatory mechanism where SAC proteins are more highly expressed. These defects in kinetochore signaling are suppressed by the contribution of SAC proteins in regulating kinetochore–MT attachments, an otherwise nonessential function. Data supporting this hypothesis follow this introduction. If true, the allowance of otherwise lethal kinetochore–MT attachments by SAC proteins leads to the genomic instability observed for such cancers, albeit other factors likely contribute (e.g., tetraploidization, chromothrypsis, telomere fusions, sister chromatid cohesion defects).

The kinetochore–MT attachment activities of SAC proteins may represent much sought-after cancer-specific therapeutic targets for GBM and other refractory late-stage cancers. This particular mechanism may transcend the heterogeneity of molecular subclasses and combinations of oncogenic drivers that has thwarted most pharmacologic interventions for aggressive malignancies in the past.

CHAPTER 2

DOCUMENTING CANCER-SPECIFIC KINETOCHORE-MICROTUBULE ATTACHMENT DEFECTS IN GLIOBLASTOMA PATIENT ISOLATES²

2.1 Introduction

GBM is the most aggressive, lethal, and common form of brain cancer in adults (35). While a standard of care treatment exists for this cancer including surgery, radiation, and chemotherapy, the five-year survival rate is below 10% (36). The aggressive and therapy resistant nature of these tumors is likely the result of a cancer stem cell population. Consistent with this notion, glioblastoma stem cells (GSC) have recently been isolated that retain the development potential and specific genetic alterations found in real patient tumors (37,40–42). RNA profiling has confirmed that the aggressive behavior of glioblastoma tumors arises from their ability to enhance many pathways including: self-renewal or developmental programs (63), DNA repair pathways (64), angiogenesis (65), and/or invasiveness (66). The failings of current chemotherapy in GBM may arise from an inability to target the cancer stem cell population, and for future

² The work in this chapter was published in February 2013 under the title “Cancer-specific Requirement for BUB1B/BUBR1 in Human Brain Tumor Isolates and Genetically Transformed Cells”. Here I have written the contents of that work to focus on my contributions and findings important to our following studies.

Y.D., P.J.P, and J.M.O conceived the content; Y.D. and P.J.P. co-wrote the original manuscript with input from J.G.D, J.Z. and J.M.O. I contributed in experimental design, data collection, analysis, and interpretation for Figures 2.4 and 2.5.

Ding Y, Hubert CG, Herman J, Corrin P, Toledo CM, Skutt-Kakaria K, Vazquez J, Basom R, Zhang B, Risler JK, Pollard SM, Nam DH, Delrow JJ, Zhu J, Lee J, DeLuca J, Olson JM, Paddison PJ. Cancer-Specific Requirement for BUB1B/BUBR1 in Human Brain Tumor Isolates and Genetically Transformed Cells. *Cancer Discov.* 2013;3:198–211

therapies to succeed they would need to overcome this challenge. A key advance in screening for new therapeutic targets is the ability to isolate and grow GSCs in serum-free, defined monolayer culture (41,42). By this method, GSCs retain tumor-initiating potential and tumor-specific genetic and epigenetic signatures over extended outgrowth periods (67). Here we perform short hairpin RNA (shRNA) kinome screens in GSCs and neural stem cells (NSC) for genes required for progenitor expansion. Combining screen results with a glioblastoma bionetwork created from patient molecular signatures in the cancer genome atlas, allowed us to identify cancer-specific activities within GSCs. From this approach BUBR1, a critical mitotic checkpoint pseudokinase, (4) was determined as the top hit for proteins required specifically for viability in GSCs. We further demonstrate that a specific activity within BUBR1 is required to suppress lethal chromosome alignment defects during mitosis. We also suggest that these defects are the result of oncogenic signaling fundamentally altering kinetochore function in a subset of GSCs. Finally, we further observe that altered kinetochore activity in glioblastoma and genetically transformed cells may serve as a predictive biomarker for cancer-specific sensitivity to BUBR1 inhibition and perhaps other mitotic targets that affect kinetochore–MT stability.

2.2 Results

An RNA Interference Kinome Screen for Genes Differentially Required for GSC Expansion

To discover targets for therapeutic inhibition in GBM patients, we conducted an shRNA screen against 713 human putative kinases in order to identify which kinase activities are required for ex vivo expansion of GSCs. To ensure the hits within our screen

represented truly selective therapeutic targets for GBM, a parallel screen was conducted in human fetal NSC-CB660 cells (Figure 2.1A) (68). These neural stem cells (NSCs) were isolated and grown in exactly the same fashion as GSCs. Both populations share molecular and phenotypic features, including doubling times, expression profiles, and differentiation potential. However, NSCs retain a normal karyotype and are not tumorigenic, thereby serving as ideal controls for GCSs (68).

Through our screening approach we identified approximately 48 candidate kinase targets with shRNAs absent in GSCs relative to NSCs, due to lethality of the target depletion in GSCs specifically. Gene ontology analysis did not help prioritize these hits because most kinases are involved in numerous biologic processes. Instead, we examined the occurrence of screen hits in a glioblastoma-specific regulatory network, constructed de novo from more than 421 glioblastoma samples from The Cancer Genome Atlas (TCGA) (69) by integrating gene expression and DNA copy number variation data (70,71). By this analysis, 37 of 48 shRNA candidate hits appeared as nodes in the glioblastoma network. Examination of subnetworks in the glioblastoma network revealed 15 biologic processes significantly enriched (5 cell-cycle related and 9 general phosphorylation related), including the M-phase of mitotic cell cycle ($P < 0.001$). The largest glioblastoma-specific subnetwork contained 4 screen hits, including ABK, BUBR1, MELK, and PLK1 (Figure 2.1B). On the basis of key driver node analysis (72), BUBR1 scored as the top-ranked screen hit (Figure 2.1C).

To control for glioblastoma network comparisons, we also examined screen hits in a normal brain network constructed from 160 nondementia human prefrontal cortex

samples. Only 20 of 48 candidate hits appeared in the normal brain network and produced smaller subnetworks enriched for general phosphorylation-related biologic processes (data not shown). Although BUBR1 appeared in this network, it was connected to only one gene and had no down nodes (Figure 2.1B), and thus was not a key driver node.

BUBR1 Is Differentially Required for Growth in GSCs and RAS-Transformed Cells.

Due to the heterogeneous nature of GBM it was essential to verify ABK, BUBR1, MELK, and PLK1 as hits in GSCs from multiple glioblastoma isolates. These short-term outgrowth assays revealed that BUBR1 inhibition gave the largest differential effect in eight different GSC isolates without observable toxicity in proliferating NSCs or astrocytes (Figure 2.2A-D). For these outgrowth assays shRNA targeting mitotic kinesin KIF11 was used as a positive control as it blocks the growth of GSCs, NSCs, and astrocytes equally. Importantly, BUBR1 was the only hit we were able to verify as we observed decreased viability after BUBR1 depletion in 80% of GSCs tested. Further tests with ABK were lethal in NSCs and GSCs alike, MELK had no effect, and PLK1 gave only partial response in GSCs.

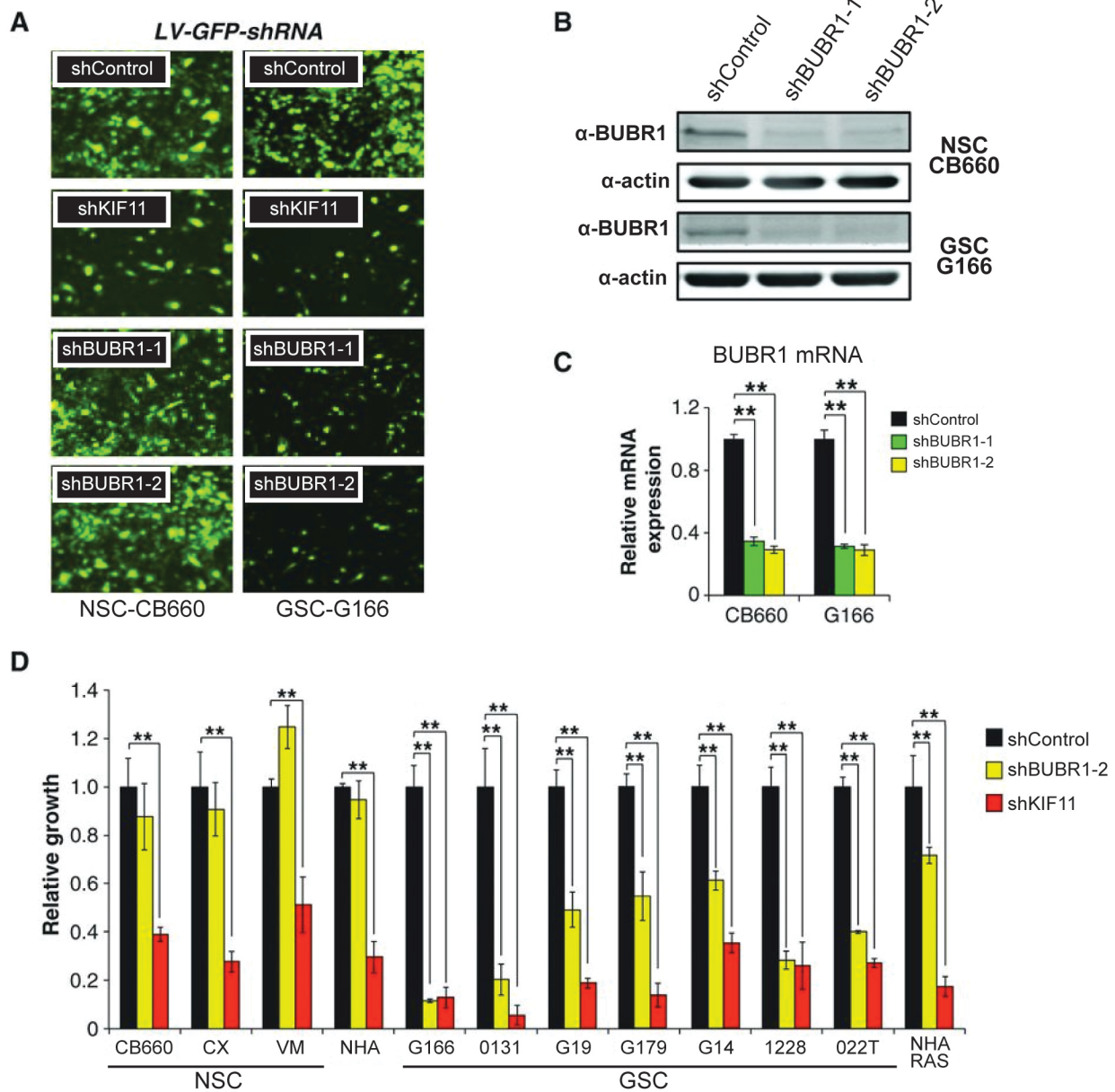


Figure 2.2. BUBR1 is validated as a candidate glioblastoma-lethal gene in vitro.

(A) GSC-specific effects of BUBR1 knockdown, visualized using shRNA–green fluorescent protein (GFP+) GSCs and NSCs 6 days after posttransduction with pGIPz-shRNA virus. Knockdown of KIF11/EG5 was used as a positive control for both RNAi pathway activity and cell proliferation. (B) and (C) Examination of BUBR1 knockdown by western blot and quantitative real-time PCR (qRT-PCR) in GSC-G166 and NSC-CB660 cells. (D) Comparison of the effects of BUBR1 knockdown on in vitro expansion of multiple GSC and NSC lines including normal human astrocytes and genetically transformed normal human astrocytes (NHA RAS). **, Student t test; $P < 0.01$.

The fact that a small fraction of GSCs did not exhibit the requirement for BUBR1 suggested that a unique oncogenic pressure was driving this defect. To understand what oncogene was sufficient to induce this differential requirement in growth for BUBR1 we used genetically transformed normal human astrocytes (NHA). These cells were transformed with an oncogenic version of RAS because PDGFR or EGFR mutations are common in GBM and the RAS GTPase is the immediate downstream transducer of such receptor tyrosine kinases (43,73,74). We found that RAS^{V12} expressed in NHA induced the BUBR1 requirement for outgrowth (Figure 2.2D).

Genetic Dissection of the Added Requirement of BUBR1 in GSCs

BUBR1 is a highly conserved BUB1-like pseudokinase whose activity is essential for SAC signaling as well as growth and development (4,75,76). As mentioned previously the SAC serves as a surveillance mechanism to monitor the attachment status of kinetochores to the plus ends of spindle microtubules. The SAC prevents anaphase onset until all sister kinetochores are properly attached and bioriented at the spindle equator (4). Mouse knock out models have demonstrated that the SAC activity of BUBR1 is an essential gene function in non-transformed cells which suggested that our RNAi approach produced a hypomorphic state where GSCs, but not NSCs or astrocytes, are sensitive to loss of one or more of BUBR1's multiple functions.

BUBR1 has multiple functional domains that have been implicated in SAC control, mitotic timing, and regulating kinetochore–MT attachment (3,4). These include N- and C-terminal KEN box domains involved for CDC20 binding and APC/C inhibition (77–79);

a C-terminal pseudokinase domain required for protein stability (80); and a GLEBS-like motif necessary for kinetochore localization during mitosis (Figure 2.3A) (81,82).

Although BUBR1 is necessary for mammalian development (83), its essential function is contained solely within the N-terminal KEN box, which enables BUBR1 to act as a pseudo-substrate inhibitor of APC/C and prevent a precocious anaphase (77,84).

Previously knockout and rescue experiments in MEFs with floxed BUBR1 alleles demonstrated that the N-terminal KEN box of BUBR1 was the essential domain for development and cell viability (75,77). However, these studies did not test if cellular transformation altered this requirement. Using this same system we also observed that only the N-terminal KEN box was required to ensure viability after BUBR1 deletion in non-transformed cells. However, when MEF cells were genetically transformed with an oncogenic RAS^{V12}, which was previously shown to induce the outgrowth requirement for BUBR1 in NHA, the results differed. In RAS-transformed MEFs deletion of the N-terminal KEN box failed to compensate for BUBR1 deletion, and, additionally, a single charge reversal mutant in the GLEBS motif also failed to rescue viability (Figure 2.3B).

The GLEBS motif is required for BUBR1 to bind BUB3 and localize to kinetochores (81,82,85). This suggested the GBM- and RAS-specific requirement for BUBR1 was contained within BUBR1's activity at kinetochores. These results in the transformed MEF system were observed in GSCs using the same genetic constructs, whereby deletion of either the N-terminal KEN box or the GLEBS mutant could not restore growth in BUBR1 depleted GSCs (Figure 2.3C).

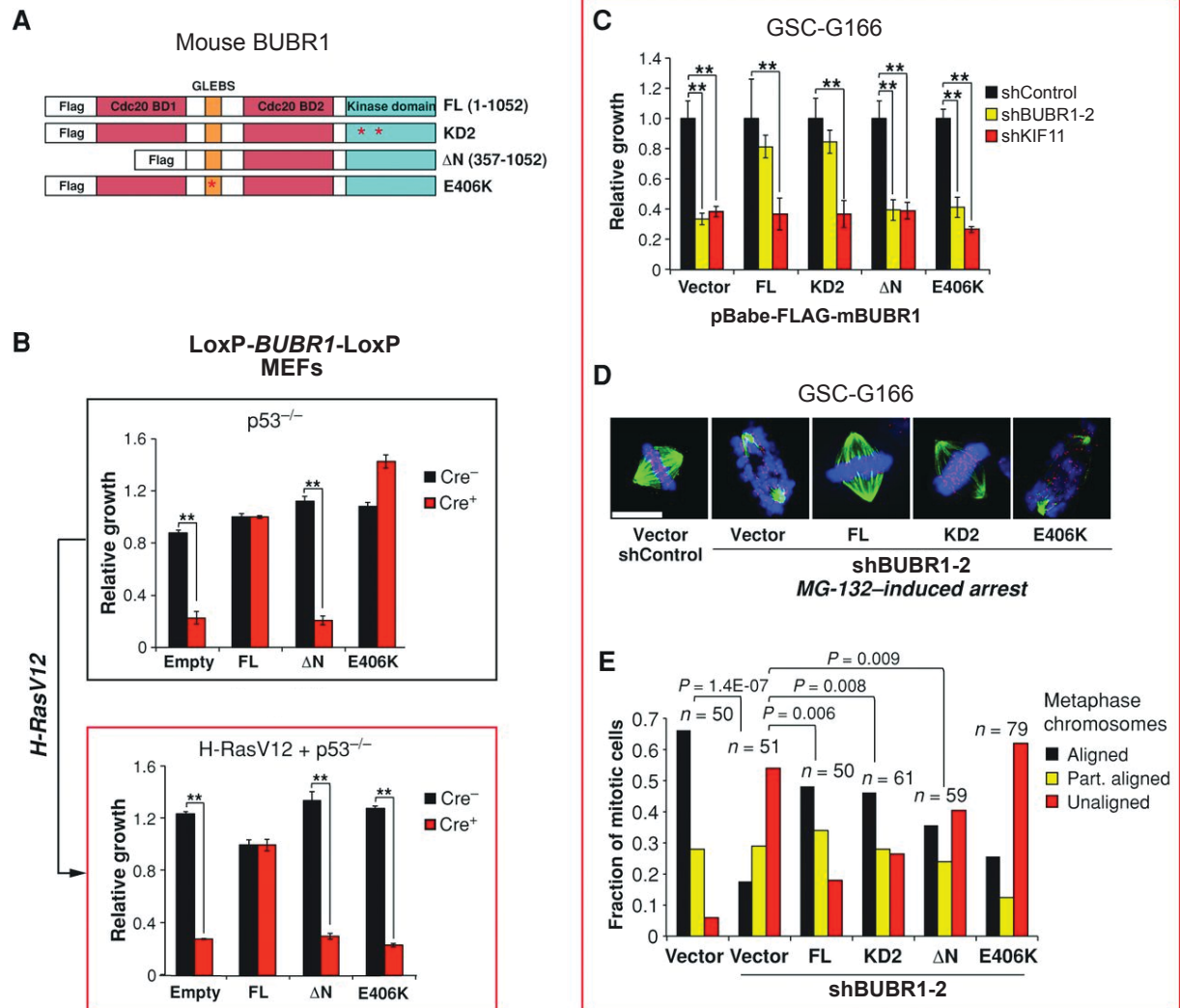


Figure 2.3. Allelic complementation studies with mouse BUBR1 (mBUBR1) mutants in BUBR1 $-/-$ MEFs and GSCs.

(A) The mouse alleles used in these studies were previously published and include FL; KD2, which harbors 2 point mutations in the kinase domain (K784>R in the ATP binding domain and K802>R in the catalytic domain); Δ N, which lacks the N-terminal Cdc20 binding domain 1; and E406K, a point mutation in the GLEBS motif that interferes with kinetochore localization and Bub3 binding. (B) Viability assessment of complementation studies using p53 $-/-$ MEFs with floxed alleles of BUBR1, with and without transformation via H-RasV12. Knockdown of BUBR1 in RAS-transformed NHAs phenocopies the BUBR1 requirement observed in GSCs with respect to viability. MEFs were transduced with murine stem cell virus (MSCV)-GFP-mBUBR1 constructs, sorted for GFP, outgrown, transduced with pMSCV-Puro-Cre, selected, and seeded into microtiter growth dishes for proliferation assays. (C) Viability of complementation studies using GSC-G166 with shBUBR1 (or controls) expressing each of 4 mBUBR1 alleles from A. Assays were conducted as in Fig. 1C. (D) and (E) Chromosome alignment after complementation of BUBR1 knockdown with mBubR1 alleles, as in Fig. 4A and B. Scale bar, 10 μ m.

To also understand the nature of the growth defects we used high-resolution fluorescence microscopy to observe any possible mitotic defects. As deleting the KEN box was lethal to transformed and non-transformed cells alike, we hypothesized SAC activity was not the source of lethality and instead it was BUBR1's role in forming kinetochore-MT attachments. To characterize this role of BUBR1 we depleted GSCs of BUBR1 and arrested them in MG132 to prevent premature anaphase onset. These cells failed to make robust kinetochore-MT attachments or align their chromosomes to a metaphase plate as previously observed in HeLa cells (18,19). This activity could be restored with all variants of BUBR1 except the GLEBS point mutant, which failed to rescue cell growth in GSCs, suggesting the GSC-specific requirement for BUBR1 is to form kinetochore-MT attachments and align chromosomes at the metaphase plate (Figure 2.3D,E). This confirmed that a specific oncogenic pressure drove the requirement for BUBR1 because a subclass of GSCs survived after BUBR1 depletion.

To further analyze this phenomenon we depleted BUBR1 and treated with MG132 in three different cell types: NSCs (CB660), and two classes of GSC, one which required BUBR1 for growth (G166), and one which did not (0827). These experiments were consistent with our mutational analysis, cell lines which required BUBR1 for growth, could not form robust kinetochore-MT attachments or align their chromosomes after BUBR1 depletion (Figure 2.4A,B).

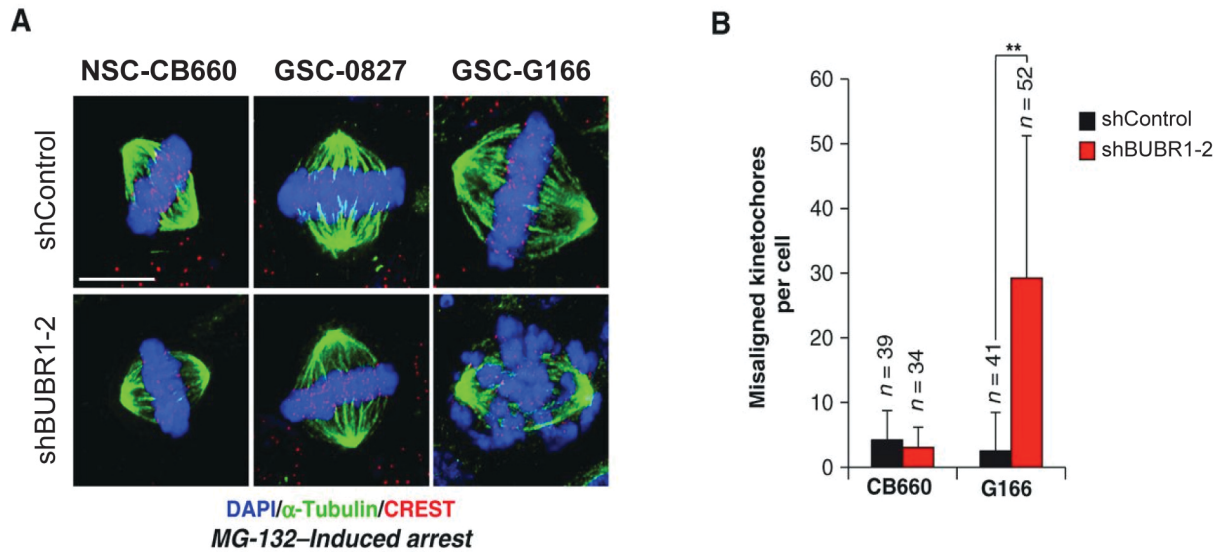


Figure 2.4. Only a subset of GSCs require BUBR1 activity to suppress kinetochore-MT attachment defects.

(A) Chromosome alignment assays in GSCs and NSCs with BUBR1 knockdown. Transduced cells were treated with 10 μ M MG-132 for 2 hours to arrest them at metaphase and then fixed, stained as indicated (CREST antiserum stains human kinetochores), and visualized using deconvolution microscopy. Scale bar, 10 μ m. (B) Quantification of misaligned kinetochores (n, number of metaphase cells counted; **, $P < 0.001$ by Student t test).

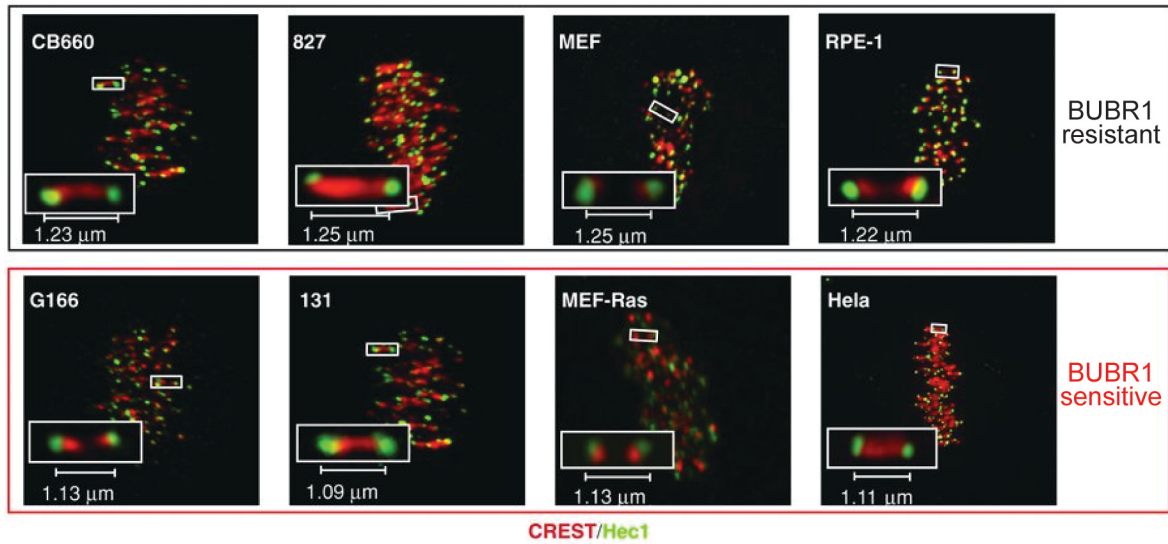
Kinetochores Function is Fundamentally Altered in Cells with BUBR1 Requirement

These findings indicated that RTK/RAS and perhaps other oncogenic signaling in GSCs were fundamentally altering kinetochore function in transformed cells. Due to these oncogene-induced changes, BUBR1 was suppressing a lethal kinetochore-MT attachment defect, which was not present in non-transformed cells and 20% of GSCs. To begin understanding how kinetochore activity was being altered we measured inter-kinetochore distance (IKD), the maximum distance achieved between sister kinetochores when stable end-on MT attachment has occurred (12). IKDs are indirect measures of the pulling force generated by MT attachment. Thus shorter IKD generally mean weaker kinetochore-MT attachments. We first measured IKDs for shBUBR1-insensitive NSCs (CB660) and 2 shBUBR1-sensitive GSC isolates (G166 and 0131). We found that IKDs were significantly shorter in both GSC isolates (1.23 μm for CB660 vs. 1.13 μm for G166 and 1.09 μm for 0131; Figure 2.5A,B). Thus, GSC IKDs were shorter by 100 to 140 nm or 50 to 70 nm for each sister kinetochore (Fig 2.5A,B). These numbers represent 15% of the overall change in IKDs from 'rest length' (0.55 μm) to MT attachment. Moreover, at metaphase kinetochores undergo a significant molecular reorganization whereby HEC1 is moved only 50 nm towards the spindle pole (86,87). These findings were consistent with the idea that kinetochore-MT attachments were fundamentally different in GSCs.

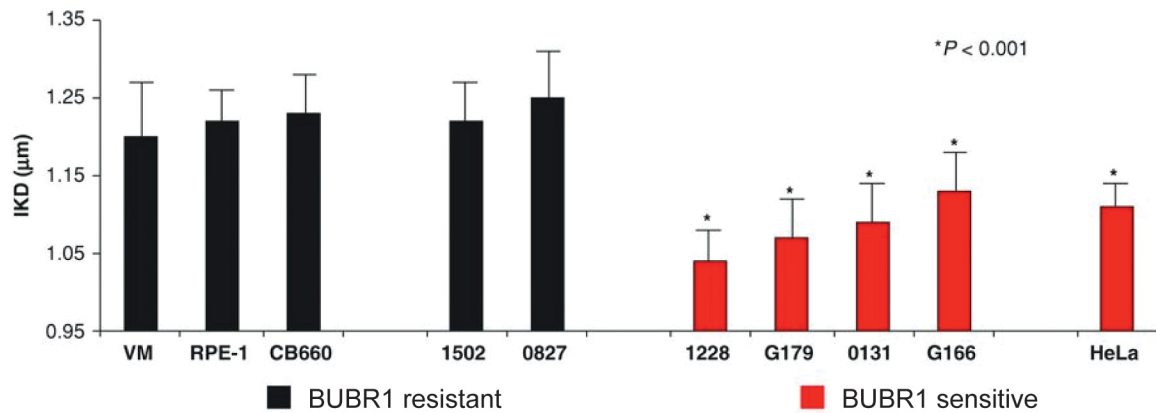
Next, we examined IKDs in two glioblastoma patient isolates, 0827 and 1502, which we had observed were completely insensitive to shBUBR1. These isolates were insensitive despite having similar knockdown efficiencies to shBUBR1-sensitive lines and among

the fastest doubling times and tumor initiation rates (data not shown). Measuring IKDs in these cells revealed that they were indistinguishable from NSCs with an IKD of 1.23 μm , suggesting that the same kinetochore alteration both weakens kinetochore-MT attachments, and induces the requirement for BUBR1. If this were true, then IKDs may predict BUBR1 sensitivity (Figure 2.5A,B). To further examine this possibility, we tested IKDs in the RAS transformed MEFs previously used for molecular dissection. In $p53^{-/-}$ control MEFs, IKDs averaged 1.25 μm , similar to those of NSCs and 827 cells. Surprisingly, Ras^{V12} expression converted long IKDs to short, averaging 1.13 μm , indistinguishable from those of G166 and 0131 cells (Figure 2.5C). Moreover, Ras^{V12} transformation also converted MEFs from being resistant to BUBR1 inhibition to being profoundly sensitive, which was true for human astrocytes as well (Figure 2.5C). Importantly, all of the IKD measurements for GSCs, NSCs, and MEFs were scored blindly to avoid experimenter bias. Because most BUBR1 experimentation has been carried out in HeLa cells, which are derived from a cervical carcinoma, we next measured IKDs in these cells (18,19). As a control, we used immortalized retinal pigment epithelial (RPE-1) cells, which are non-transformed. HeLa cells showed IKDs similar to other BUBR1-sensitive cells (1.11 μm), whereas RPE cells showed long IKDs, similar to those of insensitive cells (1.22 μm). These results suggest (i) that IKDs occur in discrete intervals: long ($\sim 1.24 \mu\text{m}$) and short ($\sim 1.12 \mu\text{m}$); (ii) that short IKDs predict sensitivity to BUBR1 inhibition; and (iii) that Ras^{V12} transformation is sufficient to induce short IKDs and sensitivity to BUBR1 loss.

A



B



C

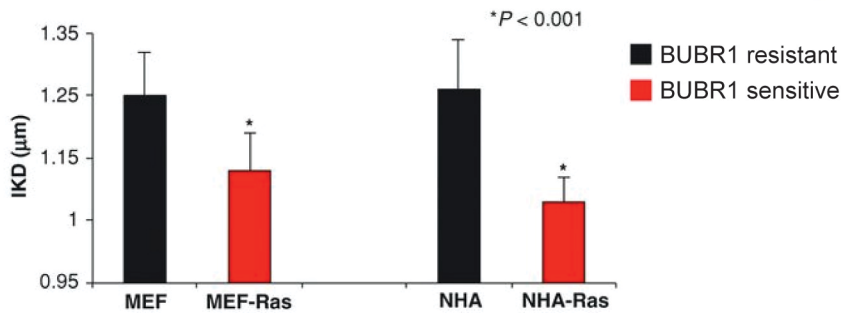


Figure 2.5. Measurement of IKD in BUBR1-resistant and -sensitive cells.

(A) Measurement of IKDs in GSCs, NSCs, MEFs, MEF-RAS cells, RPE cells, and HeLa cells, using immunofluorescent staining of kinetochores. Constitutive centromere-associated network (CCAN/CREST) proteins (red) and outer kinetochore protein, HEC1 (green) were visualized to identify kinetochore pairs. IKDs were measured between Hec1 centroids, using Applied Precision softWoRx software package. (B) and (C) quantification of average metaphase IKDs from A. *, $P < 0.001$ by Student t test.

2.3 Discussion

Here we performed a functional RNAi screen for genes differentially required for growth in glioblastoma stem cells, moreover, hits were analyzed using a bionetwork derived from multiple molecular datasets based on expression and copy number variation.

Using this novel approach we identified the mitotic pseudokinase BUBR1 as specifically required for proliferation of GSCs. The requirement for BUBR1 was validated in 80% of GSC patient isolates tested, and could be induced through genetic transformation with the RAS oncogene.

We further demonstrated that the GSC/RAS specific growth requirement for BUBR1 was contained within the BUBR1-GLEBS motif. The GLEBS domain is essential for BUB3 binding and kinetochore localization. The growth requirement was the result of lethal defects in forming kinetochore-MT attachments and aligning chromosomes. Thus either BUB3 binding, kinetochore localization, or both BUBR1 activities are required in a subset of transformed cells, but not non-transformed, in order to generate kinetochore-MT attachment. This suggested that transformation fundamentally alters kinetochore function. Such a defect was also observed by measuring IKDs, whereby every patient isolate that required BUBR1 for viability had a shorter average IKD at metaphase and likely weaker kinetochore-MT attachments.

We observed first, that not all GBM isolates required BUBR1 for proliferation, and second, that RAS transformation was sufficient to induce the requirement for BUBR1. These data together suggest that a unique oncogenic pressure drives a lethal

kinetochore defect that is suppressed by BUBR1 activity at kinetochores. Moreover, whenever we observed a BUBR1 requirement, cells also exhibited a decreased average metaphase IKD. It is likely that transformation perturbs kinetochore signaling inducing both of these defects; however, functionally, IKDs may serve as an important therapeutic biomarker. A therapy targeting BUBR1 would only function in a subset of tumors, and measuring IKDs may identify patients that would be sensitive to such an intervention.

It is important to note that RAS mutations are rarely observed in GBM, and by some means this genetic system is not an adequate model for GBM. While RAS mutations themselves are rare, it is common in GBM to identify driver mutations within EGFR, PTEN, and NF1, all of which are involved in RAS signaling pathways (73,74). While RAS-transformation was sufficient to induce the kinetochore defects observed in 80% of patient isolates, it remains unclear how/if this pathway is truly driving these defects in real tumors. However, it is conceivable that inappropriate regulation of the RAS pathway in mitosis could have a direct enzymatic effect on kinetochore–MT attachments and their regulation as downstream factors have been observed at mitotic structures (88,89). While we have identified a novel cancer-specific therapeutic target, and observed a fundamental difference between kinetochore function in transformed and non-transformed cells, two major questions remain: (1) How, mechanistically, does RAS signaling alter kinetochore function? and (2) What BUBR1 activity at kinetochores suppresses the lethal effects of RAS driven alterations? Both of these important questions are addressed below (Chapter 3).

2.4 Methods

shRNA Barcode Screens and Array Analysis

For shRNA screen and barcode array analysis, cells were infected with a pool of lentiviral shRNAs targeting 713 human kinases at a representation of approximately 1,000-fold [multiplicity of infection (MOI) < 1]. At day 3 post infection, an initial day 0 sample was taken. The rest of the population was selected with puromycin (Sigma; 2 µg/mL) to remove uninfected cells. Afterwards, cells were propagated in culture for an additional 21 days and sampled for barcode array analysis at 21 days. For each passage, a minimal representation of 1,000-fold was maintained. For each corresponding sample, shRNA barcodes were PCR recovered from genomic samples, labeled with Cy5 or Cy3, and competitively hybridized to a microarray containing the corresponding probes (Agilent Technologies). Replicate array results were analyzed using the BioConductor package limma. The change in the relative abundance of each shRNA in the library over time was measured using the normalized Cy3/Cy5 ratio of its probe signal. Barcode probes depleted in the BTIC samples were considered candidate genes, using the following criteria: (i) adjusted $P \leq 0.05$ and (ii) $|\log_2(\text{ratio})| \geq 0.585$. Cell Culture BTIC and NSC lines used in these studies have been previously published (42,63) and were grown in N2B27 neural basal media (STEMCELL Technologies) supplemented with EGF and fibroblast growth factor 2 (FGF-2) of 20 ng/mL each (Peprotech), on laminin-coated polystyrene plates (Sigma) and passaged according to Pollard and colleagues (42). Immortalized CX cells and VM cells (Millipore) were maintained in ReNcell maintenance medium with EGF and FGF-2 (20 ng/mL each; Peprotech) and also grown on laminin-coated tissue culture-treated plates and

passaged according to Pollard and colleagues (42). NHA (STEMCELL Technologies) and NHA-Ras cells (Russell Pieper, University of California San Francisco, San Francisco, CA) were grown in astrocyte growth medium (Clonetics) according to the manufacturer's instructions and published protocols (90).

RNAi

The shRNAs were obtained from the RNAi Shared Resource [Fred Hutchinson Cancer Research Center (FHCRC)] or Open Biosystems in the pGIPZ lentiviral vector. Target sequences for shRNAs are as follows: BUBR1, #1, CDS:1417, CCTACAAAGGAGACAATA; BUBR1, #2, CDS:1547, AGGAACAACCTCATTCTAA; and KIF11, CDS:571, AAGAGAGGAGTGATAATTA. For virus production, pGIPZ-shRNA plasmids were transfected into 293T cells along with psPAX and pMD2.G packaging plasmid to produce lentivirus. Approximately 24 hours after transfection, NSC expansion medium was added to replace original growth medium. Virus was harvested 24 hours after medium change and stored at -80°C . BTICs and NSCs were infected at $\text{MOI} < 1$ and selected with 2 to 4 μg of puromycin for 2 to 4 days.

qRT-PCR

qRT-PCR QuantiTect quantitative real-time PCR (qRT-PCR) primer sets and QuantiFast SYBR Green PCR Kits (Qiagen) were used according to the manufacturer's instructions with the ABI PRISM 7900 Sequence Detection System (Genomics Resource, FHCRC). Relative transcript abundance was analyzed using the $2^{-\Delta\Delta\text{Ct}}$ method. TRIzol (Invitrogen) extraction was used to collect total RNA from cells.

Western Blot Analysis

Western blots were carried out using the standard laboratory practices, except that a modified radioimmunoprecipitation assay buffer was used for protein extraction [150 mmol/L NaCl, 50 mmol/L Tris, 2 mmol/L MgCl₂, 1% SDS, 4% DOC, 4% Triton-X 100, 2 mmol/L DTT, and complete protease inhibitors (Roche)] followed by a 15-minute digestion with 125 units of Benzonase (Merck) at room temperature. The following antibodies were used for detection: BUBR1 (1:1,000; Sigma), Actin (1:1,000; Cell Signaling), and cleaved PARP (1:1,000; Cell Signaling). An Odyssey infrared imaging system was used to visualize blots (LI-COR) following the manufacturer's instruction.

Growth Assays

For short-term outgrowth assays, after selection, shRNA-transduced cells were harvested, counted (NucleoCounter, NBS), and plated onto a 96-well plate. After 7 days under standard growth conditions, the cell proliferative rate was measured using AlamarBlue reagent (Invitrogen).

Immunofluorescence

For metaphase staining, cells were treated by 10 μ mol MG-132 (TOCRIS Bioscience) for 2 hours to arrest them at metaphase and then fixed for 20 minutes at room temperature with 4% formaldehyde in PBS and 0.2% Triton X-100. For chromosome alignment assays, cells were blocked and stained with α -tubulin (DM1A; 1:1000; Sigma) and CREST anti-serum (1:1000; Immunovision) antibodies at room temperature for 1 hour. For interkinetochore distance measurements, cells were blocked and stained with

HEC1 (1:2000 GeneTex) and CREST anti-serum (1:1000; Immunovision) antibodies at room temperature for 1 hour. Cells were washed and incubated with secondary antibody and DAPI for 1 hour in the dark.

Image Acquisition and Analysis

Immunolabeled cells were imaged on a DeltaVision RT deconvolution microscope (Applied Precision Inc.). Optical sections were acquired at 0.2- μ spacing with an Olympus $\times 100/1.4$ NA UPLS Apo objective. Three-dimensional (3D) image stacks were deconvolved with Applied Precision's proprietary software softWoRx, using a constrained iterative algorithm. The number of misaligned MT-attached kinetochores was counted on the basis of CREST staining on 3D rendered images, and confirmed by visual inspection of maximum intensity projections of whole cells. Misaligned kinetochores were defined as those with normalized distance less than 0.2 μ m. At least 30 cells were analyzed for each RNAi experiment. IKDs were measured as the distance from HEC1 centroid to HEC1 centroid using SoftWoRx software.

CHAPTER 3

ONCOGENIC RAS/MAPK SIGNALING HYPERACTIVATES AURORA B KINASE AND WEAKENS KINETOCHORE-MICROTUBULE ATTACHMENTS³

3.1 Introduction

Organismal growth and development require the faithful duplication and separation of genetic material. During mitosis the kinetochore is assembled on centromeric heterochromatin where this molecular machine is primarily responsible for coupling the forces of microtubule polymerization and depolymerization with movements of whole chromosomes. These forces are used to congress and segregate chromosomes equally into two daughter cells. The kinetochore also serves as a surveillance mechanism to detect and prevent chromosome segregation errors. Chromosome segregation defects and the resulting errors in chromosome number such as aneuploidy – the missegregation of single, whole chromosomes – are linked to cancer and developmental defects. Aneuploidy was first described in transformed cells over a century ago, and only in the last two decades have we determined that errors in regulating kinetochore-MT attachments are the major causative factor (91,92). In

³ The work in this chapter is will be submitted for publication under the same title, with the suggested citation listed below.

J.G.D., P.J.P, and I conceived the content; I wrote the manuscript with input from J.G.D, and P.J.P; I contributed to all experimental design, analysis, and interpretation.

Herman JA, DeLuca KF, Toledo CM, Paddison PJ, and DeLuca JG. Oncogenic RAS/MAPK signaling hyperactivates Aurora B kinase and weakens kinetochore-microtubule attachments. In preparation for eLife.

particular, merotelic kinetochore-MT attachments commonly bypass mitotic surveillance mechanisms and persist into anaphase (30,33). Merotelic attachments occur when a kinetochore is bound to microtubules emanating from both spindle poles. To prevent the stabilization of erroneous kinetochore-MT attachments, early in mitosis ABK phosphorylates the key microtubule binding protein HEC1, which promotes kinetochore-MT attachment turnover. This results in the release of attached microtubules, including those that are incorrectly attached (12,15). Once released, microtubules are depolymerized and the erroneous attachment is prevented from growing into a robust kinetochore-fiber. Through this mechanism the cell prevents merotelic attachments from being stabilized and persisting into metaphase. When the ABK-mediated correction mechanism fails and cells enter anaphase with chromosomes bound incorrectly to microtubules, such chromosomes experience pulling forces from both spindle poles and thus may remain at the spindle equator, often resulting in a chromosome segregation error (32,33). Deregulation of multiple mitotic processes has been shown to contribute to the formation of merotelic attachments (30,92); however, it remains unclear how specific oncogenic mutations result in increased errors in regulating kinetochore-MT attachments. Moreover, there is even less understanding of how kinetochore-MT attachments can be targeted in a therapeutic manner.

We previously identified the mitotic regulator BUBR1 as specifically required for viability in a subset of glioblastoma patient isolates and in RAS^{V12} genetically transformed cells. Sensitive cells required BUBR1 to align chromosomes at the spindle equator and suppress lethal chromosome segregation defects. We found the BUBR1 GLEBS

domain was required for this cancer-specific activity suggesting BUBR1 must localize to kinetochores to prevent lethal defects. Moreover, the cells that required BUBR1 for chromosome alignment exhibited weaker kinetochore-MT attachment, as detected by measuring IKDs, suggesting an oncogene-induced fundamental alteration to kinetochore signaling (chapter 2) (58).

Here we demonstrate that oncogenic activation of the RAS/MAPK pathway enzymatically destabilizes the physical interaction of kinetochores with microtubules, while simultaneously stabilizing microtubule dynamics. We identify the former as a truly selective therapeutic target, while the latter contributes to the chromosome segregation defects and aneuploidy observed in many cancers.

3.2 Results

Generation and characterization of a cellular transformation system

Our previous work demonstrated that kinetochore function is fundamentally altered in both a subset of glioblastoma patient isolates and experimentally RAS-transformed cells. Upon RAS transformation cells were no longer able to align their chromosomes in the absence of mitotic pseudokinase BUBR1 (58). Moreover, we found that this requirement for BUBR1 correlated to a decreased metaphase IKD. IKD is an indirect measure of forces generated by kinetochore-MT attachments, where a shorter IKD is generally indicative of a weaker attachment. To understand how RAS signaling alters kinetochore function and to characterize the molecular mechanism by which BUBR1 becomes

essential for chromosome alignment in RAS transformed cells, we generated a cellular transformation model (Figure 3.1A).

Through retroviral transduction multiple tumor suppressor pathways were inactivated in a primary retinal pigment epithelial cell line, ARPE19, as previously described (93,94).

This intermediate cell line, termed ARPE19-T53D4, was then complemented with one of three oncogenic mutations: RAS^{V12} (95,96), MEK^{DD} (97), or AKT^{myr} (98) (Figure 3.1A).

These oncogenes were chosen because RAS transformation was shown previously to be sufficient to induce the kinetochore defects of interest, while MEK and AKT transformed cells each represented a signaling pathway downstream of RAS (58).

Using these cell lines we analyzed the contributions of the MAP Kinase (MAPK) and PI3 Kinase (PI3K) pathways respectively to RAS-mediated effects. Through RT-PCR we observed expression the transgenes used to inhibit tumor suppressor pathways in all cell lines (Figure 3.1B). The oncogenic activities of the MAPK and PI3K pathways were assessed through immunoblotting with phosphospecific antibodies for ERK and CREB respectively. ERK phosphorylation is increased in MEK and RAS transformed cell lines alone, as it is unique to the MAPK pathway (Figure 3.1D,E). CREB is phosphorylated in a MAPK and PI3K dependent manner and thus is increased in all transformed cell lines (Figure 3.1D,F).

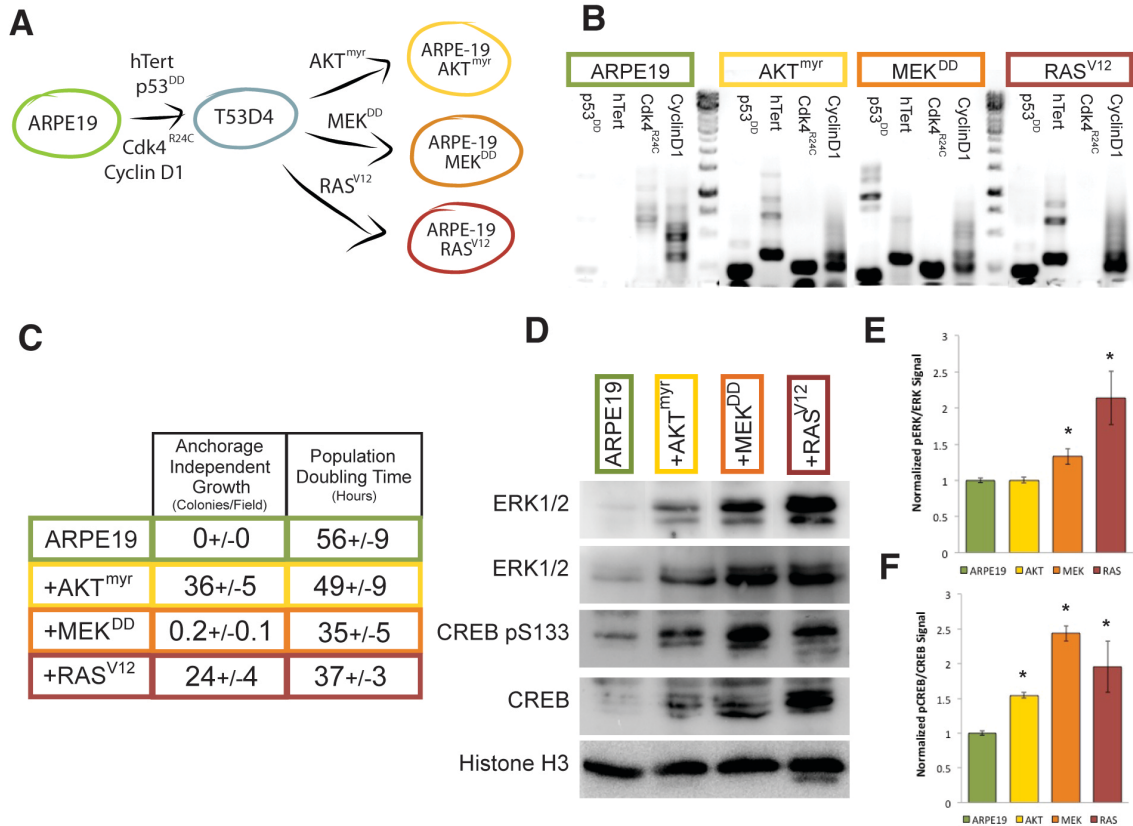


Figure 3.1. Verifying phenotype and genotype of genetically transformed cells.

(A) Transformation scheme used to generate model system; four genetic changes inactivate tumor suppressor pathways in primary retinal pigment epithelial cell line ARPE19, which is then complemented with one of three unique oncogenes. (B) RT-PCR analysis demonstrating expression of non-endogenous alleles, which inhibit tumor suppressor pathways. (C) All genetically transformed cells exhibit characteristics observed in tumor derived cell lines, including decreased doubling time and anchorage independent growth. (D) Western blot analysis of phosphorylation targets downstream of AKT and MEK oncogenes. Activation of the PI3K pathway is quantified (E) as relative CREB phosphorylation and activation of the MAPK pathway is quantified (F) as relative ERK phosphorylation both normalized to histone H3. (N=2; error bars SEM; *, $p < 0.01$ students t test)

To phenotypically analyze the transformation state of these cell lines in culture we measured their population doubling time and ability to grow independent of anchorage. In all instances the transgenic cell lines had an increased doubling time, which is common in many cancer cell lines. Whereas RAS and AKT transformed cell lines grew robustly in an anchorage independent manner, MEK transformed cells performed weakly in this assay (Figure 3.1C). This result suggests that despite the elevated MAPK signaling, these cells may be incompletely transformed.

With this system we first determined which cells demonstrated the kinetochore defects previously observed in glioblastoma patient isolates. To determine the ability of these cell lines to align chromosomes independent of BUBR1, cells were depleted of BUBR1 and arrested in MG132 to prevent premature anaphase onset due to BUBR1's role in activating the spindle assembly checkpoint. As previously determined, RAS transformed cells could not align chromosomes in the absence of BUBR1. Importantly, AKT transformed cells could still align chromosomes in the absence of BUBR1, but there was a significant decline in the ability of MEK transformed cells to do so (Figure 3.2A,B). This result suggests that oncogenic MAPK signaling, and not transformation *per se* is responsible for altering kinetochore function. This idea is further reinforced by the fact that MEK expressing cells demonstrated weak transformation behavior when assayed by anchorage independent growth (Figure 3.1C).

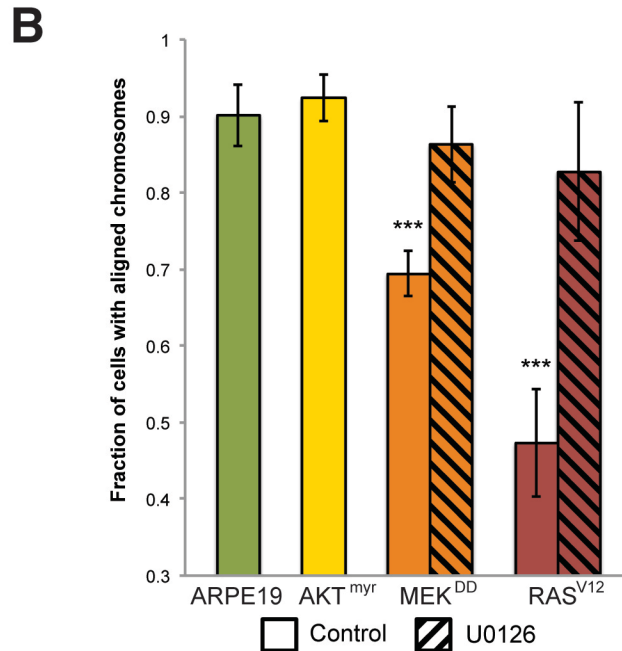
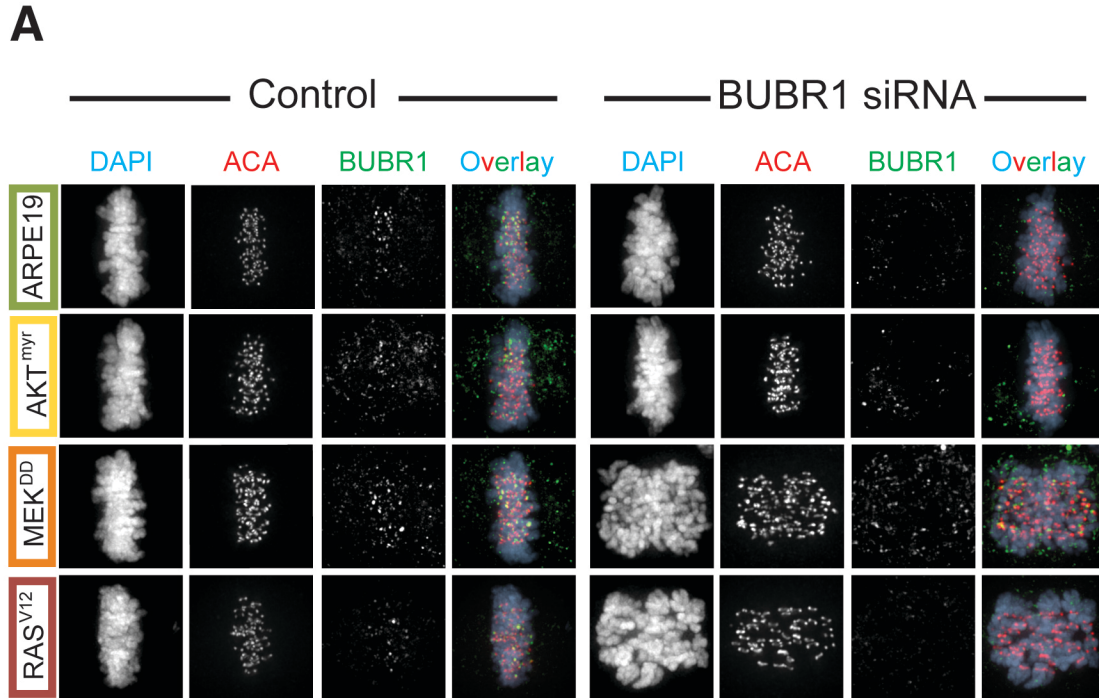


Figure 3.2. Oncogenic RAS/MAPK signaling induces the requirement for BUBR1 in forming kinetochore-microtubule attachments observed in glioblastoma stem cells.

(A) Representative images of cells expressing oncogenic MEK or RAS which have decreased ability to align chromosomes after depletion of BUBR1, which is rescued by inhibiting MAPK signaling with MEK inhibitor U0126. Oncogene induced requirement for BUBR1 in chromosome alignment first observed in figure 2.4 (B) Quantification of chromosome alignment within BUBR1 depleted populations.

(N=3; >100 cells/experiment; error bars are SD; ***, p<0.001 students t test).

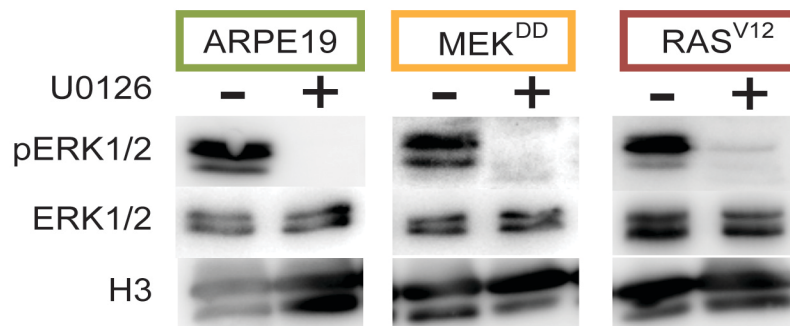


Figure 3.3. Chemical inhibition of MEK with U0126 abolishes MAPK signaling downstream. (A) Selective MEK inhibitor, U0126, robustly prevents phosphorylation of ERK at 10 μ M final concentration. Images for each blot were adjusted independently.

The MAPK pathway is composed of multiple kinases that ultimately alter nuclear transcription factors. To investigate if enzymatic activity or altered transcription activity caused kinetochore defects, we treated RAS and MEK transformed cells with the selective MEK inhibitor U0126 (Figure 3.3) (99). Treatment for one hour restored the ability of both RAS and MEK transformed cells to align chromosomes after BUBR1 depletion, suggesting that direct enzymatic activity, rather than a change to the transcriptional profile, was contributing to kinetochore regulation (Figures 3.2B, 3.5).

Consistent with previous findings, the RAS and MEK transformed cells, which are BUBR1 sensitive, also exhibited a decreased metaphase IKD ($\sim 1.11 \mu\text{m}$), whereas IKDs in AKT transformed cells maintained an IKD similar to non-transformed ARPE19 ($1.22 \mu\text{m}$). Again, a single hour treatment with a MEK or ERK inhibitor, U0126 and pp6p respectively, restored the IKDs in RAS and MEK transformed cells to those of non-transformed cells (Figure 3.4A,B). Having identified the MAPK pathway as the downstream effector of oncogenic RAS, we inhibited this pathway in mutationally diverse glioblastoma patient isolates and measured IKDs. In these tissue-specific cancer models we observed the same behavior as in our model system. Non-transformed neural stem cells (CB660) and BUBR1 insensitive glioblastoma patient isolates (1502, 0827) exhibited IKDs similar to ARPE19 and AKT transformed cells (Figure 3.5). Patient samples G166, 131, and G179 all had decreased IKDs, which were restored after MAPK inhibition with U0126 (Figure 3.5). Thus our simplified transformation system successfully models kinetochore deregulation observed in complex patient derived glioblastoma samples.

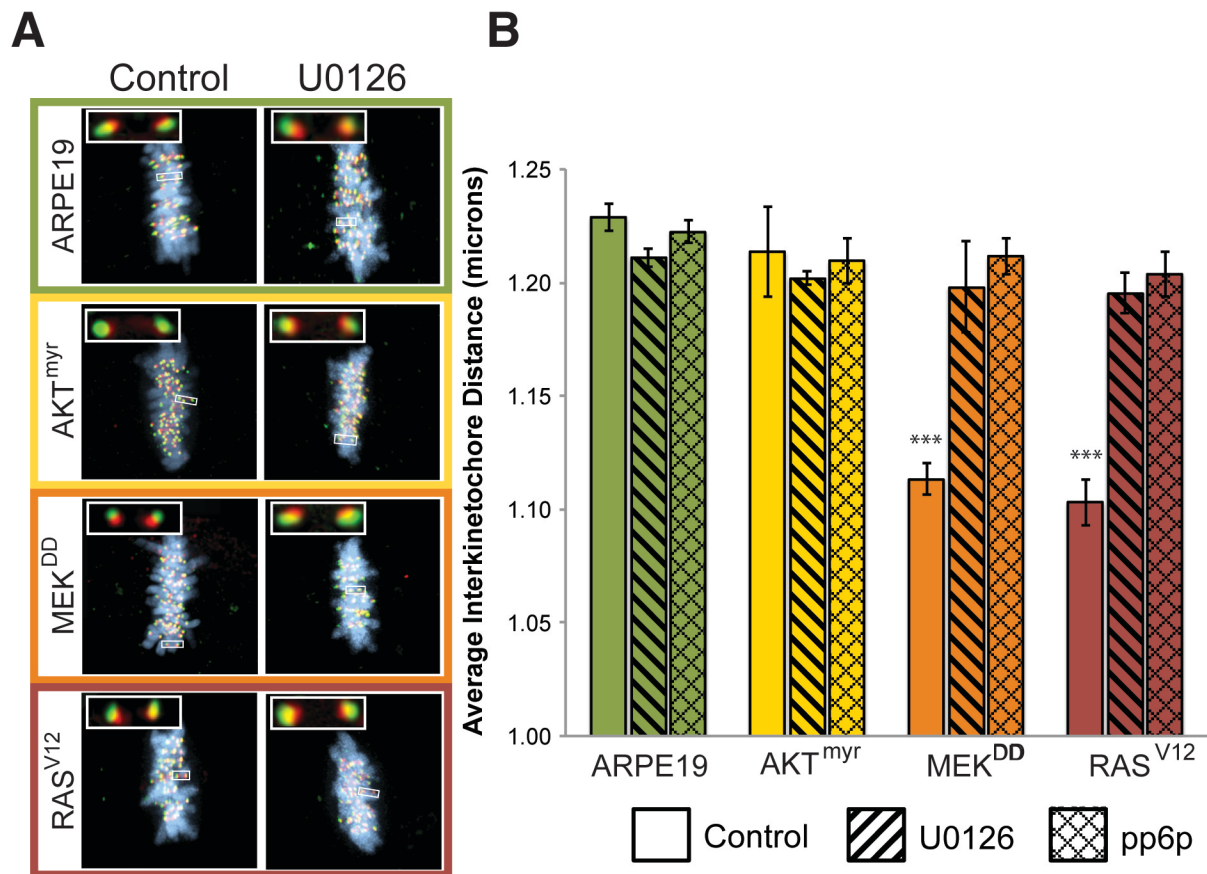


Figure 3.4. Oncogenic RAS/MAPK signaling alters kinetochores causing decreased metaphase interkinetochore distances observed in glioblastoma stem cells.

(A) Representative images of metaphase cells under unique oncogenic pressures with a single kinetochore pair inset. Left are control cells and right are cells treated with MEK inhibitor, U0126. Decreased IKD in GSCs first observed in figure 2.5 (B) Quantification of average IKD showing MEK and RAS transformed cells have decreased IKDs which are rescued through two chemical inhibitors of the MAPK pathways, MEK inhibitor U0126 and ERK inhibitor pp6p.

(N=3; >28 cells; >700 kinetochore pairs; error bars are SEM; ***, p<0.001 students t test)

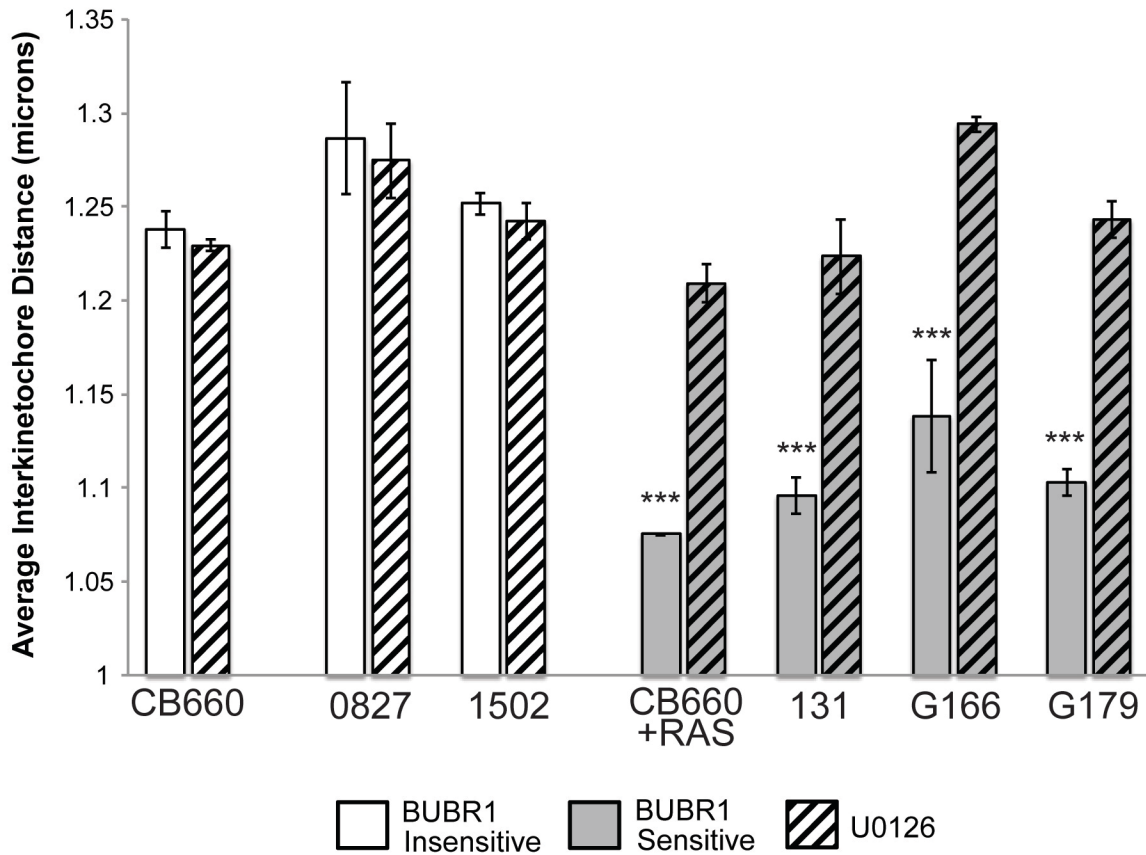


Figure 3.5. Inhibiting MAPK signaling in GSCs restores interkinetochore distances to non-transformed levels.

Inhibiting the MAPK pathway with MEK inhibitor U0126 in glioblastoma cells which were previously shown to be sensitive to BUBR1 depletion and have 'short' IKDs (Figure 2.5) restores average interkinetochore distances to non-transformed levels.

(N=2; >24 cells; >725 kinetochores; error bars are SEM; ***, students t test p<0.001)

BUBR1-mediated PP2A recruitment is specifically required by RAS/MAPK transformed cells for normal kinetochore function

Using cells with oncogenic RAS/MAPK signaling we could now ask why BUBR1 was additionally required for chromosome alignment. BUBR1 has long been known to counteract ABK activity at kinetochores, and recently was shown to accomplish this through direct recruitment of the phosphatase PP2A (Figure 1.3) (18,19,21–23). We hypothesized that BUBR1 was required for chromosome alignment in RAS/MAPK transformed cells because the balance between phosphatase and kinase activity at kinetochores had been altered. To assay this, we depleted RAS transformed cells of BUBR1, then expressed RNAi resistant BUBR1 mutants, and measured chromosome alignment in the presence of MG132 (Figure 3.6A-C). As expected, expressing wild type BUBR1 restored chromosome alignment in RAS transformed cells; however a phosphodeficient KARD-domain mutant that has previously been shown to be defective in PP2A kinetochore recruitment could not rescue chromosome alignment. To further verify that BUBR1-mediated recruitment of PP2A was the essential function of BUBR1 in RAS cells, a phosphomimetic KARD domain was fused to another kinetochore protein, MIS12, to constitutively target PP2A to kinetochores (21). This chimeric protein was able to rescue chromosome alignment in the absence of BUBR1 (Figure 3.6A-C). Importantly, these mutants all localize to kinetochores, though the MIS12 fusion concentrates at lower levels and also decorates the mitotic spindle – likely due to the low turnover of endogenous MIS12 (Figure 3.6B).

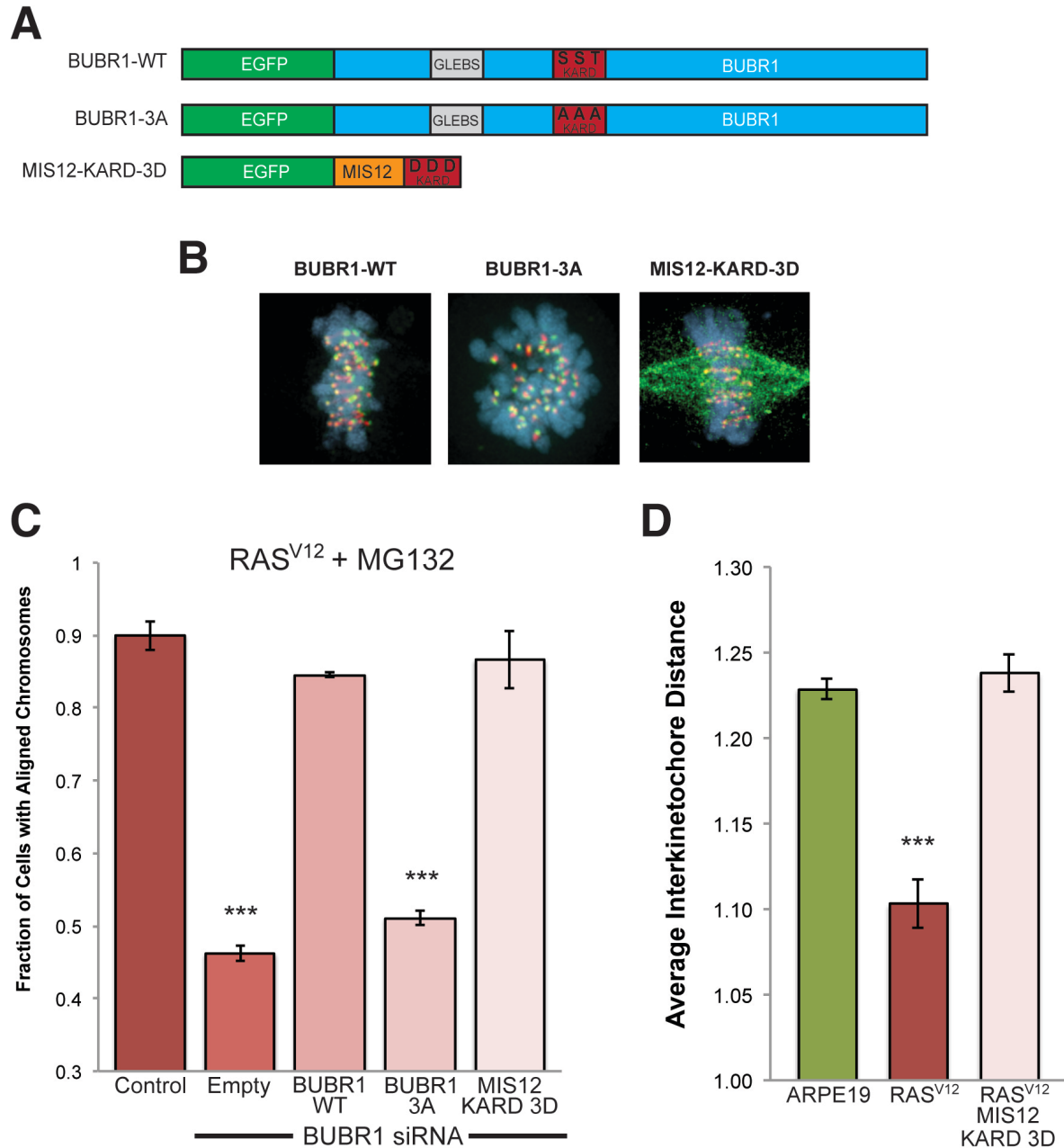


Figure 3.6. Cancer-specific activity of BUBR1 is to recruit the phosphatase PP2A to kinetochores.

(A) Schematic of RNAi resistant alleles used to rescue BUBR1 depleted cells: wild type BUBR1 (BUBR1-WT), phosphodeficient BUBR1 (BUBR1-3A), and a chimera of MIS12 and the BUBR1 KARD domain (MIS12-KARD-3D). (B) BUBR1-WT and BUBR1-3A localize to kinetochores, MIS12-KARD-3D localizes to both kinetochores and the mitotic spindle. (C) Only constructs which can recruit PP2A (BUBR1-WT and MIS12-KARD-3D) rescue chromosome alignment after BUBR1 depletion in RAS transformed cells. (N=3; >100 cells; error bars are SD; students t test *** p<0.001). (D) Expression of MIS12-KARD-3D fusion protein restores average IKD to non-transformed levels in RAS-transformed cells. (N=3; >35 cells; >1000 kinetochores; error bars are SEM; students t test *** p<0.001)

Consistent with previous observations, we found that the MIS12-KARD fusion was also sufficient to restore the decreased IKDs in RAS-transformed cells to the similar lengths as non-transformed cells, further demonstrating that the requirement for BUBR1 to align chromosomes and weaker kinetochore-MT attachments are the result of the same oncogenic pressure altering kinetochore function (Figure 3.6D).

Increased ERK activity in RAS/MAPK transformed cells hyperactivates ABK

Identifying PP2A recruitment as the essential BUBR1 function in RAS/MAPK transformed cells suggested that ABK activity may be altered in these cell lines, as PP2A is known to dephosphorylate ABK substrate KNL1 at the outer kinetochore (21). We measured ABK activity using phosphospecific antibodies against two outer kinetochore ABK substrates DSN1 and HEC1, as well as an antibody targeting an activating autophosphorylation site on ABK itself (15,100,101). By all three measures, ABK activity was increased upon oncogenic RAS/MAPK signaling and was restored to non-transformed levels after MEK inhibition with U0126 (Figure 3.7B). Importantly, the increase in ABK activity in RAS transformed cells was not the result of decreased BUBR1 kinetochore recruitment (Figure 3.8). Thus RAS/MAPK transformed cells additionally require BUBR1-mediated recruitment of PP2A in order to counteract elevated ABK activity and stabilize kinetochore-MT attachments. While these findings explain the observed BUBR1 sensitivity, they failed to identify the molecular mechanism by which RAS/MAPK signaling was enzymatically altering kinetochores.

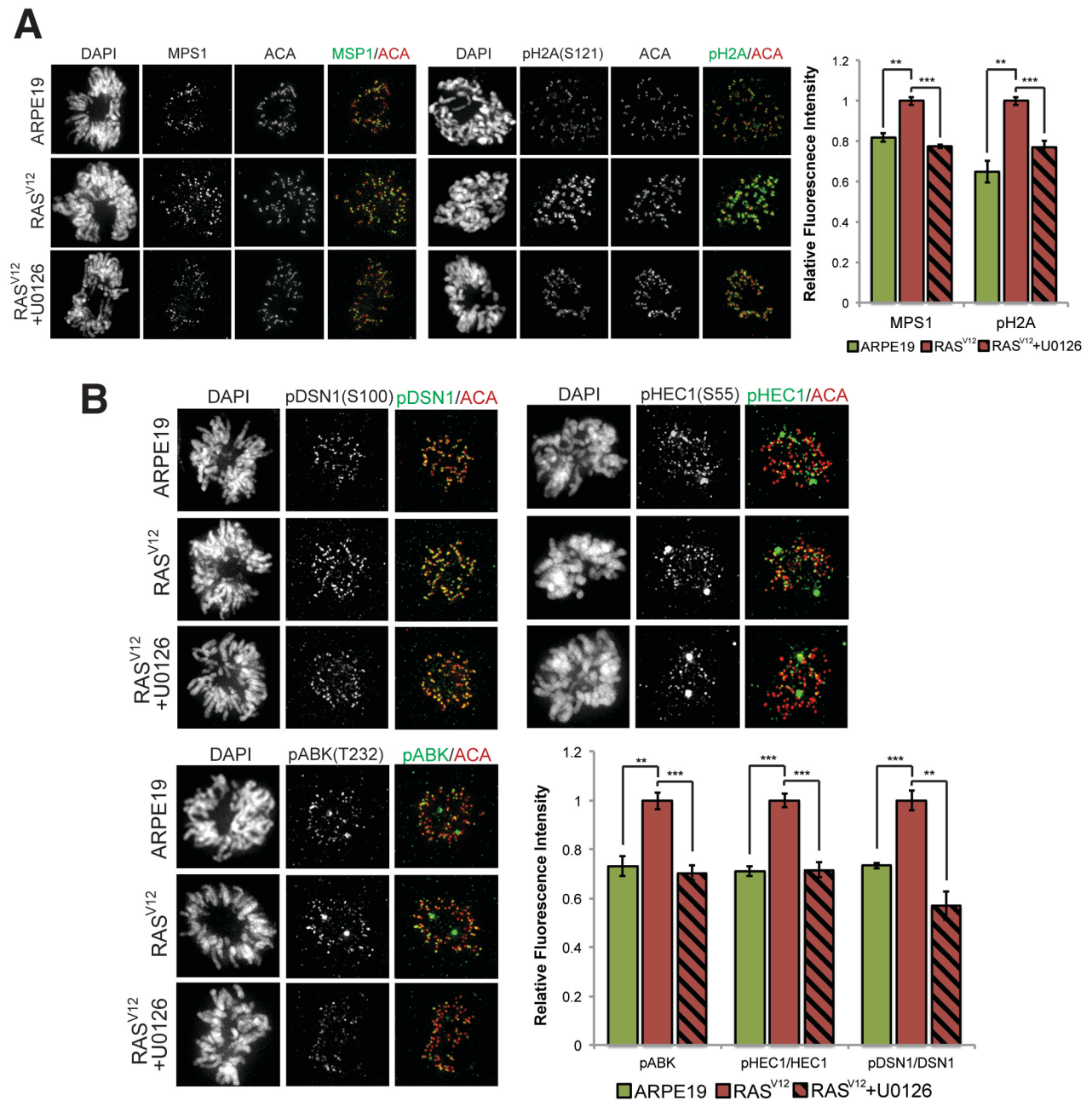


Figure 3.7. Oncogenic MAPK signaling stimulates ERK1/2 dependent activation of kinetochore kinases resulting in elevated ABK activity at kinetochores.

(A) As previously reported, increased signaling through MAPK pathway stimulates MPS1 kinetochore localization and BUB1 kinase activity, which are restored to non-transformed levels via MEK inhibition. (B) Increased MPS1 localization and BUB1 activity stimulate ABK phosphorylation at outer kinetochore substrates, particularly the key microtubule binding protein, HEC1. (N=3; >35 cells; 1800 kinetochores; error bars are SEM; students t test ** $p < 0.005$, *** $p < 0.001$)

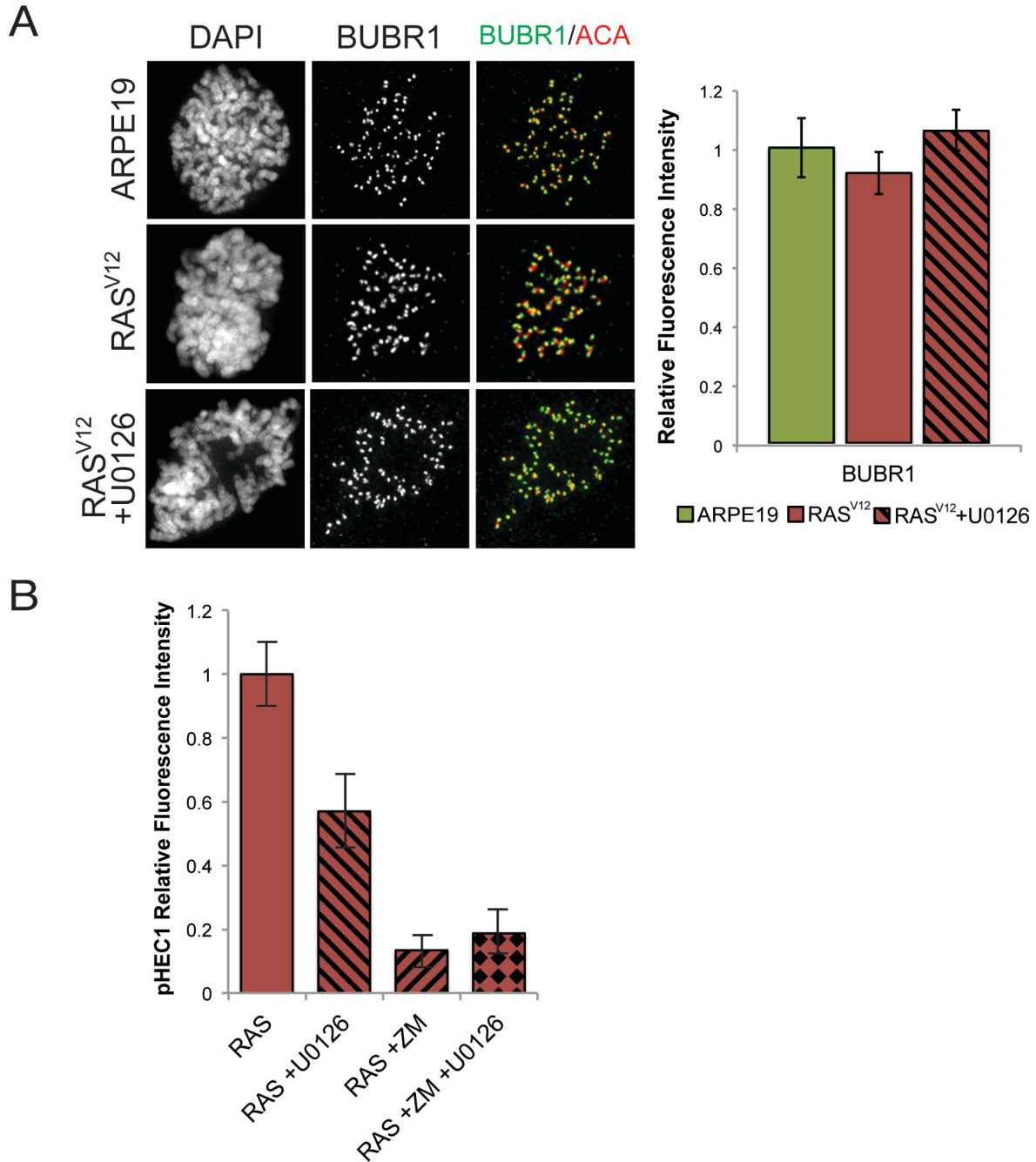


Figure 3.8. BUBR1 kinetochore levels are unchanged by transformation or U0126 treatment; MAPK-dependent HEC1 phosphorylation is likely indirect.

(A) No changes in BUBR1 kinetochore recruitment is detected using quantitative immunofluorescence (N=3; >36 cells; >1800 kinetochores; error bars are SEM)

(B) Phosphorylation of HEC1 Ser55 is reduced equally when either ABK alone, or ABK and MEK are chemically inhibited. This suggests MAPK proteins do not directly phosphorylate the HEC1 tail

(N=1; >12 cells; >400 kinetochores error bars are SD among cell averages).

Previous studies indicate that the terminal MAP kinase, ERK, affects kinetochore function in two manners: first, by phosphorylating and recruiting the mitotic kinase MPS1 to kinetochores, and second, by phosphorylating and activating another mitotic kinase BUB1 (102,103). Both MPS1 and BUB1 activities are known to contribute to ABK activation through multiple pathways (17,62,104,105). To test these activities in RAS-transformed cells we measured both MPS1 kinetochore localization and BUB1 activity (H2A phosphorylation) by quantitative immunofluorescence. We observed an increase in both measures upon RAS-transformation and similarly to ABK activity, these increases were restored to non-transformed levels by the MEK inhibitor, U0126 (Figure 3.7A). We also determined that members of the MAPK pathway likely do not directly phosphorylate HEC1, as chemically inhibiting both MEK and ABK did not reduce HEC1 phosphorylation beyond treating inhibiting ABK alone (Figure 3.8).

Increased ABK activity results in more labile kinetochore-microtubule attachments

The observed increase in ABK activity after RAS/MAPK transformation is a subtle change of 20-30%. To determine if this small change was sufficient to functionally alter normal mitotic processes we first measured the amount of time cells spent in mitosis. Early in mitosis ABK is essential for turning over erroneous kinetochore-MT attachments and ensuring they do not persist into metaphase and anaphase. Thus, increased ABK activity can prolong the time required to form stable kinetochore-MT attachments and congress chromosomes to the spindle equator.

On average, RAS and MEK transformed cells required more time to progress through mitosis, 15% to 10% respectively. The increased mitotic duration was again restored to non-transformed levels by chemically inhibiting the MAPK pathways with U0126 (Figure 3.9A).

An increase in mitotic duration could be the result of numerous perturbations. To further verify the role of ABK in this process we challenged RAS and MEK transformed cells by generating an increased numbers of erroneous kinetochore-MT attachments. Using the reversible Eg5 inhibitor STLC, we generated monopolar cells, which generate a large number of syntelic attachments. Upon STLC washout, release of these erroneous kinetochore-MT attachments is the rate-limiting step for spindle pole separation and chromosome biorientation (14). RAS and MEK transformed cells both bioriented chromosomes faster after STLC washout than non-transformed ARPE19 cells (Figure 3.9B). These results, together with those from IKD measurements and mitotic timing, indicate that kinetochore-MT attachments in RAS/MAPK transformed cells are more labile than in their non-transformed counterparts. This was further verified by testing the relative stability of kinetochore-bound microtubules against cold induced depolymerization. After 10 minutes in cold medium we observed that partially transformed ARPE19-T53D4 cells exhibited a minor decrease in cold stability of microtubule polymer (20%). Both RAS and MEK transformed cells exhibited a further decrease in cold stability (50%), which was rescued to the ARPE19-T53D4 levels by inhibiting the MAPK pathway with U0126 (Figure 3.10).

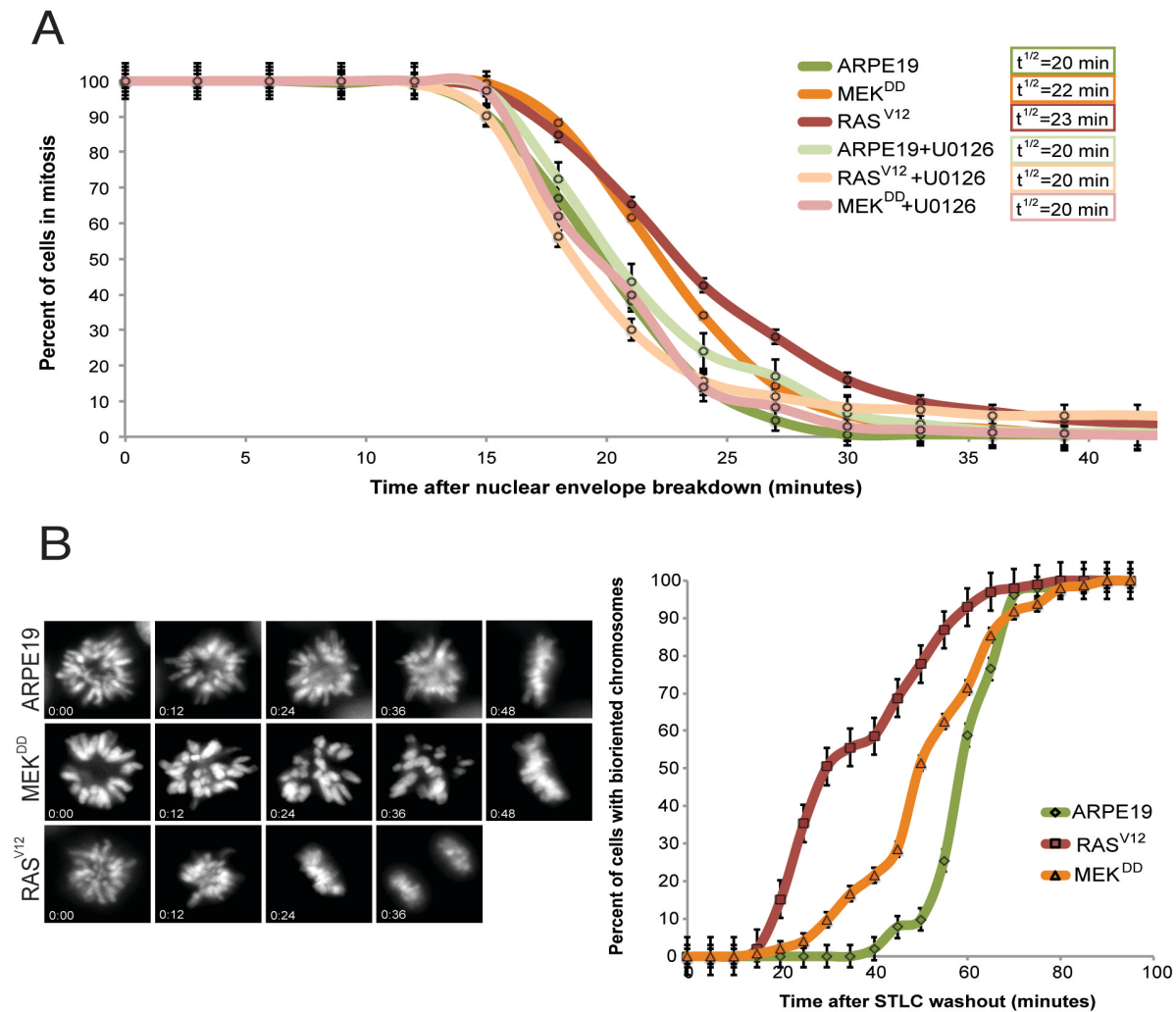


Figure 3.8. Cell with increased Aurora B kinase activity require more time to progress through mitosis and when experimentally challenged turnover kinetochore-microtubule attachments more readily.

(A) Oncogenic RAS/MAPK signaling results in a 10-15% increase in mitotic duration, which is rescued by inhibiting MEK (N=3; >200 cells; error bars are SD). (B) Cells with oncogenic RAS/MAPK signaling have increased Aurora B kinase functionality as they biorient their chromosomes after release of Eg5 inhibition more rapidly than non-transformed cells. Chromosome biorientation is only possible after Aurora B kinase mediated microtubule release from kinetochores and spindle pole separation. (N=3; >50 cells; error bars are SD).

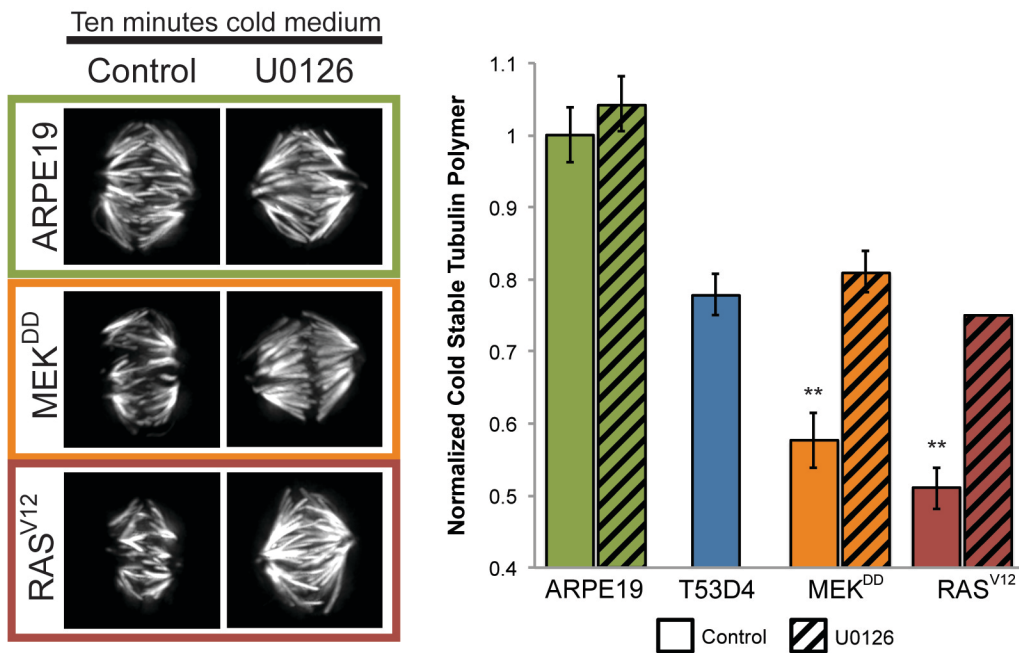


Figure 3.10. Cell with increased Aurora B kinase are more sensitive to cold induced microtubule depolymerization.

When challenged by cold temperatures k-fibers depolymerize more readily in cells with RAS/MAPK oncogenic activity. This is rescued by inhibition of the MAPK pathway, and likely represents a weaker kinetochore-microtubule interface. (N=3; >80 cells; error bars are SD; students t test ** p<0.005)

Thus four different assays demonstrate characteristic signs of weakened kinetochore-MT attachment upon RAS/MAPK transformation, due to increased ABK activity.

RAS/MAPK transformed cells have increased incidence of lagging chromosomes and merotelic attachments.

Increased ABK activity at outer kinetochores, and thereby turnover of erroneous kinetochore-MT attachments would presumably result in transformed cells with highly stable diploid genomes. However, upon RAS/MAPK transformation we observe a minor, but significant increase in the number of chromosome segregation errors such as lagging chromosomes and micronuclei (0.5% to 2.5%) (Figure 3.11A). As mentioned previously, lagging chromosomes often arise from merotelic kinetochore-MT attachments, thus we measured the incidence of merotelic attachments persisting into anaphase in these cells. Merotelic attachments are a common phenomenon, even in non-transformed cells; however, they are increased significantly upon RAS or MEK transformation (Figure 3.11B). Not only do more cells form merotelic attachments on average, but in addition, each individual cell generates more merotelic attachments. These results were surprising, and at first glance appear inconsistent with ABK hyperactivation. To fully characterize the interface between kinetochore and MTs, we needed to evaluate the stability of the MT polymer itself, not kinetochore-MT attachments.

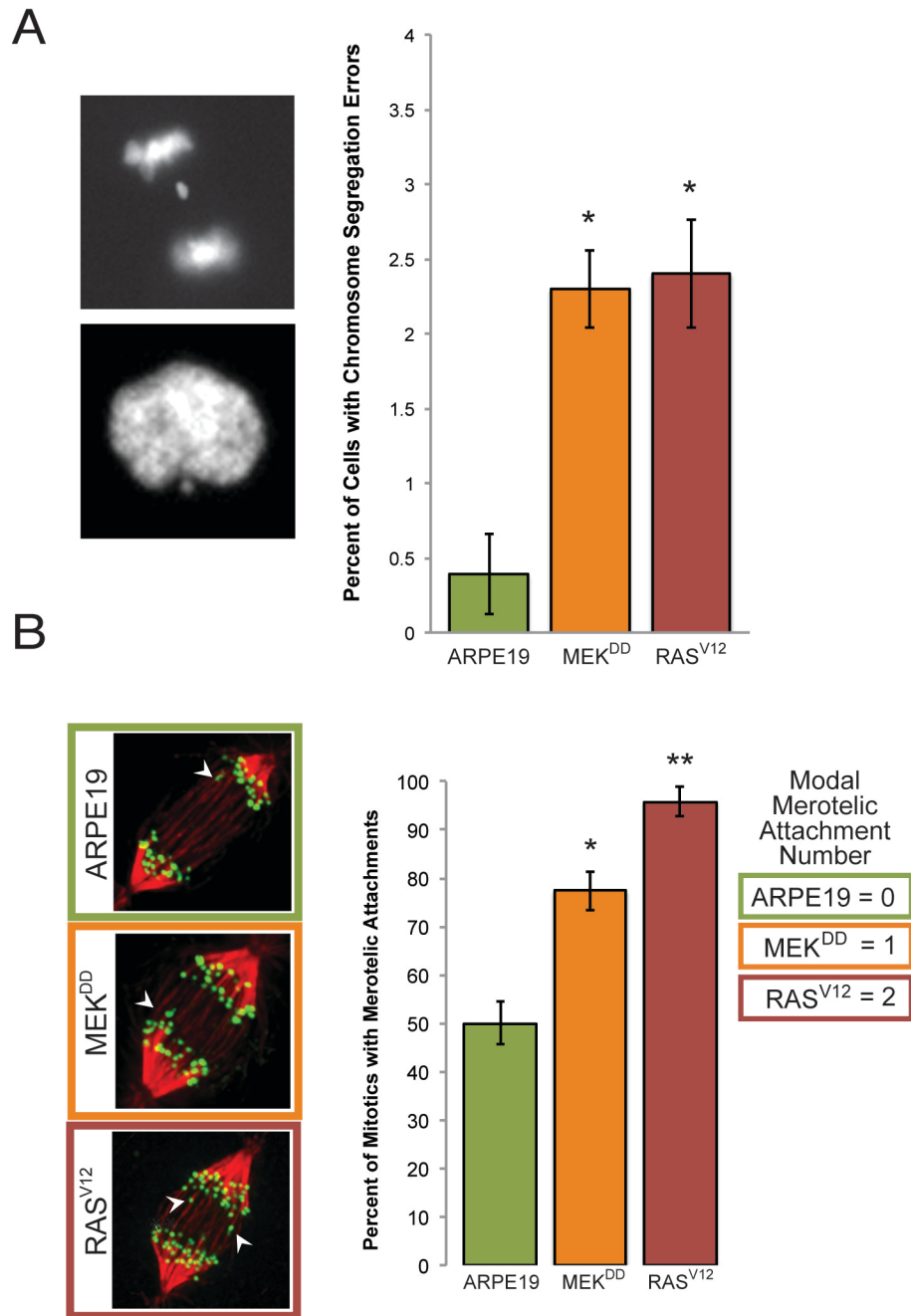


Figure 3.11. Oncogenic RAS/MAPK signaling increases the incidence of chromosome segregation defects, likely due to generation of merotelic kinetochore-microtubule attachments.

(A) Cells expressing oncogenic MEK or RAS genes have an increased incidence of chromosome segregation errors including lagging chromosomes and micronuclei. (N=3; >200 cells; error bars are SD; students t test * p<0.01). (B) MEK and RAS expressing cells have an increased incidence of forming merotelic kinetochore-microtubule attachments, and form more merotelic attachments per individual cell. (N=3; >42 cells; error bars are SD; students t test * p<0.01, ** p<0.005)

Kinetochores-bound microtubules have an increased lifetime and spend less time depolymerizing after RAS/MAPK transformation.

In previous studies kinetochores-bound microtubules were found to have longer half-lives in cancer cell lines as compared to non-transformed cells. This increased stability of the microtubule polymer was shown to contribute to the formation of merotelic attachments and chromosome segregation defects. (27,31)

To assess kinetochores-bound microtubule stability we first measured the fluorescence intensity of metaphase kinetochores-fibers. Results demonstrated that RAS or MEK transformation increased the size of microtubule bundles terminating at kinetochores (Figure 3.12A). Increased microtubule bundles are often seen in cells with merotelic attachments; however, a common way to build a larger kinetochores-fiber is by increasing the HEC1 affinity for MTs. Decreasing the phosphorylation state of the HEC1 tail increases its affinity for MTs, resulting in larger bundles presumably because binding reduces depolymerization events (14). As HEC1 phosphorylation is increased in RAS-transformed cells (Figure 3.7B), kinetochores-fibers must be stabilized through an alternative mechanism independent of physical attachment. Another means to stabilize MTs is through the inhibition of microtubule depolymerases. Upon attachment to kinetochores, MTs remain dynamic and forces from depolymerizing MT bundles cause kinetochores to oscillate about the spindle equator. If MT dynamics are perturbed this can be indirectly observed through imaging these movements in living cells. If the increased MT bundle intensities in RAS/MEK-transformed cells are the result of less dynamic microtubules we would predict longer, less frequent oscillations. Both MEK and RAS transformed cells have increased average oscillation amplitudes (0.71 +/- 0.11 μm)

when compared to non-transformed cells ($0.53 \pm 0.04 \mu\text{m}$) (Figure 3.12B). This phenotype is also observed when microtubule depolymerases such as KIF2B or KIF18A are depleted in human cells. Thus the dynamics of kinetochore-bound microtubules are consistent with a polymer that is less prone to depolymerization. To directly compare our results obtained with RAS transformed cells to previous studies of MT dynamics in cancer populations we next performed fluorescence decay after photoactivation experiments (27,31). In these experiments, we photoactivate a small portion tubulin within the metaphase spindle and measure the persistence of the kinetochore-bound microtubule population in transformed and non-transformed cells. Thus more stable microtubule bundles will have an increased fluorescence half-life. The loss of tubulin fluorescence from the metaphase spindle after photoactivation was measured independently from microtubule flux and fit to a double exponential decay curve. The average kinetochore-bound microtubule half-life in RAS-transformed cells was 1.4 fold longer than in non-transformed cells, further demonstrating the stable nature of kinetochore-fibers after this oncogenic pressure (Figure 3.12C).

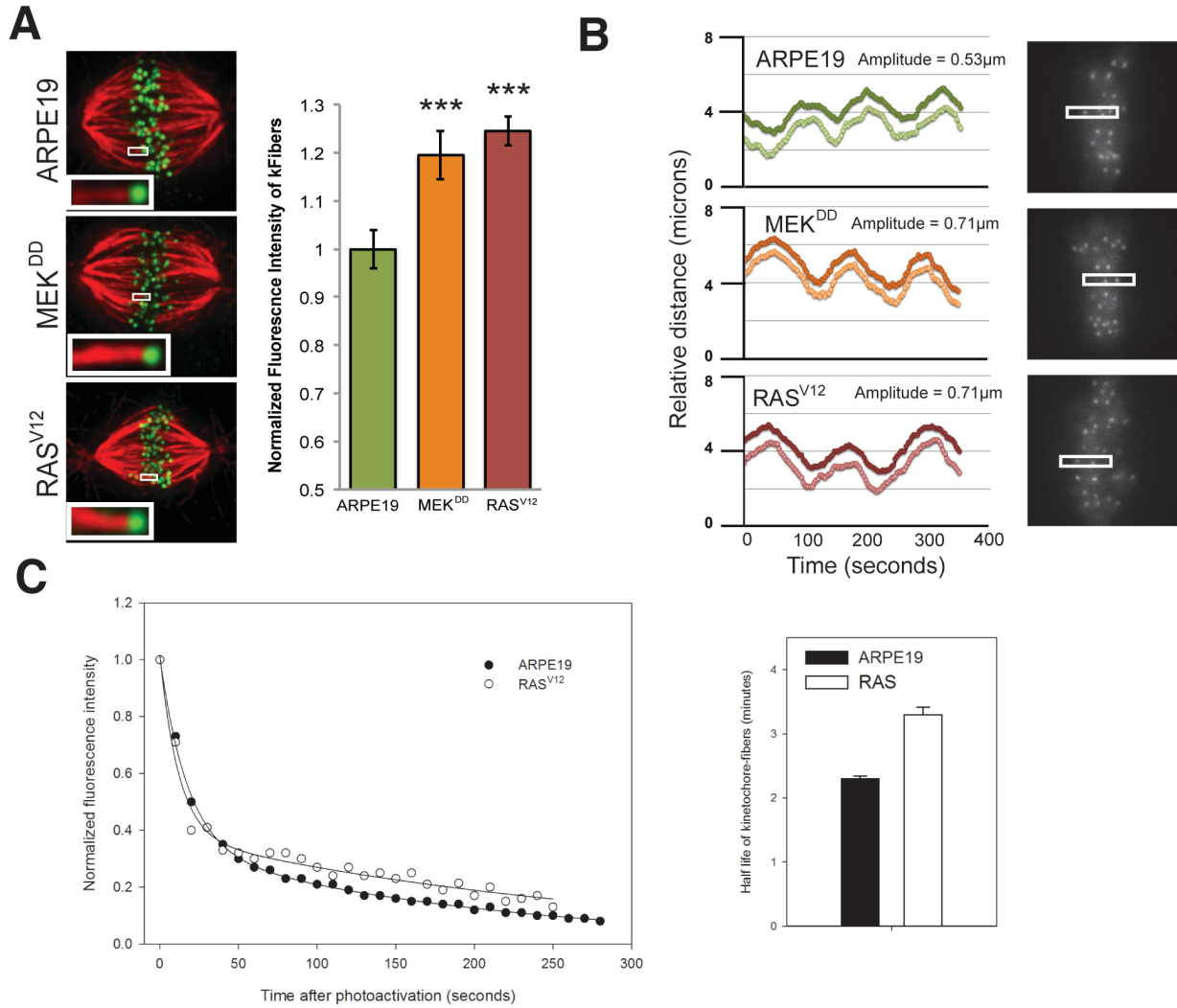


Figure 3.12. MT dynamics stabilize kinetochore-fibers independent of attachment status.

(A) Fluorescence intensity of kinetochore fibers is increased upon MEK/RAS transformation corresponding to a largest kinetochore fiber. (N=3; >35 cells; >1100 kinetochore-fibers; error bars SEM; students t test *** p<0.001). (B) The amplitude of metaphase oscillations is increased by MEK/RAS transformation consistent with a MT polymer that depolymerizes less often. Left, Single kinetochore pair traces over time; right, single time points for oscillatory mCherry-CENPA expressing cells (>5 cells; >20 kinetochore pairs; students t test p<0.01) (C) Kinetochore-fiber lifetime is increased in RAS transformed cells. Left, double exponential decay of photoactivated non-kinetochore and kinetochore-bound MTs; right, RAS transformed cells have a 1.4 fold increase in average half-life of kinetochore-bound microtubules. (>11 cells; >27 kinetochore-fibers; R²>0.99; error bars SEM).

Taken together these data illustrate a previously undocumented phenomenon. We observe that after oncogenic activation of the RAS/MAPK pathway kinetochore components have a decreased affinity for microtubule binding resulting in *decreased attachment stability*, yet depolymerization of kinetochore-bound microtubules is also suppressed resulting in *increased kinetochore-fiber stability* (Figure 3.13). While NDC80/HEC1 interactions with the microtubule lattice can stabilize MT polymer and lead to larger kinetochore bundles, MT dynamics are the rate-limiting step in loss of kinetochore fibers (13,14). Here we have described a situation where increased HEC1 phosphorylation increases the release of kinetochore-MT attachments, which based on our own in-vitro experiments, is likely due to an increased k_{off} for binding MTs. If no other perturbations were present in cells, this would result in weaker attachments and a smaller kinetochore-fiber; however, in RAS transformed cells there is a simultaneous alteration to MT dynamics. Independent of HEC1 binding, MTs in RAS-transformed cells favor the addition of tubulin polymer resulting in an increased occupancy at or near kinetochores. Thus HEC1 binding turns over more rapidly resulting in decreased attachment stability, yet decreased MT dynamics supersede stabilizing effects normally contributed by HEC1 binding and result in larger, more stable kinetochore-fibers. While attachment stability and kinetochore-fiber stability are closely related features of kinetochore-MT attachment, there is a growing body of evidence that they can also be altered separately as we have documented after RAS/MAPK transformation (106,107).

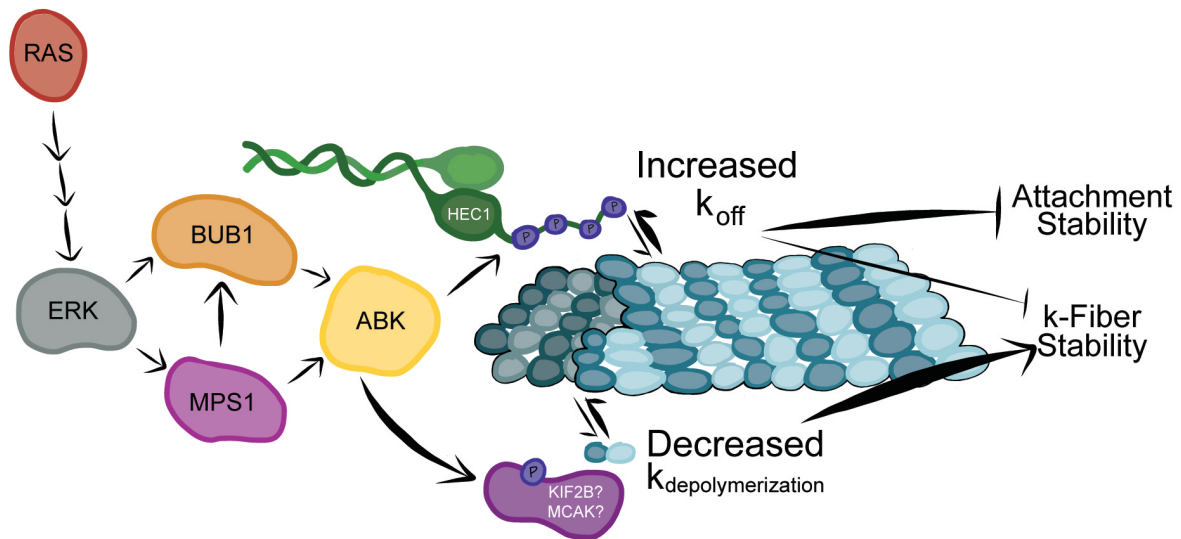


Figure 3.13. Model for RAS/MAPK signaling through ABK differentially affects kinetochore-MT attachment and k-fiber stability.

RAS activation of the MAPK cascade ultimately activates ABK. ABK activity inhibits both HEC1 MT binding and depolymerase MCAK. This results in less MT depolymerization despite a weaker attachment to kinetochores. This results in weakened attachment stability but an overall increase in the stability of k-fibers themselves. Weakened attachment stability drives the BUBR1 requirement and is an exciting therapeutic target as perturbing this interface creates lethal chromosome alignment defects specifically in cancer cells.

3.3 Discussion

Here we have demonstrated that a direct enzymatic cascade originating with oncogenic RAS/MAPK signaling fundamentally alters kinetochore regulation. This oncogenic pressure fundamentally alters kinetochore function and induces two correlated defects previously observed in GBM: (i) a cancer-specific requirement for BUBR1 to form kinetochore-MT attachments and align chromosomes at the metaphase plate, and (ii) a decreased average metaphase inter-kinetochore distance. Through molecular dissections we found that BUBR1's cancer-specific function is to recruit PP2A to transformed kinetochores. If this activity is compromised in any way (preventing BUBR1 from binding either PP2A or kinetochores) we observed lethal chromosome alignment defects in RAS/MAPK transformed cells demonstrating a cancer-specific therapeutic target (Figures 3.2 and 3.6C) (58). We also directly linked BUBR1 activity to decreased IKDs in RAS transformed cells by artificially recruiting PP2A to kinetochores and restoring non-transformed IKD lengths. This led us to verify that RAS/MAPK transformation hyperactivates ABK activity at kinetochores resulting in weak, labile kinetochore-MT attachments. Despite hyperactivation of the cell's "error correction machinery", RAS/MAPK transformed cells are characterized by increased levels of chromosome segregation errors, and an extremely high incidence of merotelic attachments persisting in anaphase. These increases in error rates likely arise from a stabilization of microtubule dynamics independent of physical attachment to kinetochores. Consistently, RAS/MAPK cells build larger kinetochore-fibers, have less dynamic metaphase oscillations, and an increased kinetochore-bound microtubule half-life.

The ABK dependent phosphorylation of HEC1 has been exhaustively demonstrated to affect kinetochore-MT binding affinity in a tunable fashion (13–15). Our results clearly indicate that in RAS/MAPK transformed cells ABK activity weakens kinetochore-MT interactions. While we also observe changes to microtubule dynamics, we have not directly tested the role of ABK activity specifically in microtubule stability independent of physical attachment. It is an intriguing, albeit, confusing hypothesis that ABK activity directly releases erroneous kinetochore-MT attachments, yet simultaneously inhibits depolymerase activity required to correct such an error. Uncovering the molecular mechanism for this altered microtubule stability is the next step in fully understanding how oncogenesis compromises mitotic processes. While we did not directly test any depolymerase activity, both KIF2B and KIF2C/MCAK are ideal candidates for such activity as they both contribute to error correction activities in human cells and MCAK is phosphoregulated by ABK in *Xenopus* extract and cells (27–29). In previous studies, overexpression of MCAK increased MT dynamics, which decreased the incidence of merotelic attachments and lagging chromosomes (27,31). Presumably the same behavior would be observed in cells with oncogenic RAS/MAPK signaling.

It is also possible that RAS/MAPK stimulation of ABK is a novel function in transformed cells, which is normally prevented or not present in non-transformed cells. Such a possibility is supported by the fact that MEK and ERK inhibition did not phenotypically affect non-transformed cells in any of our assays. Further characterizing the spatial and temporal activities of MEK and ERK during mitosis may further uncover their role in the

observed oncogenic alterations, as both potentially localize to mitotic structures (88,102,108).

These findings also stress the importance of understanding the function and limits of our experimental manipulations. It is clear that microtubule dynamics can be altered by physical interaction with kinetochores; however, these features of attachment can also be affected separately. Using our transformation model we measured the kinetochore-microtubule interface through most common techniques demonstrating that not all assays measure kinetochore-MT 'stability' equally.

The translational possibilities of this work are very exciting. Fully characterizing the molecular mechanism of the cancer-specific requirement of BUBR1 has yielded at least three unique targets for therapeutic intervention. Through our molecular dissections we now know that we can target three unique cellular processes: (i) BUBR1 kinetochore binding, (ii) BUBR1 physical interaction with PP2A, and (iii) phosphoregulation of BUBR1-PP2A interaction by PLK1 (21,58). Successful inhibition of these activities may yield a truly selective therapy. The hyperactivation of ABK in these cells serves as a figurative Achilles heel for certain cancers. It is important to note that indirectly inhibiting ABK by depleting BUGZ, a molecular chaperone of BUB3, also results in a cancer-specific mitotic viability defect (chapter 4) (109). Thus minor perturbations to either inhibit or activate ABK both take advantage of the kinetochore-MT interface as an important therapeutic target by inducing lethal chromosome alignment defects in cancer cells specifically.

Another success of this work has been to identify at least one oncogenic signaling event that induces these defects. Successful therapies must have a cancer-specific target, but they must also be prescribed to the right patients. The rescue of IKD length in our panel of GBM patient isolated cells suggests that despite their unique molecular signatures, these cells all amplify MAPK signaling in some fashion. Screening patients for MAPK activity or decreased IKDs may be key to ensuring a future therapy is effectively administered. Comparable therapeutic biomarkers are currently used for drugs targeting HER2 positive breast cancers (110) and BCR-ABL fusion in CML (111).

Finally, we must further understand how RAS/MAPK activity alters microtubule dynamics. An increased rate of aneuploidy is known to contribute to evolution and drug resistance in cancers (112,113). If these phenomena are in fact both a result of ABK activity, it may be important to destabilize microtubule dynamics while also targeting BUBR1 in order to prevent the evolution of a compensatory mechanism.

3.4 Methods

Cell Culture

ARPE19 (ATCC) and derivative cell lines were cultured in DMEM/F12 media (Life Technologies) and supplemented with 1X penicillin/streptomycin and 10% FBS at 37°C in 5% CO₂. Living cells were imaged in acid-washed, glass-bottom 35mm cell culture dishes, at 37°C in Leibovitz's L-15 media (Invitrogen) supplemented with 10% FBS, 7 mM HEPES, pH 7.0, and 4.5 g/L glucose.

Stable cell lines were negatively selected using either 1.0 mg/mL G418 (MediaTech) or 2 µg/mL puromycin (Calbiochem). For chromosome alignment assays cells were treated with 10 µM MG132 (Tocris) for 1 hour prior to fixation. To inhibit the MAPK pathway cells were treated with 10 µM U0126 (Calbiochem) or 1 µM pp6p (Santa Cruz Biotech; sc-222229), which selectively target MEK1/2 and ERK2 respectively, for 1 hour prior to fixation. Similarly, ABK inhibitor ZM447439 (Tocris) was used at 2 µM for 1 hour prior to fixation. STLC washouts were performed by arresting cell lines in 1 µM STLC (Tocris) for 2 hours, then washing 4 times with 5 mL of PBS, and imaging cells. Cold-induced depolymerization experiments were performed by incubating cells in ice cold medium for 10 minutes, then fixing with paraformaldehyde as described below. Taxol (Tocris) was used at 10 µM for photobleaching controls in photoactivation experiments.

Transient and Viral Transductions

To silence BUBR1 cells were transfected with siRNA (Quiagen) using Oligofectamine (Life Technologies) according to manufacturer instructions and fixed 48 hours later. For silence and rescue experiments, 800 ng of plasmids were concurrently transfected with siRNA. BUBR1 siRNA sequence: 5'-GAGAAUACCUAAUAUGUGATT-3'.

Retroviral particles were generated at previously described (114). Briefly, Phoenix packaging cells were transfected with pCMV-TAT and pCSIG to VSV-G psuedotype viruses in addition to a donor plasmid of choice described below. The combination of plasmids were transfected at a 3:1 volume to DNA mass ratio using Fugene 6 (Promega) transfection reagent. Growth medium was replaced 24 hours after

transfection. Viral particle-containing supernatant media were harvested 48 and 72 hours after transfection, centrifuged, aliquoted, and used or frozen at -80°C. To generate lentiviral particles the same method was used with minor substitutions. Rather than Phoenix, HEK-293T cells served as the host cell line, and were transfected with psPax2 and pMD2.G plasmids.

To perform viral infections, target cells were grown in 6 cm or 24-well cell culture dishes in viral particle-containing supernatant media for 24 hours. This was repeated with fresh viral containing-supernatant media for 24 more hours. 48 hours after initial infection cells were exposed to media containing a negative selective pressure. H2B-GFP expressing cells were isolated not through negative selection but rather GFP-positive cells were isolated using a MoFlo (Dako Colorado, Inc.) flow cytometer and high speed cell sorter equipped with a solid state iCyt 488 nm laser.

Plasmids

To inactivate tumor suppressor pathways in ARPE19 cells viral particles were generated using two dually encoding plasmids: pbabe-hTERT+p53DD (Addgene plasmid # 11128) and pbabe-cyclinD1+CDK4R24C (Addgene plasmid # 11129), which were gifts from Christopher Counter (93). After infection with these donor plasmids cells were infected with viral particles containing one of the following donor plasmids: pLXSN-H-Ras_V12 (Addgene plasmid # 39516), a gift from Julian Downward (115); 901-pLNCX-myr-HA-Akt, (Addgene plasmid # 9005) a gift from William Sellers (116); or pBabe-Puro-MEK-DD (Addgene plasmid # 15268) was a gift from William Hahn (117).

From these populations the cells were modified with the following fluorescent fusion proteins. PGK-H2BeGFP (Addgene plasmid # 21210) was a gift from Mark Mercola (118). To incorporate a red fluorescence fusion protein, mCherry was subcloned into the pBabe-Neo backbone. From a cDNA library, CENP-A was cloned at the c-terminus of this novel mCherry backbone. Alpha-tubulin was cloned into the backbone, pPAGFP-C1 (Addgene plasmid # 11910), a gift from Jennifer Lippincott-Schwartz (119). The PAGFP-alpha-tubulin fusion protein was then subcloned into the pBabe-Neo backbone.

BUBR1 was amplified from a cDNA library and cloned into pEGFP-C2 (Clontech). Silent mutations were introduced in the siRNA target sequence using site directed mutagenesis to create an RNAi resistant clone. From this construct we introduced three alanine mutations at Ser670, Ser676, and Thr680 to generate BUBR1-3A (21).

Immunoblotting

Cells were lysed in lysis buffer (50 mM TrisHCl, pH 7.4; 150 mM NaCl; 0.5% SDS; Complete proteases inhibitor cocktail (Roche). Samples were transferred to PVDF after SDS-PAGE and blocked in TBS + 3% BSA (Calbiochem). Western blotting was performed using the following antibodies diluted in TBS + 3% BSA: ERK1/2 at 1:1000 (Cell Signaling), pT202/204 ERK1/2 1:1000 (Genetex), CREB at 1:1000 (Cell Signaling), pS133 CREB at 1:1000 (Cell Signaling), H3 at 1:5000 (Abcam).

Immunofluorescence

Fixation and immunostaining of all cells were performed as described previously (15). In brief, cells were rinsed in 37°C PHEM buffer (60 mM Pipes, 25 mM Hepes, 10 mM EGTA, and 4 mM MgSO₄, pH 7.0), extracted in PHEM buffer + 0.5% Triton X-100 for 5 min, and then fixed in 2% paraformaldehyde for 20 min. To stain microtubule bundles cells were extracted in PHEM buffer + 0.5% Triton X-100 for 5 min then fixed with ice cold methanol at room temperature for 5 minutes and then -20°C for 20 minutes, followed by rehydration in PHEM buffer for 10 minutes. Immunostaining was performed using the following antibodies: anti-phosphorylated Ser55-HEC1 (pSer55 against antigen KPTSERKV(pS)LFGKR) was used at 1:1000; mouse anti-HEC1 9G3 at 1:2000 (GeneTex); rabbit anti-phosphorylated DSN1 (Ser100 against peptide SWRRA(pS)MKETN) at 1:1000; rabbit anti-DSN1 at 1:500 (GeneTex); human anti-centromere antibody at 1:500 (ACA; Antibodies, Inc.); mouse anti-tubulin at 1:300 (Sigma-Aldrich); rabbit anti-phosphorylated Aurora B (pThr232) at 1:2000 (Rockland); mouse anti-BUBR1 at 1:1000 (EMD Millipore); rabbit anti-phosphorylated histone H2A (Thr120) at 1:1000 (Active Motif); mouse anti-MPS1 at 1:1000 (EMD Millipore). Secondary antibodies conjugated to either Alexa 647, Alexa 488, or Rhodamine Red-X (Jackson ImmunoResearch Laboratories, Inc.) were used at 1:300.

Image acquisition and analysis

Images were acquired on a DeltaVision personal DV imaging system (Applied Precision) equipped with a CoolSNAP HQ² camera (Photometrics/Roper Scientific), and 60x/1.42 NA PlanApochromat objective (Olympus). Image collection and analysis were

performed with SoftWoRx acquisition software (Applied Precision). All fixed cell imaging was collected as Z-stacks at 0.2 μm intervals.

Inter-kinetochore distances were measured in SoftWoRx as the distance from HEC1 centroid to HEC1 centroid and averaged for every cell measured. Kinetochore intensities were also quantified using SoftWoRx, whereby the integrated fluorescence intensity minus the calculated background was determined for each kinetochore in non-transformed and manipulated samples and normalized to the average value obtained from non-transformed cells (120). To assay cold-induced depolymerization an equal number of Z-stacks were collected for all cell lines and then max projected. From these images the integrated intensity of the entire mitotic spindle was measured and then normalized to average result in non-transformed cells. Kinetochore bundle intensities were measured proximal to a kinetochore marker, within a single z-plane. Background intensities were also collected for each bundle and subtracted from the integrated intensities, then averaged for every cell.

All live cell experiments reporting mitotic duration used cell lines stably expressing H2B-EGFP and were imaged for 10-12 hours total at 3 minute intervals, using either a 60x/1.42 NA PlanApochromat objective or a 40x/0.75 NA UPlanFL objective (Olympus).

For kinetochore oscillations, cells were imaged with a 60x/1.42 NA PlanApochromat oil immersion objective (Olympus) every 3 seconds for 10 minutes. At each time-point, three images were collected in 1.5 μm z-stack. For all measurements, measured

kinetochores were located within the middle of the spindle. Kinetochore movements were tracked on maximum projection movies using the 'track points' function in Metamorph software. The oscillation amplitude, or deviation from average position, developed by Stumpff et al. (121) was determined using SigmaPlot software (Systat Software, Chicago, IL). To calculate the deviation from average position, time and distance data were exported into SigmaPlot, where a scatter plot (time on the x-axis, distance on the y-axis) was created. A linear regression line was then fit to the plot and the position on the regression line was subtracted from the corresponding original kinetochore position. This produced a distance value for each time-point, which represented the distance away from the average position of that kinetochore. These numbers were averaged to produce the final deviation from average position value.

To determine the half-life of kinetochore bound microtubules images were acquired on a Olympus IX81 Inverted Spinning Disk Microscope equipped with a phasor holographic photoactivation system (3i) and a cascade II EMCCD camera (Photometrics/Roper Scientific), and 100x/1.40 NA UPlanSApo oil immersion objective (Olympus). Image collection was performed using Slidebook software. Immediately following photoactivation with a 405 nm diode laser cells were imaged every 10 seconds for five minutes collecting three images separated by 1 μm each. The fluorescence decay after photobleaching was measured as previously described (12). Briefly, integrated pixel intensities within a region of interest were collected through the time course using Metamorph. These measurements were background subtracted by collecting the same measurements on the half spindle not activated. To correct for photobleaching effects

taxol stabilized spindles were activated and imaged under the same conditions. All measurements were normalized to their initial time point and averaged for each cell line. These data were fit with SigmaPlotX using a double exponential decay regression. The equation was $F(t) = A_1e^{-k_1t} + A_2e^{-k_2t}$, where $F(t)$ is the measured fluorescence and A_1 represents a non-kinetochore bound population of microtubules with the rapid decay rate k_1 , while A_2 represents the kinetochore bound microtubules with a decay rate k_2 .

CHAPTER 4

BUGZ IS REQUIRED FOR BUB3 STABILITY, BUB1 KINETOCHORE FUNCTION, AND CHROMOSOME ALIGNMENT⁴

4.1 Introduction

During mitosis, the spindle assembly checkpoint (SAC) monitors the attachment of kinetochores to the plus ends of spindle microtubules (MTs) and prevents anaphase onset until chromosomes are aligned and kinetochores are under proper tension (3,5). The SAC machinery contains multiple kinetochore proteins (i.e., BUB1, BUBR1, BUB3, MAD1, MAD2, and Mps1) that monitor MT attachment and regulate anaphase progression (3,5). The SAC proteins MAD2, BUBR1, and BUB3 comprise the soluble Mitotic Checkpoint Complex and prevent the activation of the ubiquitin ligase anaphase promoting complex/cyclosome (APC/C) by targeting APC/C's co-factor CDC20 (4). Following proper chromosome alignment and tension at the kinetochore, CDC20 inhibition is released to activate the APC/C, which begins the cascade of events that lead to anaphase (4).

⁴ This chapter was published in February 2014 under the same title.

C.M.T., P.J.P., J.G.D., and I conceived the content; P.J.P. and I co-wrote the original manuscript with input from C.M.T., J.M.O., and J.G.D. I contributed to experimental interpretation for all figures and contributed to experimental design, data collection, and analysis from figures 3-6.

Toledo CM, Herman JA, Olsen JB, Ding Y, Corrin P, Girard EJ, et al. BuGZ Is Required for Bub3 Stability, Bub1 Kinetochore Function, and Chromosome Alignment. *Dev Cell*. Elsevier Inc.; 2014;1–13.

In addition, BUB1, BUBR1, and BUB3 have been implicated in promoting chromosome alignment through regulation of Aurora B kinase (ABK) activity at kinetochores during chromosome congression (19,62,122). In prometaphase, BUB1 kinase phosphorylates threonine 120 of centromere-bound Histone 2A (pH2A-T120), which facilitates recruitment of ABK to the kinetochore (60,85,104). ABK, in turn, phosphorylates kinetochore-MT attachment proteins, which reduces their binding affinity for MTs and prevents the premature stabilization of kinetochore-MT attachments (12,15,100,123). In contrast to BUB1, BUBR1 activity opposes ABK dependent phosphorylation of kinetochore binding factors by recruiting PP2A phosphatase to the kinetochore (21–23). The interplay between these opposing activities regulates the formation of stable-end on kinetochore-MT attachments(19,21,22). BUB3 is required to recruit both BUB1 and BUBR1 to kinetochores (81,82), and BUB3 inhibition results in chromosome congression defects consistent with loss of BUB1 function at kinetochores (122).

BUB1 and BUBR1 both interact with BUB3 at the kinetochore through highly conserved GLEBS domains (82,85,124). These are short disordered regions of about 40 amino acids that form a series of salt bridges between the WD40 domains of BUB3 and two glutamate residues in the GLEBS domain (125). As a result of BUB3 binding, the GLEBS domain undergoes a conformational shift from a disordered to a well-ordered structure with fixed interaction points on the top face of BUB3's WD40 propeller (125). This interaction is critical for BUB3-dependent recruitment of BUB1 and BUBR1 to kinetochores (81,82,85). For example, a single amino-acid change in BUBR1's GLEBS

domain (E406K) is sufficient to prevent BUB3 interaction and BUBR1's kinetochore localization (81).

We have previously found that human Glioblastoma multiforme (GBM) brain tumors, the most common and lethal form of brain cancer, differentially require BUBR1's GLEBS domain to suppress lethal consequences of altered kinetochore function by promoting attachment of MTs to kinetochores (58). Removal of BUBR1 from kinetochores of GBM stem cells (GSCs) or transformed fibroblasts results in lethality due to a lack of kinetochore-MT attachments, while non-transformed cells are unaffected (58,77). Thus, GBM isolates appear to be more sensitive to perturbation of certain activities of SAC proteins than non-transformed cells. This added sensitivity in GSCs has led us to isolate a novel facilitator of BUB3 function, ZNF207, an uncharacterized C2-H2 zinc-finger domain gene (94,126). Since we implicate ZNF207 below as a key effector of BUB3 function, we rename the gene BUGZ (BUB3 interacting GLEBS domain-containing Zinc finger protein). Here, we report that the human BUGZ/ZNF207 gene encodes a novel GLEBS domain-containing and kinetochore binding protein that is required for BUB3 stability, BUB1 kinetochore function, and chromosome alignment.

4.2 Results

BUGZ was isolated from an RNAi screen targeting putative human transcription factors to identify key regulators of GSC's expansion and survival. As with our previous studies (58,94) we compared GSCs screen results with those from non-transformed human neural stem cells (NSCs), a candidate cell of origin for GBM, to identify GBM-specific

lethality hits (Figure 4.1). We found BUGZ shRNAs in this category. Thus, we set out to validate BUGZ as a candidate cancer lethal gene and then attempted to ascertain its cellular function.

Figures 4.1A-D show that, consistent with the screen data, BUGZ knockdown results in differential growth inhibition of GSCs when compared to proliferating human NSCs. Multiple shRNAs provided robust GSC-specific growth inhibition and penetrant knockdown in both GSCs and NSCs (Figure 4.3). Knockdown of KIF11/Eg5 was used as a positive proliferation control. Its inhibition blocks growth of cultured cells regardless of transformation status (Figure 4.1B,F) (58,94).

BUGZ knockdown also inhibited the growth of SSEA1+ GSC subpopulations, which are enriched for tumor initiating cell activity (Figure 4.1E) (127), and inhibited tumor sphere formation, a surrogate assay for stem cell self-renewal (Figure 4.3B) (39,40). However, BUGZ knockdown did not alter expression of SSEA1 or other progenitor markers, including SOX2 and NESTIN, or neural lineage markers, including GFAP and TUJ1 (data not shown). Moreover, BUGZ-knockdown-insensitive-NSCs could be converted to sensitive by genetic transformation with hTERT, dominant-negative p53^{DD}, CyclinD1, CDK4^{R24C}, H-RasV12, and MYC (Figure 4.1F) (93,94).

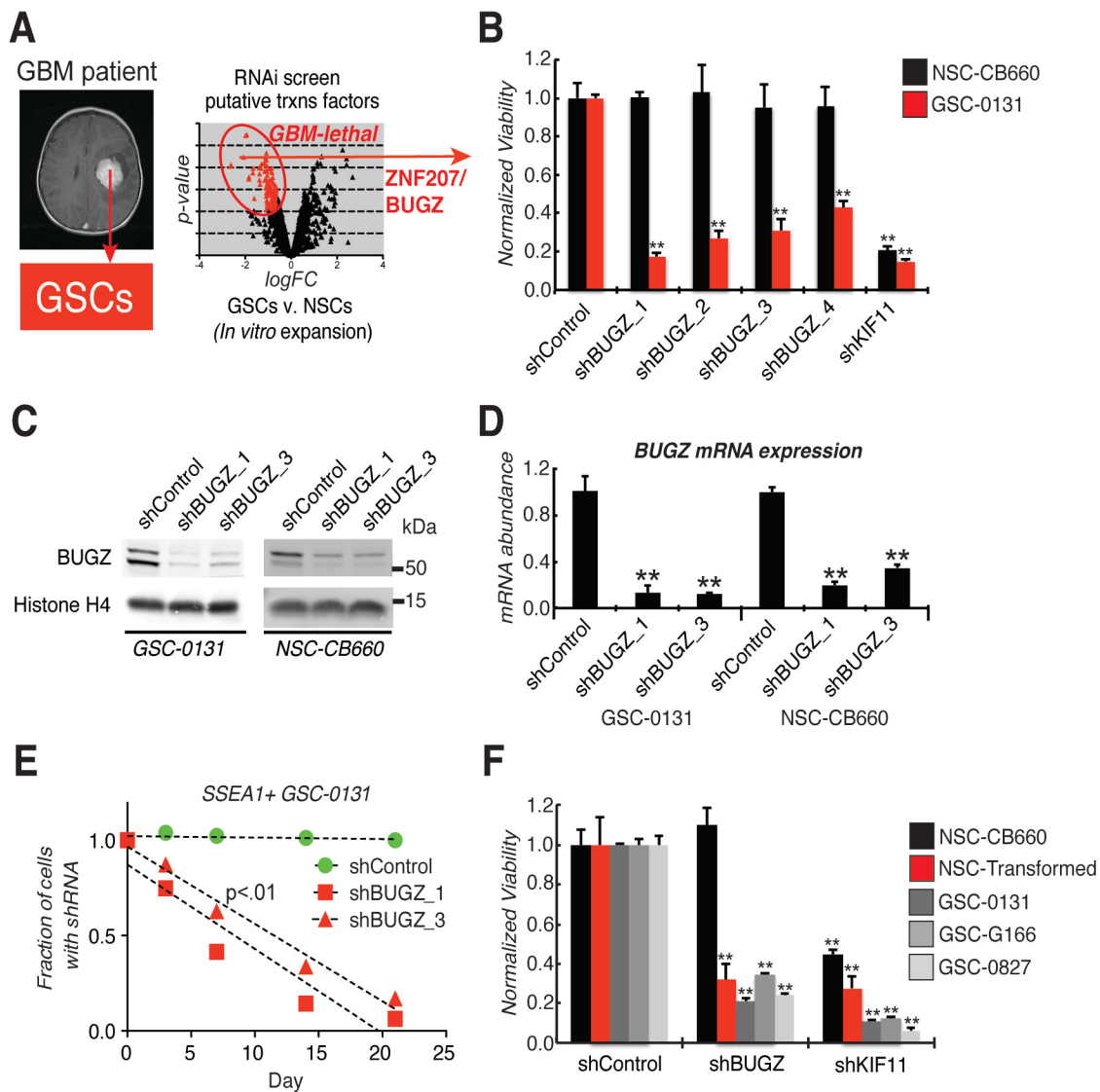


Figure 4.1. BUGZ is a candidate GBM-lethal gene.

(A) An RNAi screen of putative transcription factors revealed ZNF207/BUGZ as differentially required for GSC expansion as compared to NSCs. (B) BUGZ knockdown causes loss of viability in GSCs but not NSCs. Cells were infected with lentiviruses expressing BUGZ, KIF11 or control shRNAs, outgrown for 7 days, and assayed for growth. Knockdown of KIF11 was used as a positive control for both RNAi knockdown and cell proliferation. (C and D) Western blot analysis and quantitative real time PCR (qRT-PCR) for BUGZ protein and mRNA expression, respectively, of whole cell extracts from GSC-0131 and NSC-CB660 following shRNA knockdown. (E) BUGZ knockdown compromises growth of SSEA1+ GSC subpopulations. Flow cytometry analysis of SSEA1+ GSC-0131 cells infected with shBUGZ-GFP+ or shControl-GFP+ mixed with untreated cells during in vitro outgrowth in self-renewing conditions. (F) BUGZ knockdown compromises growth of transformed NSCs and multiple GSC isolates, but not NSCs (assay same as (B)).

Other GSC patient isolates also showed sensitivity to BUGZ knockdown, demonstrating that the effect is not patient-specific (Figure 4.1F). Finally, we performed an *in vivo* competition experiment to directly test the effects of BUGZ suppression in an orthotopic xenograft model of GBM by mixing GSCs containing GFP-expressing shBUGZ or shControl with non-shRNA control GSCs at an approximate 9:1 ratio respectively (94). Following 17 days post injection, non-shRNA control GSCs drastically outcompeted shBUGZ GSCs, while shControl GSCs comprised the bulk tumor mass (Figures 4.2 and 4.3C). Thus, BUGZ expression is required for GBM tumor formation *in vivo*. Taken together, these results suggest that GSCs have a differential requirement for BUGZ, which is likely driven by oncogenic activity.

To gain insight into the molecular function of BUGZ, we next performed affinity purification mass spectrometry to identify candidate protein binding partners. This analysis revealed BUB3 as the top-scoring hit (Figure 4.4A). We confirmed this interaction in reciprocal co-immunoprecipitation experiments. BUGZ was able to pull down BUB3 and vice versa in GSCs (Figure 4.4B) and 293T cells (Figure 4.5), demonstrating the proteins interact in cells.

Since SAC signaling is an essential and highly conserved process, we performed phylogenetic analysis to identify BUGZ orthologs and examine available data on their function in model genetic systems. BUGZ shows strong conservation among eukaryotes with the exception of budding and fission yeast, where no orthologs could be identified (Figure 4.4C) (128).

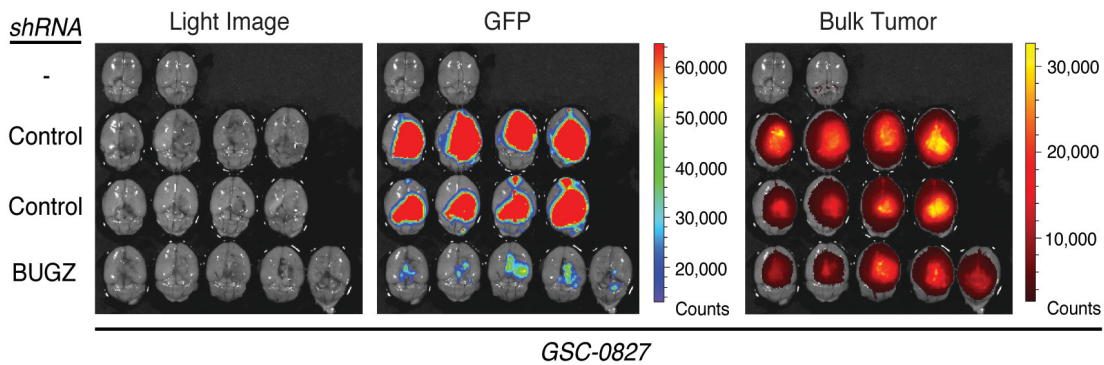


Figure 4.2. Suppression of BUGZ expression compromises GBM tumor formation in vivo.

Images of in vivo competition mouse brains 17 days post orthotopic xenograft of GSC-0827 cells expressing GFP-shControl or GFP-shBUGZ mixed with non-shRNA GSC-0827 cells. Left, light images of brains. Middle, GFP+ fluorescence marking shRNA-containing cells. Right, fluorescent signal from Tumor paint (Chlorotoxin: indocyanine green) to identify total tumor mass. First mouse brain of top row did not receive GSC-0827 cells or Tumor Paint, while the second mouse brain of top row did not receive GSC-0827 cells but received Tumor paint. Quantification of GFP fluorescence is shown in Figure 4.3 **Student t test, $p < 0.01$.

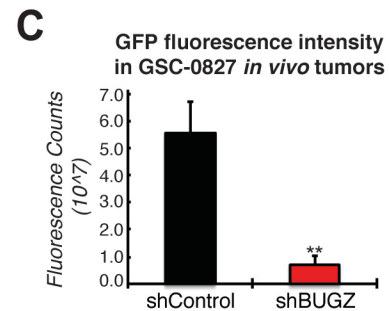
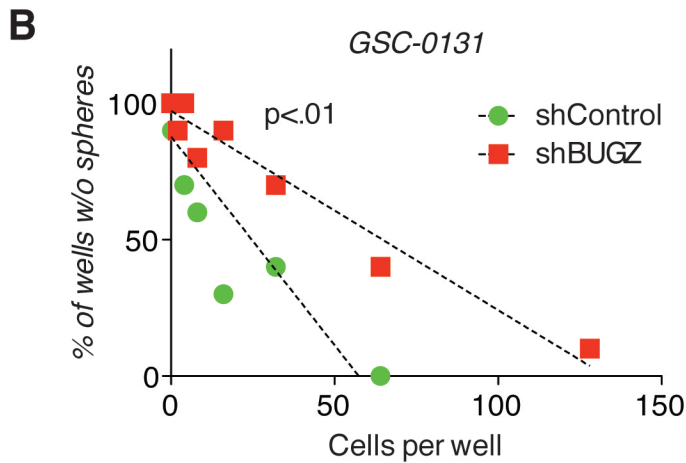
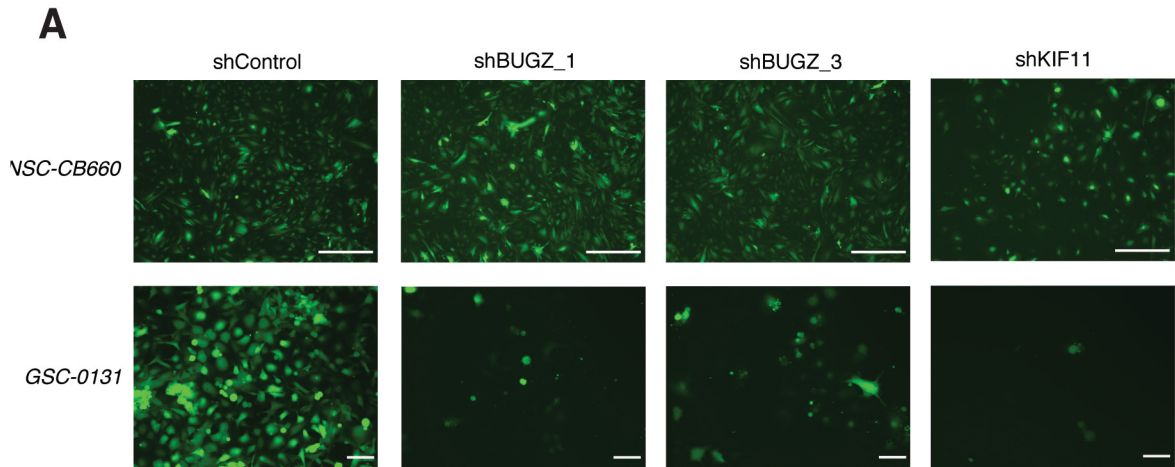


Figure 4.3. BUGZ knockdown differentially inhibits growth of GSCs in monolayer culture, in a tumor sphere formation assay, and in vivo mouse orthotopic xenograft competition experiment. (A) Images of NSC-CB660 and GSC-0131 isolates' viability after 7 days of infection with shControl or two independent shRNA clones targeting BUGZ. Visualization of the cells using pGIPZ-shRNA-green fluorescent protein (GFP). An shRNA targeting KIF11 was used as a positive control for both RNAi pathways activity and cell proliferation. Bar (NSC-CB660) 500 μ m; Bar (GSC-0131) 100 μ m. (B) Limiting dilution sphere forming assay of GSC-0131 infected with two independent shRNA viral clones for in vitro tumor sphere formation and clonogenicity. (C) Quantification of GFP fluorescence from in vivo mouse brain orthotopic xenograft GSC-0827 competition experiment. GFP-shBUGZ expressing GSCs were unable to contribute to the formation of their tumors and yielded tumor masses dominated by non-shRNA GSCs with no detectable GFP expression. **, Student t test, unequal variance, 2 tails; $P < 0.01$.

This is in contrast to BUB3, which is highly conserved in all eukaryotes, including budding and fission yeast, where it was first identified (129). Additionally, examination of protein-protein interaction databases available for humans, worms, flies, and plants revealed additional evidence for BUGZ ortholog interaction with BUB3 from genome-scale yeast two-hybrid screens or mass spectrometry analysis (Table 4.1). However, other candidate proteins identified in our mass-spectrometry analysis were not found. This suggests that BUGZ-BUB3 interactions are highly conserved among higher eukaryotes.

We next examined whether BUGZ interacts with BUB3 through a GLEBS domain, similar to BUB1 and BUBR1. We observed that BUGZ orthologs also harbor a single conserved GLEBS domain motif (AA 344-376 for human), which contains the characteristic two glutamate residues found in all GLEBS domains (AA 358 and 359 for human BUGZ) (Figure 4.4D). Furthermore, mutational analysis of human BUGZ followed by immunoprecipitations revealed that BUGZ's GLEBS domain is required for interaction with BUB3, while its zinc finger domains are dispensable (Figure 4.4E,F). Thus, similar to BUB1 and BUBR1, BUGZ interacts with BUB3 through a GLEBS domain.

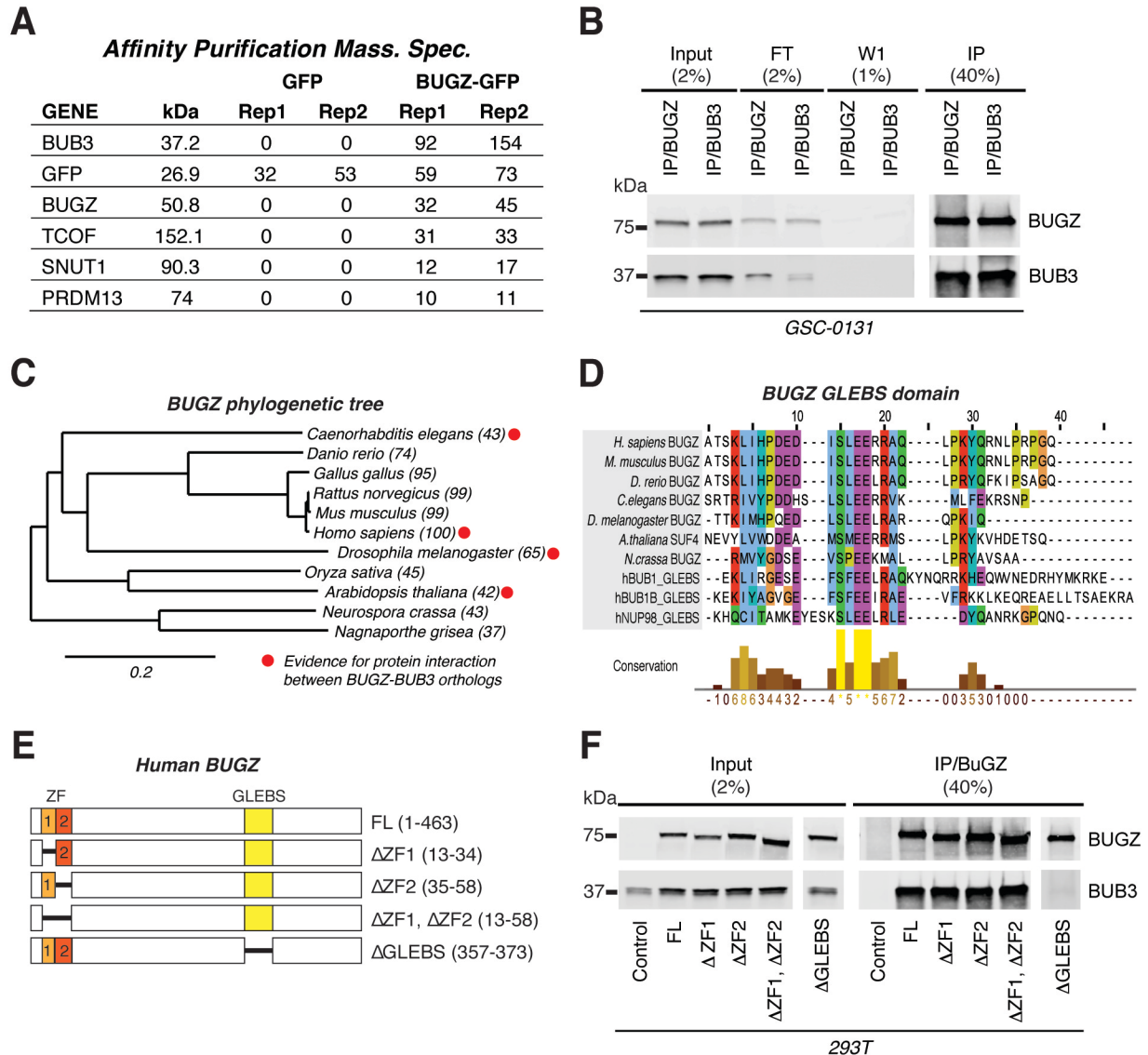


Figure 4.4. BUGZ binds to BUB3 through a highly conserved GLEBS domain.

(A) BUB3 was identified as the top candidate protein to interact with BUGZ by affinity purification mass spectrometry of 293T cells transfected with GFP-tagged ZNF207. GFP control was used to identify non-specific protein interactions. (B) BUGZ binds to BUB3 and vice versa. Western blot analysis with anti-turboGFP (BUGZ) and anti-BUB3 of immunoprecipitates with the turboGFP antibody (BUGZ) or V5 antibody (BUB3) from GSC-0131 cells infected with V5-BUB3 and turboGFP-BUGZ constructs. (C) Evolutionary distance between orthologs of BUGZ/ZNF207 sampled from major phyla. Percent protein identity to human BUGZ from pair-wise protein alignments is indicated in parentheses (NCBI, HomoloGene data base). (D) BUGZ orthologs contain a highly conserved GLEBS domain. GLEBS domains from hBUB1 (AA240-280), hBUBR1 (AA400-440), and hNUP98 (157-213) (Larsen et al., 2007; Wang et al., 2001) were used to create pair-wise alignments of indicated BUGZ orthologs using CLUSTW. (E) Human BUGZ alleles generated and used in these studies. (F) BUGZ binds to BUB3 through its GLEBS domain. Western blot analysis with anti-turboGFP and anti-BUB3 of immunoprecipitates with the turboGFP antibody (BUGZ) from 293T cells transfected with the mutant alleles in (E) or the control (V5-BUB3).

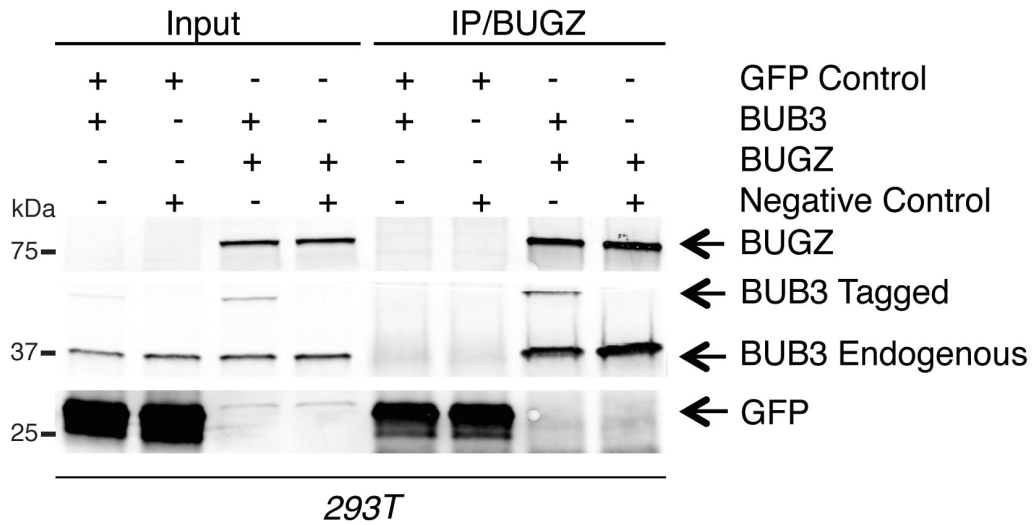


Figure 4.5. Co-immunoprecipitation of BUGZ and BUB3 in 293T cells.

Western blot analysis with anti-turboGFP (BUGZ) and anti-BUB3 of immunoprecipitates with the turboGFP antibody (BUGZ) from 293T cells infected with mCherry-BUB3 and turboGFP-BUGZ constructs. IP = immunoprecipitation.

Table 4.1. Evidence of BUGZ ortholog interaction with BUB3 from protein-protein interaction databases.

Multiple methods have detected the highly conserved BUGZ-BUB3 interaction. Y2H=Yeast-two-hybrid screen. MS=Mass spectrometry

BUGZ ortholog	Gene ID	Method	Reference
Homo Sapiens	7756	Co-fractionation, Y2H	(Havugimana et al., 2012; Hegele et al., 2012; Wang et al., 2011)
Drosophila melanogaster	35004	Y2B	(Giotet al., 2003)
Caenorhabditis elegans	178042	Y2H	(Li et al., 2004)
Arabidopsis thaliana	839984	Affinity capture-MS	(Van Leene et al., 2010)

To further explore the role of BUGZ-BUB3 binding, we evaluated the protein levels of each binding partner after RNAi depletion. We found that depletion of BUGZ led to ~2-fold depletion of BUB3 protein in GSCs, NSCs, and HeLa cells, while other SAC and kinetochore proteins (including BUB1, BUBR1, MAD2L1, HEC1, and Cdc20) were unaffected (Figures 4.6A,B, and 4.7A-C). However, mRNA levels of BUB3 remain unchanged with BUGZ knockdown (Figure 4.6C), suggesting the effects are not due to transcriptional regulation or to off-target RNAi. In addition, BUB3 loss due to BUGZ depletion can be rescued by overexpressing a BUGZ allele that is resistant to the shBUGZ (Figure 4.6D). Moreover, mutational analysis revealed that the glutamic acid residues E358 and E359 of BUGZ's GLEBS domain are critical for BUB3 stability (Figure 4.6D). These two glutamic acid residues are invariant among consensus residues for BUB1, BUBR1 and Nup98 GLEBS domains (Figure 4.4D) and are essential for their binding to BUB3 or Rae1 (82,85,124,125,130,131). These results suggest that the BUGZ-BUB3 GLEBS-mediated interaction decreases protein turnover of BUB3.

We next addressed whether BUGZ and BUB3 have overlapping localization patterns in cells. Similar to reports for BUB3 (85), a BUGZ-GFP fusion localized primarily to the nucleus in interphase, concentrated at kinetochores prior to nuclear envelope breakdown and during early prometaphase, and disappeared from kinetochores upon MT binding (Figure 4.6E). Immunostaining of BUGZ revealed a similar localization pattern (Figure 4.8A).

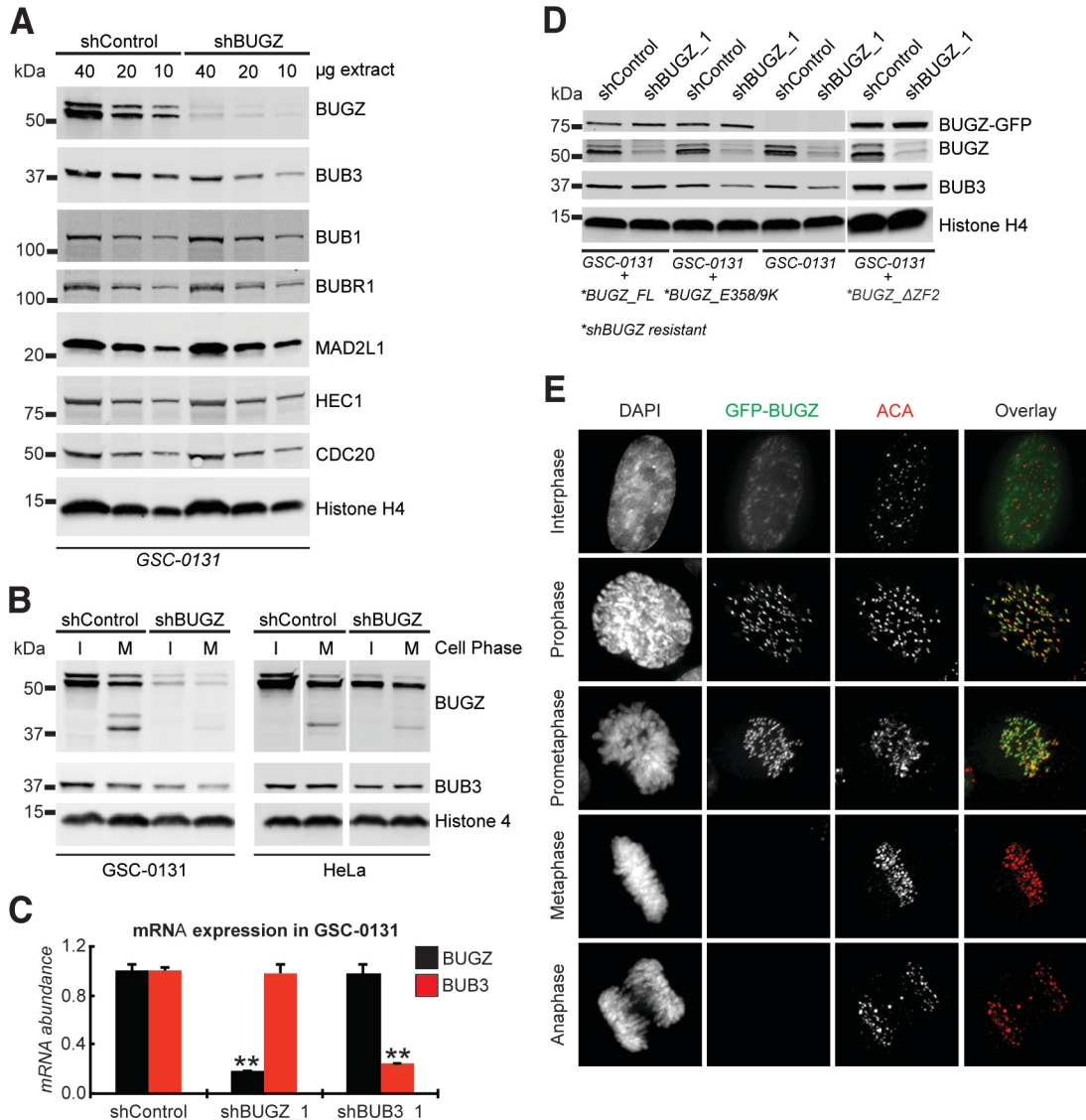


Figure 4.6. BUGZ stabilizes BUB3 expression and localizes to the kinetochore. (A) BUGZ stabilizes BUB3 expression. Western blot analysis of multiple KT-associated proteins after infection with shControl or shBUGZ virus. (B) BUGZ stabilizes BUB3 expression in interphase and mitotic cells. Western blot analysis of interphase or mitotic cell extracts for BUGZ and BUB3 levels after infection with shControl or shBUGZ virus and treatment with MG-132 for 18.5 hours. *Mitotic extracts contain lower molecular weight species of BUGZ, which could represent a cleavage or degradation product. (C) Knockdown of BUGZ does not alter BUB3 mRNA levels and vice versa as determined by quantitative real time PCR. **Student t test, $p < 0.01$. (D) Expression of BUGZ in BUGZ-depleted GSCs rescues BUB3 expression, but BUGZ-GLEBS domain mutants do not. Western blot analysis of cells infected with BUGZ Δ ZF2 (shBUGZ_1 targets the second zinc finger motif), shBUGZ resistant (denoted by *) full length (FL) BUGZ, or shBUGZ resistant BUGZ E358K E359K. Following selection, these cells were virally transduced with shControl or shBUGZ. (E) BUGZ localizes to kinetochores in prophase and prometaphase but diminishes during metaphase. HeLa cells were transfected with GFP-BUGZ fusions and imaged for DAPI, GFP, and ACA. Representative images are shown.

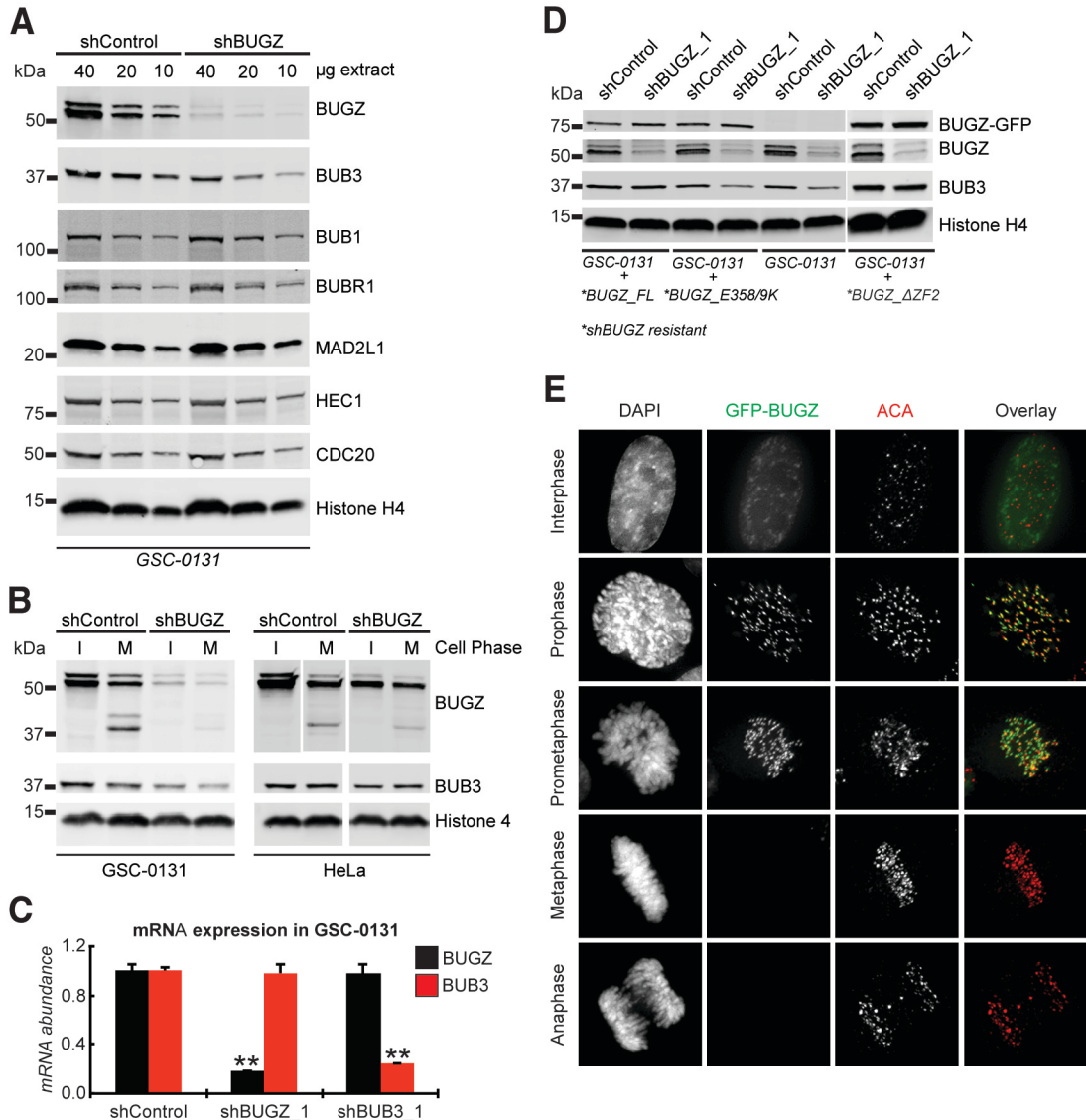


Figure 4.6. BUGZ stabilizes BUB3 expression and localizes to the kinetochore. (A) BUGZ stabilizes BUB3 expression. Western blot analysis of multiple KT-associated proteins after infection with shControl or shBUGZ virus. (B) BUGZ stabilizes BUB3 expression in interphase and mitotic cells. Western blot analysis of interphase or mitotic cell extracts for BUGZ and BUB3 levels after infection with shControl or shBUGZ virus and treatment with MG-132 for 18.5 hours. *Mitotic extracts contain lower molecular weight species of BUGZ, which could represent a cleavage or degradation product. (C) Knockdown of BUGZ does not alter BUB3 mRNA levels and vice versa as determined by quantitative real time PCR. **Student t test, $p < 0.01$. (D) Expression of BUGZ in BUGZ-depleted GSCs rescues BUB3 expression, but BUGZ-GLEBS domain mutants do not. Western blot analysis of cells infected with BUGZ Δ ZF2 (shBUGZ_1 targets the second zinc finger motif), shBUGZ resistant (denoted by *) full length (FL) BUGZ, or shBUGZ resistant BUGZ E358K E359K. Following selection, these cells were virally transduced with shControl or shBUGZ. (E) BUGZ localizes to kinetochores in prophase and prometaphase but diminishes during metaphase. HeLa cells were transfected with GFP-BUGZ fusions and imaged for DAPI, GFP, and ACA. Representative images are shown.

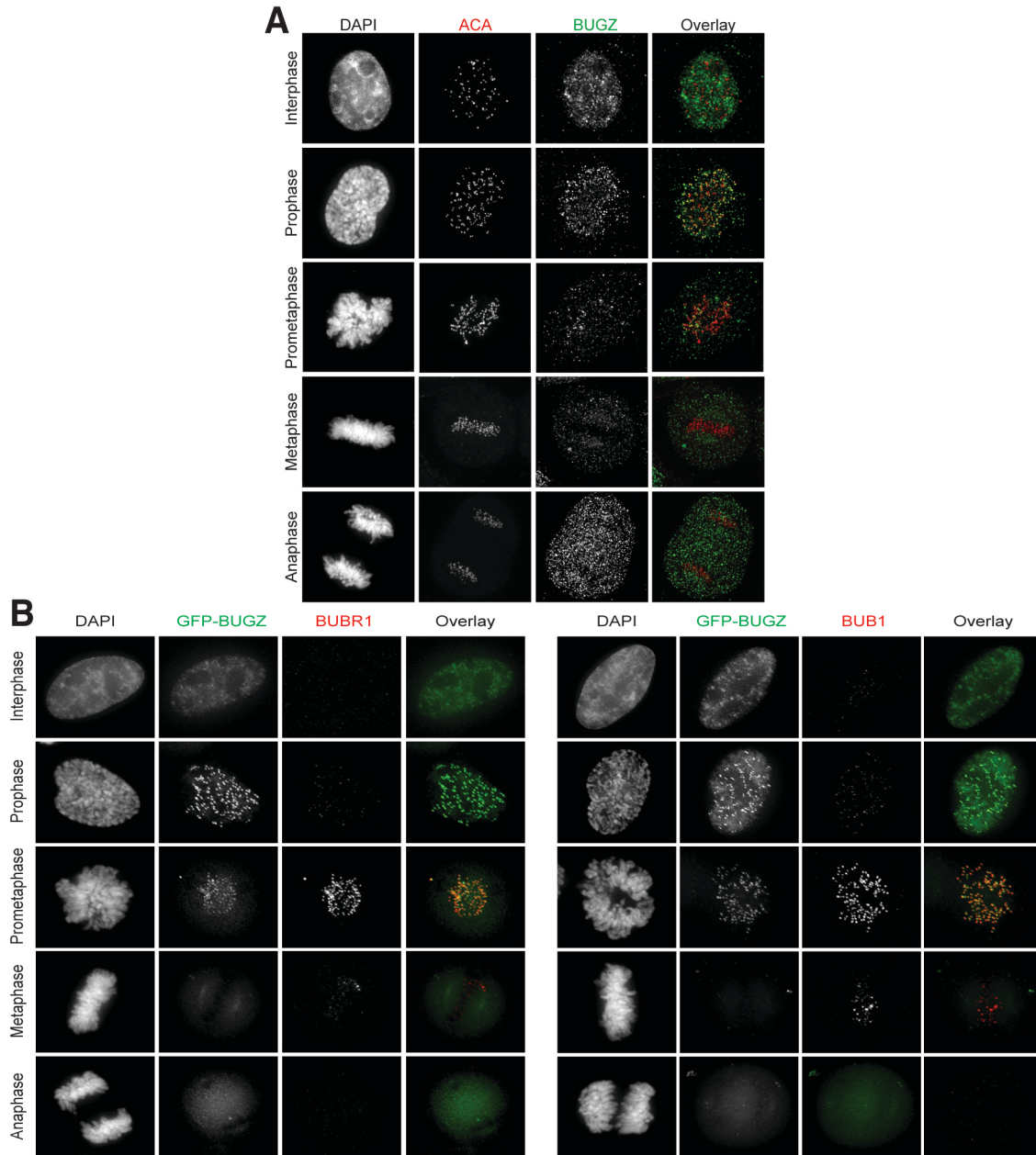


Figure 4.8. BUGZ localizes to the nucleus in interphase and to kinetochores prior to nuclear envelope breakdown, while BUBR1 and BUB1 localize to the kinetochore after BUGZ in early mitosis.

(A) Immunofluorescent staining of BUGZ in HeLa cells. Consistent with observations using GFP-BUGZ fusion protein, BUGZ is primarily nuclear in interphase and localizes to kinetochores in prophase before nuclear envelope breakdown. Upon microtubule attachment at metaphase, BUGZ kinetochore levels drastically reduce. (B) Immunofluorescent co-staining of BUB1 or BUBR1 with GFP-BUGZ through mitotic phases in HeLa cells. BUGZ concentrates at kinetochore prior to nuclear envelope breakdown and before significant levels of BUBR1 or BUB1 kinetochore localization. BUGZ is undetectable at metaphase and anaphase, while BUBR1 and BUB1 levels are low, but detectable.

We next determined co-localization patterns of BUGZ and BUB3 in HeLa cells. BUB3, just like BUGZ, maximally localized to kinetochores prior to nuclear envelope breakdown and remained bound throughout prometaphase as previously described (Figure 4.9A) (132). However, unlike BUGZ, low levels of BUB3 persisted at metaphase kinetochores.

In contrast to BUGZ and BUB3 kinetochore localization, BUB1 and BUBR1, which also associate with BUB3 via GLEBS domains, concentrate at kinetochores after nuclear envelope breakdown (Figure 4.8B), consistent with previously published results (133,134). Similar to these proteins, BUGZ's GLEBS domain is required for kinetochore localization (Figure 4.9B), while its zinc finger motifs are dispensable (Figure 4.9B). In addition, depletion of BUB3 using RNAi prevented BUGZ localization to the kinetochore (Figure 4.9C). Previous reports demonstrated that BUB3, BUB1, and BUBR1 all require KNL-1 in order to bind kinetochores (135–138). We found that KNL-1 depletion also resulted in a loss of BUGZ from kinetochores (Figure 4.9D). Moreover, when cells were treated with nocodazole, causing spindle MTs to depolymerize, unattached kinetochores re-accumulated BUGZ (Figure 4.9E). Conversely, treating cells with taxol, which stabilizes kinetochore-MTs attachments, did not recruit BUGZ to MT-attached kinetochores (Figure 4.9E). This behavior is similar to BUB3 and other SAC proteins (120). Together, these results indicate that BUGZ localizes to kinetochores by binding to BUB3 through its GLEBS domain and BUGZ's kinetochore localization is regulated by attachment of MTs.

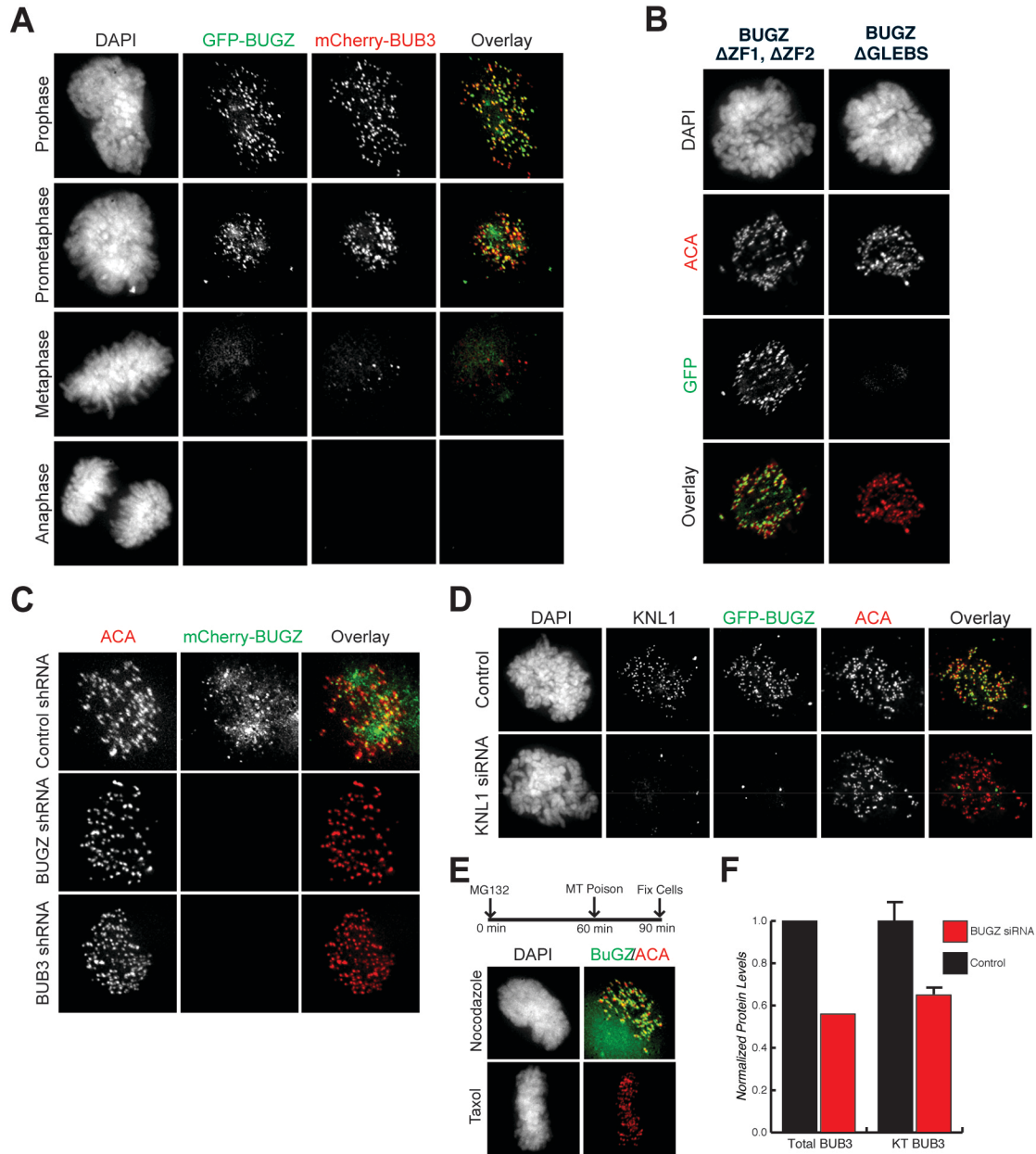


Figure 4.9. BUGZ co-localizes with BUB3 at KT early mitosis by virtue of its GLEBS domain and reduces BUB3 levels at KT when inhibited.

(A) BUGZ and BUB3 co-localization in HeLa cells transfected with GFP-BUGZ and mCherry-BUB3 expression constructs. BUGZ and BUB3 co-localize during prophase and prometaphase. Representative images shown. (B) BUGZ localization in HeLa cells transfected with GFP-BUGZ $\Delta ZF1, \Delta ZF2$ or BUGZ $\Delta GLEBS$ mutants. BUGZ $\Delta ZF1, \Delta ZF2$ localizes to the KTs but not BUGZ $\Delta GLEBS$. KTs are stained with anti-centromere antibody (ACA). (C) BUGZ localization is BUB3-dependent. HeLa cells stably expressing BUGZ-mCherry were infected with shControl, shBUGZ, or shBUB3. (D) BUGZ KT localization requires KNL1. HeLa cells stably expressing BUGZ-GFP were transfected with siControl or siKNL1. (E) BUGZ KT binding is regulated by KT-MT attachment. GFP-BUGZ stable HeLa cells were treated as shown with nocodazole or taxol and imaged.

Previous studies report that BUB3 and its binding partners BUB1 and BUBR1 exhibit interdependencies for kinetochore localization (3,5). We therefore analyzed kinetochore localization of BUB3, BUB1, and BUBR1 in BUGZ-depleted HeLa cells. After BUGZ depletion, BUB3 levels are reduced at kinetochores, which is not unexpected due to the decrease in total protein (Figure 4.9F). BUB1 kinetochore localization is also significantly decreased (Figure 4.10A), which is likely due to loss of its obligate kinetochore recruitment factor BUB3 (85,134,139). Intriguingly, BUBR1 kinetochore association is not affected after BUGZ depletion (Figure 4.10A), though previous studies have demonstrated that BUBR1 kinetochore recruitment relies on BUB3 (140,141). It is possible that BUBR1 out-competes BUB1 for limiting BUB3 binding sites that remain post- BUGZ depletion, or alternatively, that BUGZ plays a more direct role in BUB1 kinetochore recruitment.

In addition to their well-known roles in SAC signaling, BUB1, BUBR1 and BUB3 have also been implicated in facilitating chromosome alignment during mitosis (19,62,140). We therefore examined chromosome alignment in BUGZ-depleted HeLa cells treated with the proteasome inhibitor MG132 (to prevent precocious anaphase entry), and found that this process was significantly compromised (Figure 4.10B). In control populations, >95% of cells were able to fully align chromosomes, whereas proper chromosome alignment was observed in less than 55% of BUGZ-depleted cells (Figure 4.10B). We also detected similar chromosome alignment defects in GSC-0131 and transformed NSC-CB660 upon BUGZ depletion and MG132 treatment (Figure 4.10C).

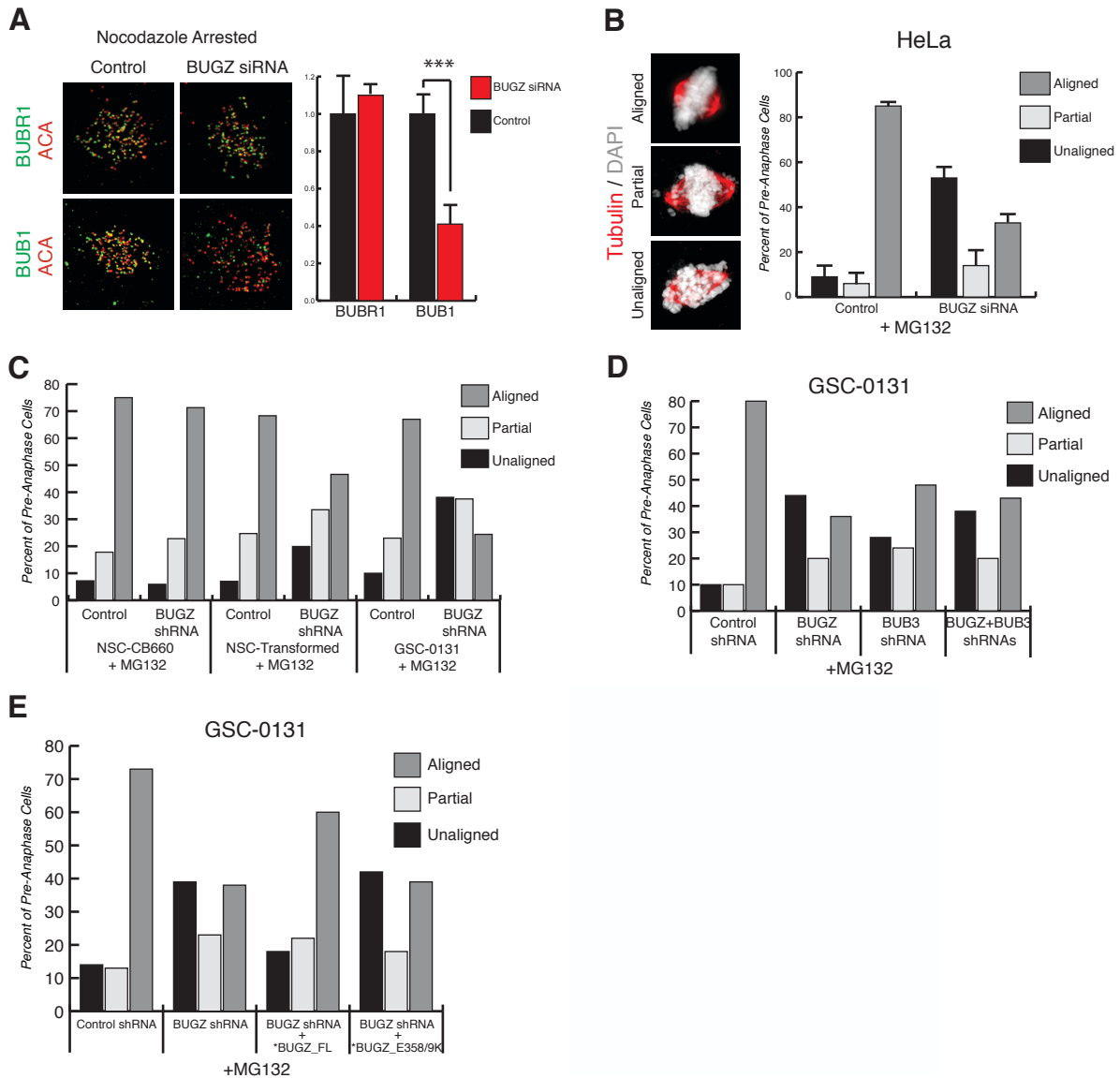


Figure 4.10. BUGZ activity is required for proper chromosome alignment.

(A) Representative images (left) and quantitative analysis (right) show BUGZ depletion does not alter BUBR1 levels, but BUB1 localization significantly reduces (student t test $p < 0.001$). BUBR1 and BUB1 total protein levels are unaltered ($N=2$). (B) BUGZ depletion causes chromosome alignment defects in HeLa cells. 35% of BUGZ depleted cells align chromosomes compared to 85% of control cells. ($N=2$; >800 cells/condition). (C) BUGZ depletion causes chromosome alignment defects in transformed NSC and GSC- cells, but not in non-transformed NSC cells. 71% of BUGZ depleted NSC cells align chromosomes compared to 46% of BUGZ depleted genetically transformed NSC cells. (>170 cells/condition). (D) In GSC cells, BUGZ and BUB3 co-depletion causes chromosome alignment defects similar to BUGZ and BUB3 depletion alone. 43% of BUGZ/BUB3 co-depleted GSC cells align chromosomes compared to 36% of BUGZ depleted and 49% of BUB3 depleted cells. (>110 cells/condition). (E) Expression of wt BUGZ, not BUGZ GLEBS domain mutant (E358/9K), rescues chromosome alignment defects in GSCs depleted for endogenous BUGZ. 60% of BUGZ depleted GSCs expressing shBUGZ resistant *BUGZ_FL align chromosomes compared to 39% for the BUGZ E358/9K GLEBS domain mutant. (>115 cells/condition).

However, non-transformed NSC-CB660 cells were able to fully align chromosomes following BUGZ loss (Figure 4.10C). In addition, co-depleting both BUGZ and BUB3 in GSC-0131 resulted in partial to severe chromosome alignment defects similar to BUGZ and BUB3 depletion alone (Figure 4.10D). The chromosome alignment defects in GSC-131 following depletion of endogenous BUGZ could be rescued by ectopic expression of the BUGZ ORF (Figure 4.10E), which further demonstrates that the chromosome alignment defects are due to BUGZ depletion and not due to off-target RNAi. However, BUGZ GLEBS domain mutations (E358K and E359K) failed to rescue the chromosome alignment defects (Figure 4.10E). The alignment defects were also observed in live BUGZ-depleted cells, which exhibited significantly extended mitotic transit times (120 min compared to 60 min in control cells) (Figure 4.11A,B). Together, these results suggest oncogenic stress alters kinetochore function, which leads to a differential requirement for BUGZ's GLEBS domain in cancer cells for chromosome congression.

To understand the source of these attachment errors, we assayed BUB1 kinase activity, which is implicated in mediating proper chromosome alignment through localization and activation of ABK (104,142,143). BUB1 kinase activity was measured in cells by immunostaining its substrate, histone H2AT120. Consistent with loss of BUB1 at kinetochores, pH2A levels were significantly lower after BUGZ depletion (Figure 4.12A). Consistent with loss of ABK activity at kinetochores after BUGZ depletion, we also observed significant loss of phosphorylation of HEC1S44, a critical downstream kinetochore substrate of ABK involved in the regulation of kinetochore-MT attachments (Figure 4.12A) (15).

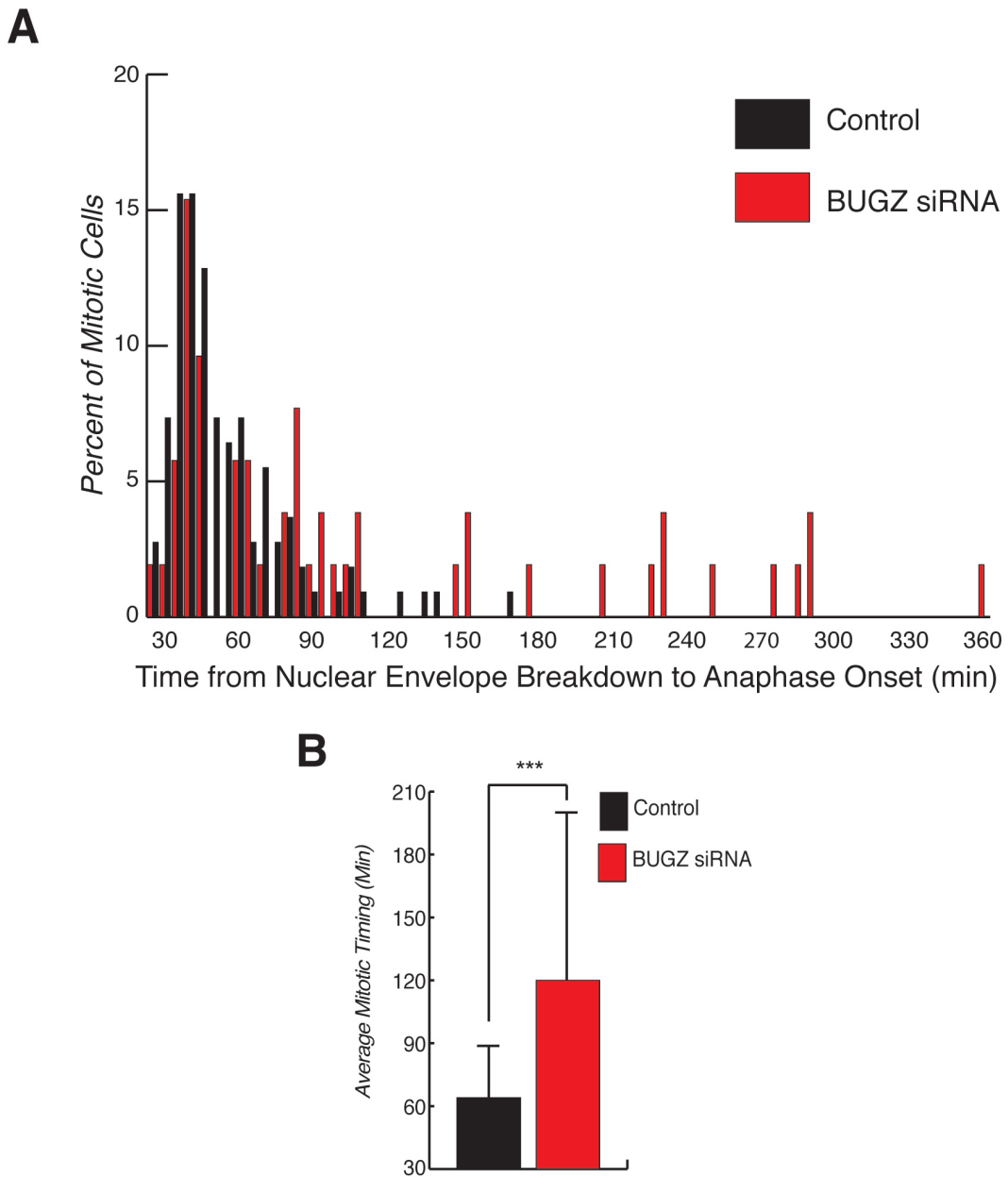


Figure 4.11. BUGZ depletion delays mitotic timing.

(A) HeLa cells expressing H2B-GFP fusion protein were imaged at five minute intervals to determine time from nuclear envelope breakdown until anaphase onset. Control cells (black) transited mitosis within 60 minutes on average. BUGZ depletion causes a significant delay in most cells, resulting in a 120 minute mitosis (Mann-Whitney test $p < 0.001$). (B) Averages summarized ($n > 60$ cells/condition).

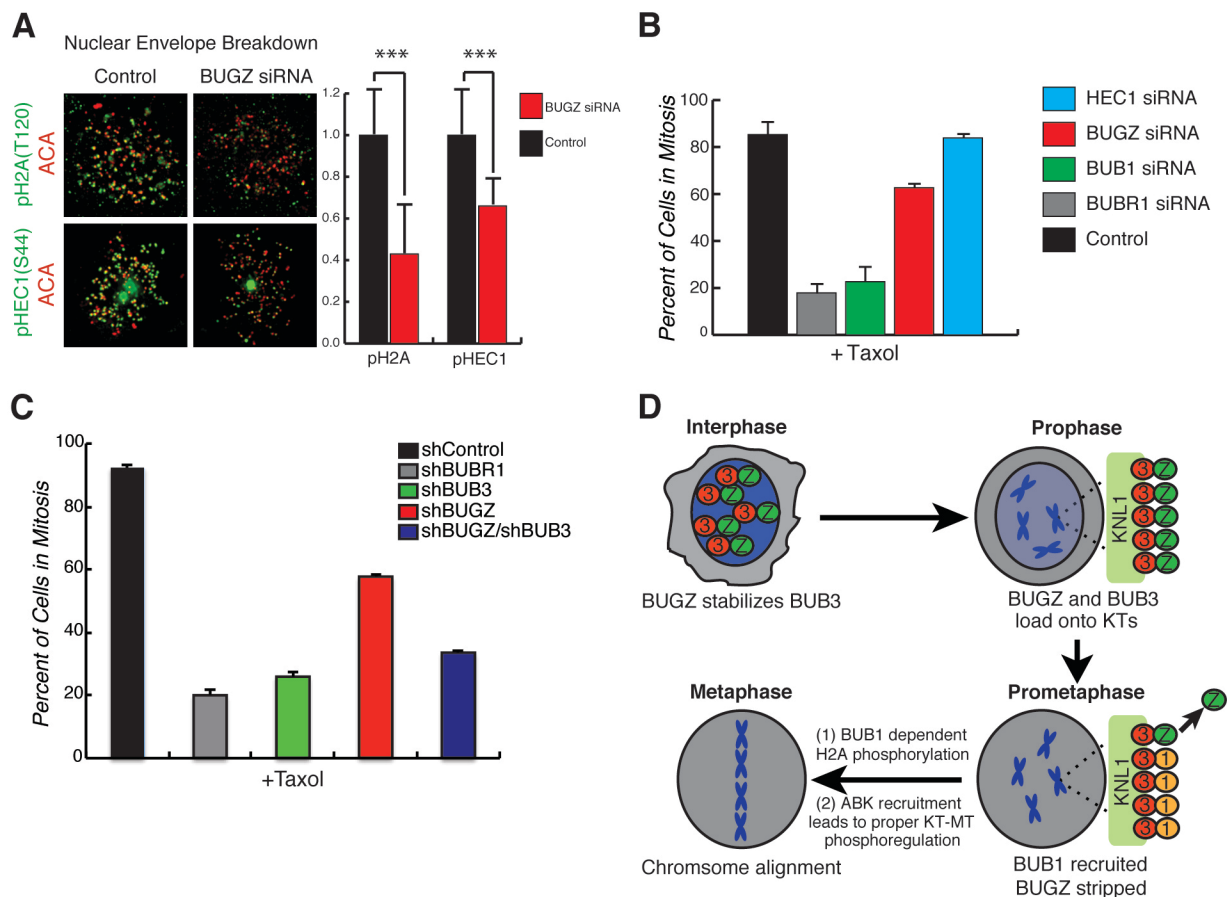


Figure 4.12. BUGZ activity is required for localization and activation of ABK, and the spindle assembly checkpoint.

(A) Immunofluorescence analysis for kinase activity of BUB1 and Aurora B. Representative images (left) and quantitative analysis (right) show BUGZ depletion decreases phosphorylation of BUB1 and Aurora B substrates, H2A and HEC1 respectively (student t test $p < 0.001$). (N=2; error bars represent cellular deviation [control] and experimental deviation [BUGZ siRNA]). (B) BUGZ depleted cells sustain a moderate mitotic arrest in microtubule poisons. A majority of control (black) and attachment factor HEC1 (blue) depleted cells are mitotic after 24 hours in taxol. Depleting SAC proteins BUBR1 (gray) and BUB1 (green) causes premature mitotic exit. BUGZ depletion (red) causes an intermediate phenotype, suggesting cells establish a SAC response but cannot maintain it. (N=2; >1000 cells counted/condition) (C) BUGZ and BUB3 (blue) co-depleted cells do not sustain a checkpoint arrest. A majority of control (black) depleted cells are mitotic after 24 hours in taxol. Depleting SAC proteins BUBR1 (gray) and BUB3 (green) causes a premature mitotic exit, while BUGZ depletion (red) causes an intermediate phenotype. Thus, BUGZ induced arrests require checkpoint signaling. (N=3; >1000 cells counted/condition). (D) Model of BUGZ function.

Thus, BUGZ affects chromosome alignment by ensuring BUB3 mediated recruitment of BUB1, which in turn ensures appropriate ABK-mediated phospho-regulation of kinetochore-MT attachments.

However, unlike BUB1 and BUBR1, BUGZ depleted cells retained a functional SAC response and elicited a significant mitotic delay in response to MT poisons, albeit at diminished levels (Figures 4.12B and 4.13). BUGZ and BUB3 co-depleted cells did not sustain a checkpoint arrest under these same conditions, which was similar to the behavior of cells depleted of BUB3 alone (Figure 4.12C). These results suggest that BUGZ depleted cells have enough residual BUB1 and BUB3 to activate the SAC.

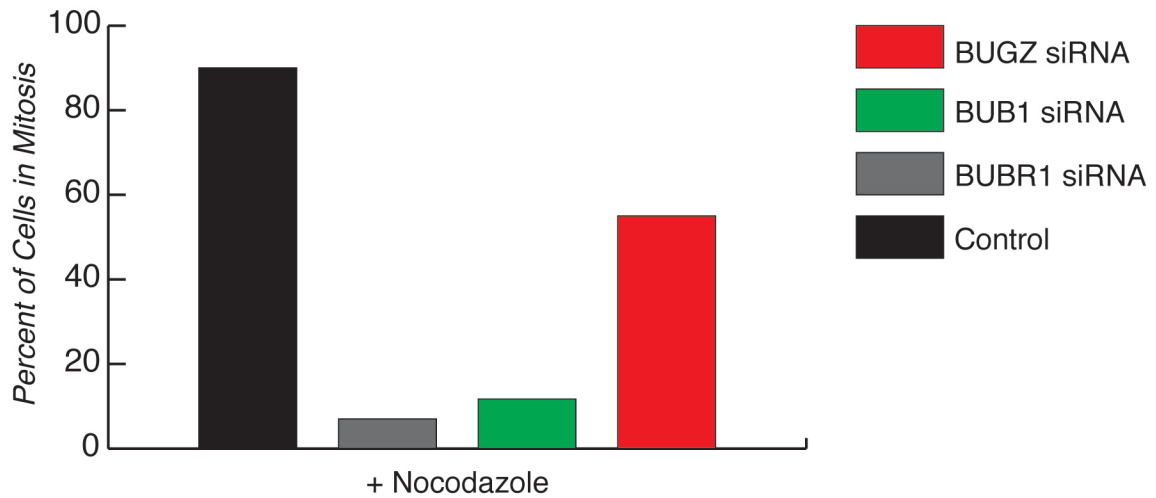


Figure 4.13. BUGZ depletion causes a weakened checkpoint arrest in response to MT poisons.

Control cells (black) robustly arrest in mitosis after 24 hours in the microtubule depolymerizing drug, nocodazole. Depletion of checkpoint proteins BUBR1 (gray) or BUB1 (green) drastically decreases the number of cells arrested in mitosis. BUGZ depletion (red) results in a moderate phenotype suggesting a functional, yet less robust SAC response. (N=2; >700 cells/condition).

4.3 Discussion

Here, we report for the first time that the human BUGZ/ZNF207 gene encodes a novel GLEBS domain-containing and kinetochore binding protein that is required for BUB3 stability, BUB1 kinetochore function, and chromosome alignment. A model for BUGZ function is presented in Figure 6D. We propose that BUGZ activity is required for BUB3 stability during interphase and mitosis. BUGZ depletion, therefore, results in a reduction of BUB3 protein levels during interphase and decreased binding to kinetochore during mitosis. As a consequence, BUB3-dependent BUB1 recruitment to kinetochores is compromised. This, in turn, compromises BUB1-dependent recruitment of ABK, which causes lethal chromosome congression defects in cancer cells. Importantly, viability defects and chromosome alignment defects resulting from BUGZ depletion were recreated in non-sensitive cells through oncogenic transformation. This suggests that oncogenic stress can drive an added requirement for BUGZ function in our GBM isolates and other cancer lines.

We previously established that GSCs differentially require BUBR1's GLEBS domain to suppress lethal consequences of altered kinetochore function by promoting attachment of MTs to kinetochores (58). Similar to BUGZ, BUBR1-GLEBS viability requirement can be reproduced in non-sensitive cells through genetic transformation with Ras^{V12}. However, the phenotypes associated with BUBR1-GLEBS domain requirement appear to be distinct from those observed for BUGZ. For example, BUBR1 knockdown results in severe defects in kinetochore-MT attachment in GBM isolates resulting in short inter-kinetochore distances at metaphase, while BUGZ knockdown results in alignment

defects similar to those produced by BUB3 depletion in all GSC isolates (Figure 4.10E). We postulate that GBM isolates and transformed NSCs have an added requirement for BUGZ due to oncogenic signaling that leads to changes in either kinetochore protein activity (e.g., through changes in stoichiometry) or feedback regulation of genes involved in chromosome congression (e.g., ABK). Based upon these studies, the RTK/RAS pathway is a likely candidate for triggering a BUGZ requirement. The RTK/RAS pathway is over activated in many cancers, including GBM, and there is evidence that RAS-down stream effectors ERK1/2 can directly phosphorylate the C-terminal domain of CENPE, a key kinetochore protein, which is predicted to decrease its MT binding ability (144).

The functional dichotomy between BUGZ and BUBR1 is also observed in the SAC. BUBR1's essential function is to maintain an intact mitotic checkpoint until all chromosomes are properly aligned and kinetochores are under proper tension. We observe a significant mitotic delay in cancer cells following depletion of BUGZ despite a significant loss of both BUB1 and BUB3 at the kinetochore (Figure 4.9C,F). This mitotic delay is checkpoint-dependent as co-depletion of BUGZ and BUB3 prevents mitotic arrest (Figure 4.12C). Thus, it is likely that unattached kinetochores present in BUGZ depleted cells are able to generate a functional SAC signal. It is known that BUB1 must be depleted >95% to cause checkpoint abrogation (62). Therefore, the >40% of BUB3 and BUB1 present in BUGZ depleted cells is likely sufficient for SAC activation. However, we cannot preclude the possibility that BUGZ is also involved in SAC silencing, which contributes to the mitotic delay observed.

Our studies raise a key question: Is BUGZ essential in non-transformed cells? BUB1, BUB3, and BUBR1 are all essential for mouse development, as null mutations of these genes cause early embryo lethality (75,83,145,146). However, the heterozygous state is permissive for normal development, albeit with increases in mitotic abnormalities. Consistent with being non-essential, BUBR1's GLEBS domain is not required for mouse embryo fibroblast proliferation or kinetochore-MT attachment (58,77). Our knockdown studies suggest that the hypomorphic BUGZ state is permissive for viability of non-transformed cells, where BUB3 expression is probably equivalent to BUB3 heterozygous cells. However, we do not know if complete removal of BUGZ would reduce BUB3 levels further, or whether BUGZ will have other essential functions not revealed by our studies (e.g., in its zinc finger domains). It will be also be interesting to see if GLEBS domains are essential for mammalian development, given that our findings suggest targeting GLEBS domain interactions with BUB3 may represent a precision therapy for GBM.

Our findings also raise a critical question regarding BUGZ's role to facilitate BUB3's function: How does BUGZ regulate BUB3's stability? One possibility is that upon BUB3 binding, BUGZ's GLEBS domain masks post-translational modifications of BUB3, such as phosphorylation, ubiquitination, or sumoylation, which prevents its degradation. However, we were unable to detect increases in BUB3 expression from BUGZ depleted cells treated with the proteasome inhibitor MG132 (Figure 4.6B) or the sumoylation inhibitor ginkgolic acid (data not shown). Another possibility is that BUGZ acts as a molecular chaperone for BUB3 by converting an unfolded or partially folded BUB3 to its

final compact and stable confirmation (125), which, for example, may prevent specific proteases from recognizing and degrading unfolded BUB3. Over expression of BUGZ increases the steady-state levels of ectopically expressed and also endogenous BUB3 (Figures 4.4F and 4.6D), suggesting that BUGZ expression is rate-limiting for BUB3 stability. Thus, further experimentation is warranted to determine the nature of the change in BUB3 turnover following BUGZ depletion.

Another question is how BUGZ-dependent BUB3 regulation affects BUB1 and BUBR1 function at kinetochores? BUB3 and its binding partners BUB1 and BUBR1 exhibit interdependencies for kinetochore localization (3,5). Our results suggest that BUGZ loss preferentially depletes BUB1 recruitment to the kinetochore, leaving BUBR1 levels unchanged (Figure 4.10A). This appears to contradict previous studies that have established roles for BUB1 and BUB3 in recruiting BUBR1 to kinetochores (85,137,140,146–148). However, these studies produce knockdowns of >90% of BUB1 or BUB3. Our studies produce more modest changes in BUB3 levels after BUGZ knock down (Figure 4F) and only partial loss of recruitment of BUB1 to kinetochores (Figure 4.10A). This suggests that BUBR1 may outcompete BUB1 at kinetochores for residual BUB3 (e.g., BUBR1 could have higher affinity for BUB3 than BUB1). Alternatively, BUGZ could act as an exchange factor facilitating BUB3-BUB1 interactions.

Further, it was recently found that BUB3 kinetochore recruitment is driven by MPS1/TTK-dependent phosphorylation of KNL1's MELT motifs (135–138). Consistent with this result, we find that BUGZ kinetochore localization is KNL1-dependent (Figure

4.9D). Interestingly, it was found that BUB3 binding of phosphorylated MELT motifs ~10-fold greater when BUB1 was present (137). Future work will be required to determine whether BUGZ, BUB1, and BUBR1 have similar effects on KNL1-dependent BUB3 kinetochore localization.

In summary, we find that BUGZ is a novel GLEBS domain-containing and kinetochore binding protein required for BUB3 stability and kinetochore function. In transformed cells, BUGZ knockdown results in defects in kinetochore-MT attachments and chromosome congression. For cancer biology, these results raise the possibility that inhibiting GLEBS domain interactions with BUB3 may be a novel therapeutic strategy for refractory cancers like GBM, which suffer from lethal kinetochore-MT instability brought about by oncogenic stress (58). For evolutionary biology, these results suggest that BUGZ function may have arisen in higher eukaryotes to facilitate BUB3 function and chromosome congression.

4.4 Methods

Western blotting, affinity purification, mass spectrometry, and immunoprecipitations were performed according to standard protocols.

Cell culture and drug treatment

GSC and NSC lines were grown in N2B27 neural basal media (StemCell Technologies) supplemented with EGF and FGF-2 (20ng/mL each) (Peprotech) on laminin (Sigma) coated polystyrene plates and passaged as described previously (58,94). Cells were

detached from their plates using Accutase (Millipore). 293T and HeLa cells (ATCC) were grown in 10% FBS/DMEM (Invitrogen). Cells were treated with 800 nM or 10 μ M nocodazole (Sigma) for 24 hours and 1 hour incubations respectively. Taxol (Sigma) was used at 10 μ M for 24 hours, and MG132 (Tocris) was also used at a final concentration of 10 μ M. Live cell imaging was performed in Leibovitz's L-15 media (Invitrogen) supplemented with 10% FBS, 7 mM HEPES, pH 7.0 and 4.5 g/l glucose.

RNAi and lentiviral production

shRNAs were obtained from Open Biosystems (Huntsville, AL) in the pGIPZ lentiviral vector. For virus production, pGIPZ-shRNA plasmids were transfected with lipofectamine 2000 (Invitrogen) into 293T cells along with psPAX and pMD2.G packing plasmids to produce lentivirus. Following approximately 24 hours after transfection, neural stem cell expansion medium was added to replace the original 293T growth medium. Virus was harvested and filtered approximately 24 hours after media change and stored at -80°C. GSCs and NSCs were infected at MOI 1). HeLa cells were infected at MOI1 with respect to the experiment in the presence of 8 μ g/mL of polybrene. Cells were infected for 48 hours followed by selection with 1-4 μ g (depending on the target cell type) of puromycin for 2-4 days.

Growth assays

For short-term single clone validation assays, cells were infected with lentivirus containing a single shRNA to the respective gene. Following selection, cells were harvested, counted (NucleoCounter, NBS) and plated in triplicate onto 96-well plates

coated with laminin (58,94). After 7 days under standard growth conditions with 0.5 $\mu\text{g}/\text{mL}$ of puromycin to maintain selection and prevent outgrowth of residual uninfected cells, cell proliferative rates were measured using Alamar blue reagent according to manufacture instructions (Invitrogen). For analysis, shRNA containing samples were normalized to their respective shControl samples.

Western blotting

Western blots were carried out using standard laboratory practices (www.cshprotocols.org), except cells were lysed in a modified RIPA buffer (150mM NaCl, 50 mM Tris, pH 7.5, 2 mM MgCl_2 , 0.1% SDS, 2 mM DDT, 0.4% deoxycholate, 0.4% Triton X-100, 1X complete protease inhibitor cocktail (complete Mini EDTA-free, Roche), and 1 U/ μL benzonase nuclease (Novagen)) at RT for 15 minutes. Additionally, some cells were subjected to treatment with the protease inhibitor MG-132 (EMD Millipore) at 10 μM for 18.5 hours following the infection/selection process. After a shake-off, cells in suspension (mitotic cells) were harvested. Cells remaining attached to the culture plate were washed with PBS to remove the remaining mitotic cells in culture and detached (interphase/asynchronous cells). Attached cells were then washed with PBS and lysed using the modified RIPA buffer.

Cells were harvested following infection with their respective shRNA and selection, washed with PBS, and lysed with the modified RIPA buffer. The shake-off method was also performed for HeLa cells to generate interphase and mitotic cells. However, HeLa cells were not treated with MG-132 due to the high mitotic index. Cell lysates were

quantified using Perce 660nm protein assay reagent and identical amounts of proteins were loaded onto SDS-PAGE for western blot. Trans-Blot Turbo transfer system was used according to the manufacture instructions. Antibodies against ZNF207 (Novus, # NBP1-89550, 1:1000), ZNF207 (Thermo Scientific, # PA5-30641, 1:1000), BUB3 (BD Transduction Laboratories, # 611730, 1:1000), turboGFP (d) (Evrogen, # AB513), histone 4 (Abcam, # 17036-100, 1:2000), BUB1 (Abcam, #548931:1000), BUBR1 (Cell Signaling, # 4116S, 1:500), MAD2L1 (D8A7) (Cell Signaling, # 4636, 1:1,000), HEC1 (Thermo Scientific, # MA1-23308, 1:500), and CDC20 (Cell Signaling, # 4823, 1:1000) were used for these experiments. An Odyssey infrared imaging system was used to visualize blots (LI-COR) following the manufacturer instructions. For quantification, an ROI using the Odyssey software for each shRNA cell lysate sample was acquired, normalized to a loading control (histone 4 or beta-actin (not shown)), and then normalized to the respective shControl.

Immunofluorescence

Cells were grown on sterile, acid-washed coverslips in 35 mm cell culture dishes. Cells were rinsed with PHEM (60 mM PIPES, 25 nM HEPES, 10 mM EGTA, 4 mM MgSO₄) and either immediately treated with 4% paraformaldehyde for 20 minutes at room temperature, or for phosphorylation specific antibodies, treated with lysis buffer (PHEM + 1.0% Triton X-100) for 5 minutes at 37°C and then PFA fixed for 20 minutes at room temperature. Fixed cells were washed, blocked for 1 hour at room temperature in PHEM+10% boiled donkey serum (BDS). Primary antibodies were diluted in PHEM+5% BDS and incubated for 16 hours at 4°C. Coverslips were washed, then incubated with

secondary antibodies conjugated to fluorescent dyes (Jackson ImmunoResearch Laboratories) again diluted in PHEM + 5% BDS for 45 minutes at room temperature. Coverslips were washed, stained with 2 ng/mL 4',6-diamidino-2-phenylindole (DAPI) diluted in PHEM, and then mounted onto microscope slides in an anti-fade solution containing 90% glycerol and 0.5% N-propyl gallate.

Commercial antibodies used: Tubulin-DM1 α (Sigma, #T9026, 1:300); CREST (Antibodies, Inc., #15-234-0001, 1:500); ZNF207/BUGZ (Thermo Scientific, #PA5-30641, 1:600); BUB1 (Abcam, #548931, 1:300); BUB3 (BD Transduction Laboratories, #611730, 1:1000); BUBR1 (Millipore, #3612, 1:1000); pH2AT120 (Active Motif, #39391, 1:2000). HEC1S44 phosphorylation specific antibody was generated and affinity purified by 21st Century Biochemicals as previously described (15).

Image acquisition and analysis

Fixed-cell images were acquired using a DeltaVision PersonalDV Imaging System (Applied Precision/GE) on a Photometrics CoolSnap HQ2 camera (Roper Scientific) and a 60x/1.42NA Planapochromat DIC oil immersion lens (Olympus). All immunofluorescence images were collected as z-stacks at 0.2 μm intervals. Kinetochore integrated pixel intensity values were measured on deconvolved images with SoftWorx software (Applied Precision) applying background correction. Live cell imaging of control and BUGZ depleted cells was performed on the same microscope using an environmental chamber to maintain the stage at 37°C. Cells

expressing a GFP-H2B fusion were imaged every 5 minutes for 12 hours on a single plane. Imaging of BUGZ depleted cells began 24 hours post siRNA treatment.

Transformed neural stem cells

Normal CB660 neural stems were simultaneously infected with retrovirus containing pbabe-hTERT + p53DD (Addgene, Plasmid 11128), pbabe-cyclinD1 + CDK4R24C (Addgene, Plasmid 11129), and pbabe-c-mycT58A + HRasG12V (Addgene, Plasmid 11130) for three consecutive rounds of infection as described (94). After recovery, cells were selected with both neomycin for Ras and blasticidin for c-MYC respectively.

SSEA1+ outgrowth assays

Cells were infected with shControl and sh BUGZ virus for 48 hours followed by selection with puromycin for 72 hours. Cells were detached from their respective plate, counted with a nucleocounter, and mixed with untreated cells. After mixing, cells were either seeded to a 6-well tissue culture dish coated with laminin for further growth. After three days in culture, cells were harvested, counted, seeded to a 6-well tissue culture dish coated with laminin for further growth or washed with cold PBS containing 0.5% bovine serum albumin (BSA) for flow analysis. Cells were analyzed at days 0, 3, 7, 14, and 21. Data analysis was performed using FlowJo (Three Star).

Cells used for flow analysis were then blocked with cold PBS containing 0.5% BSA for 15 minutes at 4°C, followed by an one hour incubation with APC mouse anti human CD15 (SSEA1, BD Pharmingen, # 551376) or APC Mouse IgM, kappa Isotype control

(BD Pharmingen, # 555585) at 4°C on a shaker in the dark. Following two washes with cold PBS containing 0.5% BSA, cells were suspended with PBS containing 0.5% BSA and analyzed using a FACS Canto flow cytometer (Becton Dickinson)

Limiting dilution assay

Cells were infected with shControl and sh BUGZ virus for 48 hours followed by selection with puromycin for 72 hours (Day 0). Cells were detached from their respective plate, dissociated into single-cell suspensions, counted with a nucleocounter, and then plated into non-tissue culture treated 96-well plates not coated with laminin at various seeding densities (0.125-256 cells per well, 10 wells per seeding density). Cells were incubated at 37°C for 3 weeks and fed with 10X EGF and FGF-2 neural stem cell expansion media every 3-4 days. At the time of quantification, each well was examined for the formation of tumor spheres.

Immunoprecipitations

GSCs and NSCs were lysed following the infection/selection process. 293Ts were transfected using Lipofectamine 2000 (Invitrogen) and lysed 48 hours later. Cell lysates were extracted using the modified RIPA buffer supplemented with PhosStop phosphatase inhibitor cocktail (Roche), 10µM sodium fluoride (anti-phosphatase inhibitor), and 10µM sodium metavanadate. After 10 minutes of incubation on ice, cell lysates were harvested and rotated at 4°C for 20 minutes. The extract was then spun and down and the supernatant was harvested. Antibodies used for immunoprecipitations were anti-turboGFP (Evrogen, 1:25) and anti-V5 (Sigma, #V8012,

1:25). Binding was performed for 3 hours at 4°C on a rotator. Immunoprecipitates were captured on Protein A/G Plus Agarose beads (Santa Cruz, #2003) and incubated at 4°C for 2.5 hours on a rotator. After a brief spin, the beads were washed three times with the supplemented modified RIPA buffer. Following the washes, 3X SDS sample buffer (New England BioLabs, #B7709S) was added, gently mixed, boiled, and analyzed by SDS-PAGE followed by Western blotting.

Mass spectrometry

Mass spectrometry experiments were performed using an online EasyLC nanopump (Thermo) fitted to a hybrid LTQ-Velos-Orbitrap instrument (Thermo), a C18 pre-column (75um i.d. x 2.5 cm length), and an uLC analytical column (75um i.d. x 10 cm length). The mass spectrometer was run in data-dependent acquisition mode (16 MS/MS scans per MS scan at 60,000 resolution). Reverse phase chromatography was performed using a 95min gradient from water to acetonitrile, each containing 0.1% FA at a flow rate of 0.3 ul/min. The acquired spectra were searched by SEQUEST using the UniProt reference human proteome, and matched peptides were filtered using a 20ppm precursor ion threshold.

Xenotransplantation

0827 GSCs were infected with pGIPZ shRNA virus and selected for 3 days in puromycin (1 µg/mL). Cells were then harvested using Accutase (Sigma), counted, resuspended in an appropriate volume of culture media, mixed 90% GIPZ plus 10% untreated cells (non-infected cells), and kept on ice prior to immediate transplantation

(94). NOD-scid IL2Rgammanull mice (Jackson Labs #005557) were sedated by inhalation of isoflourane. A small bore hole was made in the skull using a hand drill with a Meisinger #009 steel burr bit (Hager and Meisinger GmbH). 1×10^5 cells were slowly injected by pipet into the right frontal cortex approximately 2mm rostral to Bregma, 2mm lateral and 3mm deep through a 0.2-10 μ L disposable sterile aerosol barrier tip (Fisher Scientific #02-707-30). The burr hole was closed using SURGIFOAM (Johnson & Johnson) and the skin rejoined using TISSUMEND II (Veterinary Product Laboratories, Phoenix, AZ). 17 days after initial transplantation, mice were injected intravenously through the tail with 100 μ L of 10 μ M Chlorotoxin: indocyanine green (Blaze Bioscience, Seattle, WA) 4 hours prior to sacrifice by carbon dioxide inhalation. The brain and tumor were removed from the skull and imaged for GFP and indocyanine green fluorescence using the Xenogen IVIS Spectrum imaging system (Caliper Life Sciences).

CHAPTER 5

CONCLUSIONS AND FUTURE PERSPECTIVES⁵

5.1 Summary

Through these studies we have demonstrated that kinetochore-MT attachments are commonly altered upon transformation. In particular, we found that inhibiting the activity of accessory Aurora B kinase regulators provides GBM specific lethality, thus increasing the therapeutic window for chemotherapies. These studies arose from two unique genetic screens of human proteins, yet identified two mitotic proteins as specifically required for outgrowth of GSCs. These screens were designed to target human kinases and putative transcription factors yet both identified kinetochore proteins as specifically required for growth in GSCs over NSCs. This suggests that the mitotic process is commonly fundamentally altered upon transformation, either through ABK activation as demonstrated here or through another yet to be characterized mechanism. In these studies we have identified the cancer-specific activity of both BUBR1 and BUGZ, which are essential for targeted therapeutic intervention in GBM. While these studies have not

⁵ This chapter presented as a conclusion to this dissertation was published in part as a review article, "Molecular Pathways: Targeting Kinetochore-Microtubule Attachments in Cancer" in August 2014. Parts have been omitted or expanded where appropriate.

P.J.P. and I conceived the content and co-wrote this manuscript with input from J.G.D and J.M.O.

Herman JA, Toledo CM, Olson JM, DeLuca JG, Paddison PJ. Molecular Pathways: Regulation and Targeting of Kinetochore-Microtubule Attachment in Cancer. Clin Cancer Res. 2014;233–9

yielded a specific inhibitory molecule, they have clearly identified molecular targets for cancer therapy.

5.2 Repurposing currently FDA approved therapies

More conventional therapies and targets may also take advantage of oncogenically induced kinetochore defects. Both BUBR1 and BUGZ function within complex regulatory pathways to affect kinetochore phosphoregulation, and targeting other mitotic proteins in these pathways may yield GBM-specific cell death. These include kinase activities of MPS1 (136,138,149), BUB1 (17,104,142), PKM2 (150), and PLK1 (Figure 5.1; 19). As discussed previously, BUB1 activation of ABK activity requires BUGZ through an unknown mechanism. In addition, BUB1 cannot bind kinetochores without MPS1-dependent phosphorylation of MELT motifs within the kinetochore factor KNL1 (Figure 5.1; 122,124,135). Thus, kinase inhibitors specific for either MPS1 or BUB1 may exacerbate the same kinetochore–MT attachment defects in GBM that induce the requirement for the BUGZ-GLEBS domain. However, because these kinases are essential for SAC signaling, it remains unclear whether dose-limiting toxicities in noncancer cells will limit the effectiveness of MPS1 or BUB1 inhibitors, albeit there have been promising preclinical trials of MPS1 inhibitors, some of which have initiated phase I trials (151–153). Although cycloalkenepyrazole inhibitors of BUB1 kinase activity have been patented (Patent WO2013167698), no cell-based or *in vivo* studies have been published to date.

Interestingly, PKM2, which has important roles in glycolysis and gene transcription, binds BUB3 during mitosis and phosphorylates residue Y207, a regulatory event required for BUB3-BUB1 complex recruitment to kinetochores in GBM cells (150). PKM2 inhibitors have been previously developed to metabolically target cancers (154). An interesting possibility is that these drugs may have the added effect of destabilizing compromised kinetochore–MT attachments observed in GBM cells which require BUB3 for chromosome alignment; however, this activity has not been assayed.

PLK1 inhibitors have shown efficacy in preclinical work using GBM models (155) and have had clinical success in acute myeloid leukemia. Currently, at least six unique PLK1 inhibitors have reached phase I or II clinical trials for various cancers, and BI-6727 (volasertib) was recently designated a “breakthrough therapy” by the FDA in the treatment of acute myeloid leukemia after raising complete remission rates 3-fold for patients enrolled in a phase II trial (156–159).

However, without detailed mechanistic studies, it is difficult to know if the clinical success of these targets is attributable, even in part, to mitotic disruption. As these therapies demonstrate clinical success, it will be important to expand them into cancers with documented kinetochore–MT attachment defects. However, these targets, particularly MPS1 and PLK1, have many roles within the cell cycle, including centrosome duplication and mitotic entry, and thus may exhibit broad antimitotic effects.

Aneuploidy was among the first cytologic features associated with cancer cells (51), and thus chromosome segregation has long been a logical target for cancer therapies. However, our understanding of molecular drivers of chromosome instability in cancer and the interdependency of chromosome instability, tumor initiation, and evolution is only just emerging.

Antimitotic drugs, including microtubule poisons such as taxanes and vinca alkaloids, have long been instrumental in cancer therapy, but unfortunately due to their nonspecific nature can be quite toxic. Even recently developed drugs, such as Aurora kinase or KIF11/EG5 inhibitors, target all dividing cells and thus have performed poorly in clinical trials (160,161). These failings likely result from targeting mitotic master regulators that are required in healthy cells; inhibiting a ubiquitously essential target dramatically reduces the therapeutic window and efficacy of a treatment. It is clear that the next generation of antimitotic biologic chemotherapies must capitalize on defects already present in cancer cells. Proteins and processes that have become destabilized by oncogenic signaling are ideal targets for a therapy that inhibits accessory or redundant regulators. As observed with BUBR1, healthy cells with robust kinetochore signaling survive BUBR1-GLEBS inhibition, whereas GBM cells, compromised by oncogenic signaling, cannot tolerate this loss. By targeting accessory regulators in defective pathways, healthy cells with redundant or robust regulatory mechanisms are largely unaffected, and the inhibition is amplified or exacerbated in compromised cells.

Kinetochores and their dynamic attachments to microtubules are an exciting area from which to identify targets for precision cancer therapies. Mitotic factors are commonly altered in cancers through mutation, transcriptional changes, or epigenetic and posttranslational modifications. Moreover, a large body of work characterizing the complex pathways, which regulate kinetochore–MT attachments, informs the many targets for chemical intervention. Even more exciting is the possibility of applying previously FDA-approved antimitotic therapies to specific cancers with compromised kinetochore signaling.

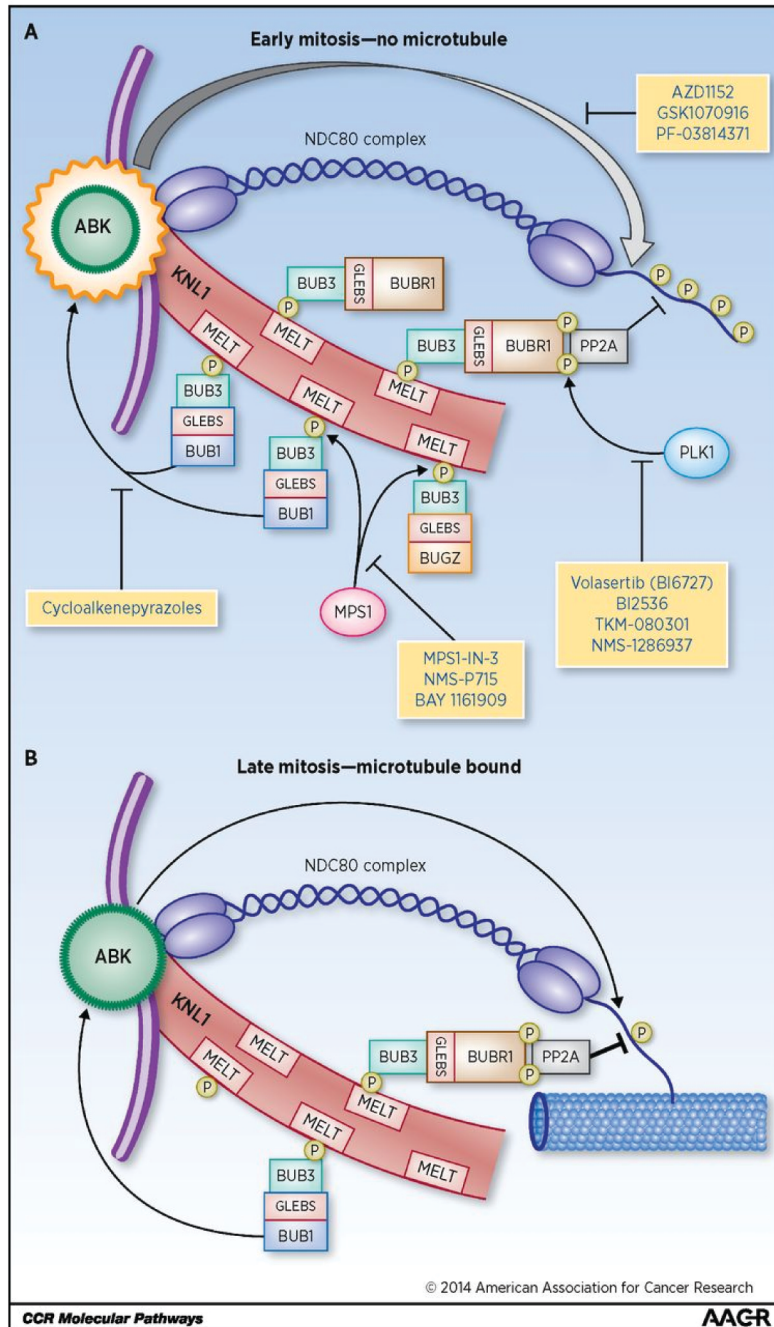


Figure 5.1. Therapeutic interventions targeting kinetochore-microtubule attachments
 (A) Early in mitosis, three GLEBS-containing proteins, BUBR1, BUB3, and BUB1, accumulate at kinetochores through BUB3 binding to regulate KT–MT attachments. The recruitment of these proteins is dependent on MPS1 phosphorylation of MELT motifs in KNL1. BUB1 and Aurora B kinases increase kinetochore phosphorylation, particularly of the Ndc80 complex, to inhibit stable microtubule attachment. Conversely, BUBR1/PLK1 recruits PP2A to counteract kinetochore phosphorylation to facilitate KT–MT attachment stabilization. (B) Late in mitosis, phosphatase activity dominates and reduces kinetochore phosphorylation to stabilize microtubule attachments. Clinically relevant chemical inhibitors of kinetochore phosphoregulation are shown in blue.

REFERENCES

1. Vleugel M, Hoogendoorn E, Snel B, Kops GJPL. Evolution and function of the mitotic checkpoint. *Dev Cell*. 2012;23:239–50.
2. Maiato H, DeLuca J, Salmon ED, Earnshaw WC. The dynamic kinetochore-microtubule interface. *J Cell Sci*. 2004;117:5461–77.
3. Santaguida S, Musacchio A. The life and miracles of kinetochores. *EMBO J*. 2009;28:2511–31.
4. Musacchio A, Salmon ED. The spindle-assembly checkpoint in space and time. *Nat Rev Mol Cell Biol*. 2007;8:379–93.
5. Lara-Gonzalez P, Westhorpe FG, Taylor SS. The spindle assembly checkpoint. *Curr Biol*. Elsevier Ltd; 2012;22:R966–80.
6. Foley EA, Kapoor TM. Microtubule attachment and spindle assembly checkpoint signalling at the kinetochore. *Nat Rev Mol Cell Biol*. Nature Publishing Group; 2013;14:25–37.
7. Rieder CL, Cole RW, Khodjakov A, Sluder G. The checkpoint delaying anaphase in response to chromosome monoorientation is mediated by an inhibitory signal produced by unattached kinetochores. *J Cell Biol*. 1995;130:941–8.
8. Mitchison T, Kirschner M. Dynamic instability of microtubule growth. *Nature*. 1984;312:237–42.
9. Tooley J, Stukenberg PT. The Ndc80 complex: Integrating the kinetochore's many movements. *Chromosom Res*. 2011;19:377–91.
10. DeLuca JG, Dong Y, Hergert P, Strauss J, Hickey JM, Salmon ED, et al. Hec1 and nuf2 are core components of the kinetochore outer plate essential for organizing microtubule attachment sites. *Mol Biol Cell*. 2005;16:519–31.
11. Ciferri C, De Lucall J, Monzani S, Ferrari KJ, Ristic D, Wyman C, et al. Architecture of the human Ndc80-Hec1 complex, a critical constituent of the outer kinetochore. *J Biol Chem*. 2005;280:29088–95.
12. DeLuca JG, Gall WE, Ciferri C, Cimini D, Musacchio A, Salmon ED. Kinetochore microtubule dynamics and attachment stability are regulated by Hec1. *Cell*. 2006;127:969–82.

13. Guimaraes GJ, Dong Y, McEwen BF, DeLuca JG. Kinetochores-microtubule attachment relies on the disordered N-terminal tail domain of Hec1. *Curr Biol*. Elsevier Ltd; 2008;18:1778–84.
14. Zaytsev A V., Sundin LJR, DeLuca KF, Grishchuk EL, DeLuca JG. Accurate phosphoregulation of kinetochores-microtubule affinity requires unconstrained molecular interactions. *J Cell Biol*. 2014;206:45–59.
15. DeLuca KF, Lens SM a, DeLuca JG. Temporal changes in Hec1 phosphorylation control kinetochores-microtubule attachment stability during mitosis. *J Cell Sci*. 2011;124:622–34.
16. Liu D, Vader G, Vromans MJM, Lampson MA, Lens SMA. Sensing chromosome bi-orientation by spatial separation of Aurora B kinase from kinetochores substrates. *Science (80-)*. 2009;323:1350–3.
17. Caldas G V, DeLuca KF, DeLuca JG. KNL1 facilitates phosphorylation of outer kinetochores proteins by promoting Aurora B kinase activity. *J Cell Biol*. 2013;203:957–69.
18. Ditchfield C, Johnson VL, Tighe A, Ellston R, Haworth C, Johnson T, et al. Aurora B couples chromosome alignment with anaphase by targeting BubR1, Mad2, and Cenp-E to kinetochores. *J Cell Biol*. 2003;161:267–80.
19. Lampson MA, Kapoor TM. The human mitotic checkpoint protein BubR1 regulates chromosome-spindle attachments. *Nat Cell Biol*. 2005;7:93–8.
20. Foley EA, Maldonado M, Kapoor TM. Formation of stable attachments between kinetochores and microtubules depends on the B56-PP2A phosphatase. *Nat Cell Biol*. Nature Publishing Group; 2011;13:1265–71.
21. Suijkerbuijk SJE, Vleugel M, Teixeira A, Kops GJPL. Integration of kinase and phosphatase activities by BUBR1 ensures formation of stable kinetochores-microtubule attachments. *Dev Cell*. Elsevier Inc.; 2012;23:745–55.
22. Kruse T, Zhang G, Larsen MSY, Lischetti T, Streicher W, Kragh Nielsen T, et al. Direct binding between BubR1 and B56-PP2A phosphatase complexes regulate mitotic progression. *J Cell Sci*. 2013;126:1086–92.
23. Xu P, Raetz E a, Kitagawa M, Virshup DM, Lee SH. BUBR1 recruits PP2A via the B56 family of targeting subunits to promote chromosome congression. *Biol Open*. 2013;2:479–86.
24. Lens SMA, Voest EE, Medema RH. Shared and separate functions of polo-like kinases and aurora kinases in cancer. *Nat Rev Cancer*. 2010;10:825–41.

25. Lampson MA, Cheeseman IM. Sensing centromere tension: Aurora B and the regulation of kinetochore function. *Trends Cell Biol.* Elsevier Ltd; 2011;21:133–40.
26. Funabiki H, Wynne DJ. Making an effective switch at the kinetochore by phosphorylation and dephosphorylation. *Chromosoma.* 2013;122:135–58.
27. Bakhoun SF, Thompson SL, Manning AL, Compton DA. Genome stability is ensured by temporal control of kinetochore-microtubule dynamics. *Nat Cell Biol.* 2009;11:27–35.
28. Knowlton AL, Lan W, Stukenberg PT. Aurora B is enriched at merotelic attachment sites, where it regulates MCAK. *Curr Biol.* 2006;16:1705–10.
29. Zhang X, Lan W, Ems-McClung SC, Stukenberg PT, Walczak CE. Aurora B phosphorylates multiple sites on mitotic centromere-associated kinesin to spatially and temporally regulate its function. *Mol Biol Cell.* 2007;18:3267–2376.
30. Thompson SL, Bakhoun SF, Compton DA. Mechanisms of chromosomal instability. *Curr Biol.* Elsevier Ltd; 2010;20:R285–95.
31. Bakhoun SF, Genovese G, Compton DA. Deviant kinetochore microtubule dynamics underlie chromosomal instability. *Curr Biol.* Elsevier Ltd; 2009;19:1937–42.
32. Cimini D, Moree B, Canman JC, Salmon ED. Merotelic kinetochore orientation occurs frequently during early mitosis in mammalian tissue cells and error correction is achieved by two different mechanisms. *J Cell Sci.* 2003;116:4213–25.
33. Cimini D, Howell B, Maddox P, Khodjakov A, Degraffi F, Salmon ED. Merotelic kinetochore orientation is a major mechanism of aneuploidy in mitotic mammalian tissue cells. *J Cell Biol.* 2001;153:517–27.
34. Thompson SL, Compton D a. Chromosomes and cancer cells. *Chromosome Res.* 2011;19:433–44.
35. Ferlay J, Shin H, Bray F, Forman D, Mathers C, Parkin D. GLOBOCAN 2008: Cancer incidence and mortality worldwide [Internet]. Int. Agency Reserach Cancer. 2010 [cited 2011 Aug 11]. Available from: <http://globocan.iarc.fr>
36. Stupp R, Mason WP, van der Bent MJ, Weller M, Fisher B, Taphoorn MJB, et al. Radiotherapy plus concomitant and adjuvant temozolomide for glioblastoma. *N Engl J Med.* 2005;352:987–96.

37. Hemmati HD, Nakano I, Lazareff JA, Masterman-Smith M, Geschwind DH, Bronner-Fraser M, et al. Cancerous stem cells can arise from pediatric brain tumors. *Proc Natl Acad Sci U S A*. 2003;100:15178–83.
38. Singh SK. Identification of a cancer stem cell in human brain tumors. *Cancer Res*. 2003;63:5821–8.
39. Galli R, Binda E, Orfanelli U, Cipelletti B, Gritti A, Vitis S De, et al. Isolation and characterization of tumorigenic, stem-like neural precursors from human glioblastoma isolation and characterization of tumorigenic , stem-like neural precursors from human glioblastoma. *Cancer Res*. 2004;64:7011–21.
40. Singh S, Hawkins C, Clarke I, Squire J, Bayani J, Hide T, et al. Identification of human brain tumour initiating cells. *Nature*. 2004;432:396–401.
41. Lee J, Kotliarova S, Kotliarov Y, Li A, Su Q, Donin NM, et al. Tumor stem cells derived from glioblastomas cultured in bFGF and EGF more closely mirror the phenotype and genotype of primary tumors than do serum-cultured cell lines. *Cancer Cell*. 2006;9:391–403.
42. Pollard SM, Yoshikawa K, Clarke ID, Danovi D, Stricker S, Russell R, et al. Glioma stem cell lines expanded in adherent culture have tumor-specific phenotypes and are suitable for chemical and genetic screens. *Cell Stem Cell*. Elsevier Ltd; 2009;4:568–80.
43. Szerlip NJ, Pedraza a., Chakravarty D, Azim M, McGuire J, Fang Y, et al. Intratumoral heterogeneity of receptor tyrosine kinases EGFR and PDGFRA amplification in glioblastoma defines subpopulations with distinct growth factor response. *Proc Natl Acad Sci*. 2012;109:3041–6.
44. Harada K, Nishizaki T, Ozaki S, Kubota H, Ito H, Sasaki K. Intratumoral cytogenetic heterogeneity detected by comparative genomic hybridization and laser scanning cytometry in human gliomas. *Cancer Res*. 1998;58:4694–700.
45. Sottoriva A, Spiteri I, Piccirillo SGM, Touloumis A, Collins VP, Marioni JC, et al. Intratumor heterogeneity in human glioblastoma reflects cancer evolutionary dynamics. *Proc Natl Acad Sci U S A*. 2013;110:4009–14.
46. Snuderl M, Fazlollahi L, Le LP, Nitta M, Zhelyazkova BH, Davidson CJ, et al. Mosaic amplification of multiple receptor tyrosine kinase genes in glioblastoma. *Cancer Cell*. Elsevier Inc.; 2011;20:810–7.
47. Bakhoun SF, Compton DA. Chromosomal instability and cancer: a complex relationship with therapeutic potential. *J Clin Invest*. 2012;122:1138–43.

48. Gao C, Furge K, Koeman J, Dykema K, Su Y, Cutler ML, et al. Chromosome instability, chromosome transcriptome, and clonal evolution of tumor cell populations. *Proc Natl Acad Sci U S A*. 2007;104:8995–9000.
49. Bhat KPL, Balasubramanian V, Vaillant B, Ezhilarasan R, Hummelink K, Hollingsworth F, et al. Mesenchymal differentiation mediated by NF- κ B promotes radiation resistance in glioblastoma. *Cancer Cell*. 2013;24:331–46.
50. Gillies RJ, Verduzco D, Gatenby RA. Evolutionary dynamics of carcinogenesis and why targeted therapy does not work. *Nat Rev Cancer*. Nature Publishing Group; 2012;12:487–93.
51. Weaver BA, Cleveland DW. Does aneuploidy cause cancer? *Curr Opin Cell Biol*. 2006;18:658–67.
52. Roschke A V, Rozenblum E. Multi-layered cancer chromosomal instability phenotype. *Front Oncol*. 2013;3:1–13.
53. Yoon D-S, Wersto RP, Zhou W, Chrest FJ, Garrett ES, Kwon TK, et al. Variable levels of chromosomal instability and mitotic spindle checkpoint defects in breast cancer. *Am J Pathol*. American Society for Investigative Pathology; 2002;161:391–7.
54. Bie L, Zhao G, Cheng P, Rondeau G, Porwollik S, Ju Y, et al. The accuracy of survival time prediction for patients with glioma is improved by measuring mitotic spindle checkpoint gene expression. *PLoS One*. 2011;6.
55. Cahill DP, Lengauer C, Yu J, Riggins GJ, Willson JK, Markowitz SD, et al. Mutations of mitotic checkpoint genes in human cancers. *Nature*. 1998;392:300–3.
56. Suijkerbuijk SJE, Kops GJPL. Preventing aneuploidy: The contribution of mitotic checkpoint proteins. *Biochim Biophys Acta - Rev Cancer*. 2008;1786:24–31.
57. Yuan B, Xu Y, Woo J-H, Wang Y, Bae YK, Yoon D-S, et al. Increased expression of mitotic checkpoint genes in breast cancer cells with chromosomal instability. *Clin Cancer Res*. 2006;12:405–10.
58. Ding Y, Hubert CG, Herman J, Corrin P, Toledo CM, Skutt-Kakaria K, et al. Cancer-specific requirement for BUB1B/BUBR1 in human brain tumor isolates and genetically transformed cells. *Cancer Discov*. 2013;3:198–211.
59. Baker DJ, Dawlaty MM, Wijshake T, Jeganathan KB, Malureanu L, van Ree JH, et al. Increased expression of BubR1 protects against aneuploidy and cancer and extends healthy lifespan. *Nat Cell Biol*. Nature Publishing Group; 2013;15:96–102.

60. Ricke RM, Jeganathan KB, Malureanu L, Harrison AM, van Deursen JM. Bub1 kinase activity drives error correction and mitotic checkpoint control but not tumor suppression. *J Cell Biol.* 2012;199:931–49.
61. Ricke RM, Jeganathan KB, van Deursen JM. Bub1 overexpression induces aneuploidy and tumor formation through Aurora B kinase hyperactivation. *J Cell Biol.* 2011;193:1049–64.
62. Meraldi P, Sorger PK. A dual role for Bub1 in the spindle checkpoint and chromosome congression. *EMBO J.* 2005;24:1621–33.
63. Stiles CD, Rowitch DH. Glioma stem cells: A midterm exam. *Neuron.* 2008;58:832–46.
64. Bao S, Wu Q, McLendon RE, Hao Y, Shi Q, Hjelmeland AB, et al. Glioma stem cells promote radioresistance by preferential activation of the DNA damage response. *Nature.* 2006;444:756–60.
65. Bao S, Wu Q, Sathornsumetee S, Hao Y, Li Z, Hjelmeland AB, et al. Stem cell-like glioma cells promote tumor angiogenesis through vascular endothelial growth factor. *Cancer Res.* 2006;66:7843–8.
66. Liu Q, Nguyen DH, Dong Q, Shitaku P, Chung K, Liu OY, et al. Molecular properties of CD133+ glioblastoma stem cells derived from treatment-refractory recurrent brain tumors. *J Neurooncol.* 2009;94:1–19.
67. Sawin KE, LeGuellec K, Philippe M, Mitchison TJ. Mitotic spindle organization by a plus-end-directed microtubule motor. *Nature.* 1992;359:540–3.
68. Sun Y, Pollard S, Conti L, Toselli M, Biella G, Parkin G, et al. Long-term tripotent differentiation capacity of human neural stem (NS) cells in adherent culture. *Mol Cell Neurosci.* 2008;38:245–58.
69. McLendon R, Friedman A, Bigner D, Van Meir EG, Brat DJ, M. Mastrogiannakis G, et al. Comprehensive genomic characterization defines human glioblastoma genes and core pathways. *Nature.* 2008;455:1061–8.
70. Zhu J, Zhang B, Smith EN, Drees B, Brem RB, Kruglyak L, et al. Integrating large-scale functional genomic data to dissect the complexity of yeast regulatory networks. *Nat Genet.* 2008;40:854–61.
71. Tran LM, Zhang B, Zhang Z, Zhang C, Xie T, Lamb JR, et al. Inferring causal genomic alterations in breast cancer using gene expression data. *BMC Syst Biol.* BioMed Central Ltd; 2011;5:121.

72. Yang X, Deignan JL, Qi H, Zhu J, Qian S, Zhong J, et al. Validation of candidate causal genes for obesity that affect shared metabolic pathways and networks. *Nat Genet.* 2009;41:415–23.
73. Frederick L, Wang XY, Eley G, James CD. Diversity and frequency of epidermal growth factor receptor mutations in human glioblastomas. *Cancer Res.* 2000;60:1383–7.
74. Verhaak RGW, Hoadley K a., Purdom E, Wang V, Qi Y, Wilkerson MD, et al. Integrated genomic analysis identifies clinically relevant subtypes of glioblastoma characterized by abnormalities in PDGFRA, IDH1, EGFR, and NF1. *Cancer Cell.* Elsevier Ltd; 2010;17:98–110.
75. Baker DJ, Jeganathan KB, Cameron JD, Thompson M, Juneja S, Kopecka A, et al. BubR1 insufficiency causes early onset of aging-associated phenotypes and infertility in mice. *Nat Genet.* 2004;36:744–9.
76. Wijshake T, Malureanu LA, Baker DJ, Jeganathan KB, van de Sluis B, van Deursen JM. Reduced life- and healthspan in mice carrying a mono-allelic BubR1 MVA mutation. *PLoS Genet.* 2012;8:e1003138.
77. Malureanu LA, Jeganathan KB, Hamada M, Wasilewski L, Davenport J, van Deursen JM. BubR1 N terminus acts as a soluble inhibitor of cyclin B degradation by APC/C(Cdc20) in interphase. *Dev Cell.* Elsevier Inc.; 2009;16:118–31.
78. Davenport J, Harris LD, Goorha R. Spindle checkpoint function requires Mad2-dependent Cdc20 binding to the Mad3 homology domain of BubR1. *Exp Cell Res.* 2006;312:1831–42.
79. Tang Z, Bharadwaj R, Li B, Yu H. Mad2-independent inhibition of APC/Cdc20 by the mitotic checkpoint protein BubR1. *Dev Cell.* 2001;1:227–37.
80. Suijkerbuijk SJE, van Osch MHJ, Bos FL, Hanks S, Rahman N, Kops GJPL. Molecular causes for BUBR1 dysfunction in the human cancer predisposition syndrome mosaic variegated aneuploidy. *Cancer Res.* 2010;70:4891–900.
81. Harris L, Davenport J, Neale G, Goorha R. The mitotic checkpoint gene BubR1 has two distinct functions in mitosis. *Exp Cell Res.* 2005;308:85–100.
82. Wang X, Babu JR, Harden JM, Jablonski SA, Gazi MH, Lingle WL, et al. The mitotic checkpoint protein hBUB3 and the mRNA export factor hRAE1 interact with GLE2p-binding sequence (GLEBS)-containing proteins. *J Biol Chem.* 2001;276:26559–67.
83. Wang Q, Liu T, Fang Y, Xie S, Huang X, Mahmood R, et al. BUBR1 deficiency results in abnormal megakaryopoiesis. *Blood.* 2004;103:1278–85.

84. Lara-Gonzalez P, Scott MIF, Diez M, Sen O, Taylor SS. BubR1 blocks substrate recruitment to the APC/C in a KEN-box-dependent manner. *J Cell Sci.* 2011;4332–45.
85. Taylor SS, Ha E, McKeon F. The human homologue of Bub3 is required for kinetochore localization of Bub1 and a Mad3/Bub1-related protein kinase. *J Cell Biol.* 1998;142:1–11.
86. Maresca TJ, Groen AC, Gatlin JC, Ohi R, Mitchison TJ, Salmon ED. Spindle assembly in the absence of a RanGTP gradient requires localized CPC activity. *Curr Biol. Elsevier Ltd;* 2009;19:1210–5.
87. Uchida KSK, Takagaki K, Kumada K, Hirayama Y, Noda T, Hirota T. Kinetochore stretching inactivates the spindle assembly checkpoint. *J Cell Biol.* 2009;184:383–90.
88. Eves EM, Shapiro P, Naik K, Klein UR, Trakul N, Rosner MR. Raf kinase inhibitory protein regulates aurora B kinase and the spindle checkpoint. *Mol Cell.* 2006;23:561–74.
89. Yin Y, Shen WH. PTEN: a new guardian of the genome. *Oncogene.* 2008;27:5443–53.
90. Sonoda Y, Ozawa T, Hirose Y, Astrocytoma A, Aldape KD, McMahon M, et al. Formation of Intracranial Tumors by Genetically Modified Human Astrocytes Defines Four Pathways Critical in the Development of Human Anaplastic Astrocytoma Advances in Brief Formation of Intracranial Tumors by Genetically Modified Human Astrocytes Defines. *Cancer Res.* 2001;4956–60.
91. Boveri T. Uber mehrpolige mitosen als mittes zur analyse des zellkerns. *Verhandlungen der Phys Gesellschaft zu Wurzburg.* 1902;35:67–90.
92. Thompson SL, Compton DA. Chromosome missegregation in human cells arises through specific types of kinetochore-microtubule attachment errors. *Proc Natl Acad Sci U S A.* 2011;108:17974–8.
93. Kendall SD, Linardic CMC, Adam SJS, Counter CCM. A network of genetic events sufficient to convert normal human cells to a tumorigenic state. *Cancer Res.* 2005;65:9824–8.
94. Hubert C, Bradley R, Ding Y. Genome-wide RNAi screens in human brain tumor isolates reveal a novel viability requirement for PHF5A. *Genes Dev.* 2013;1032–45.

95. Parada LF, Tabin CJ, Shih C, Weinberg RA. Human EJ bladder carcinoma oncogene is homologue of Harvey sarcoma virus ras gene. *Nature*. 1982;297:474–8.
96. Land H, Parada LF, Weinberg RA. Tumorigenic conversion of primary embryo fibroblasts requires at least two cooperating oncogenes. *Nature*. 1983;304:596–602.
97. Huang W, Kessler DS, Erikson RL. Biochemical and biological analysis of Mek1 phosphorylation site mutants. *Mol Biol Cell*. 1995;6:237–45.
98. Kohn AD, Takeuchi F, Roth RA. Akt, a Pleckstrin Homology Domain Containing Kinase, Is Activated Primarily by Phosphorylation. *J Biol Chem*. 1996;271:21920–6.
99. Favata MF. Identification of a novel inhibitor of mitogen-activated protein kinase kinase. *J Biol Chem*. 1998;273:18623–32.
100. Cheeseman IM, Chappie JS, Wilson-Kubalek EM, Desai A. The conserved KMN network constitutes the core microtubule-binding site of the kinetochore. *Cell*. 2006;127:983–97.
101. Wheatley SP, Henzing AJ, Dodson H, Khaled W, Earnshaw WC. Aurora-B phosphorylation in vitro identifies a residue of survivin that is essential for its localization and binding to inner centromere protein (INCENP) in vivo. *J Biol Chem*. 2004;279:5655–60.
102. Chen R-H. Phosphorylation and activation of Bub1 on unattached chromosomes facilitate the spindle checkpoint. *EMBO J*. 2004;23:3113–21.
103. Zhao Y, Chen R-H. Mps1 phosphorylation by MAP kinase is required for kinetochore localization of spindle-checkpoint proteins. *Curr Biol*. 2006;16:1764–9.
104. Yamagishi Y, Honda T, Tanno Y, Watanabe Y. Two histone marks establish the inner centromere and chromosome bi-orientation. *Science* (80-). 2010;330:239–43.
105. Saurin AT, van der Waal MS, Medema RH, Lens SMA, Kops GJPL. Aurora B potentiates Mps1 activation to ensure rapid checkpoint establishment at the onset of mitosis. *Nat Commun*. 2011;2:316.
106. Amaro AC, Samora CP, Holtackers R, Wang E, Kingston IJ, Alonso M, et al. Molecular control of kinetochore-microtubule dynamics and chromosome oscillations. *Nat Cell Biol*. Nature Publishing Group; 2010;12:319–29.

107. Kabeche L, Compton DA. Cyclin A regulates kinetochore microtubules to promote faithful chromosome segregation. *Nature*. Nature Publishing Group; 2013;
108. Shapiro PS, Vaisberg E, Hunt AJ, Tolwinski NS, Whalen AM, McIntosh JR, et al. Activation of the MKK/ERK pathway during somatic cell mitosis: direct interactions of active ERK with kinetochores and regulation of the mitotic 3F3/2 phosphoantigen. *J Cell Biol*. 1998;142:1533–45.
109. Toledo CM, Herman JA, Olsen JB, Ding Y, Corrin P, Girard EJ, et al. BuGZ Is required for Bub3 stability, Bub1 kinetochore function, and chromosome alignment. *Dev Cell*. Elsevier Inc.; 2014;1–13.
110. Slamon DJ, Leyland-Jones B, Shak S, Fuchs H, Paton V, Bajamonde A, et al. Use of chemotherapy plus a monoclonal antibody against HER2 for metastatic breast cancer that overexpresses HER2. *N Engl J Med*. 2001;344:783–92.
111. Druker BJ, Sawyers CL, Kantarjian H, Resta DJ, Reese SF, Ford JM, et al. Activity of a specific inhibitor of the BCR-ABL tyrosine kinase in the blast crisis of chronic myeloid leukemia and acute lymphoblastic leukemia with the Philadelphia chromosome. *N. Engl. J. Med*. 2001 page 1038–42.
112. Rajagopalan H, Lengauer C. Aneuploidy and Cancer. *Science* (80-). 2011;333:918–918.
113. Duesberg P, Stindl R, Hehlmann R. Explaining the high mutation rates of cancer cells to drug and multidrug resistance by chromosome reassortments that are catalyzed by aneuploidy. *Proc Natl Acad Sci U S A*. 2000;97:14295–300.
114. Serrano M, Lin AW, McCurrach ME, Beach D, Lowe SW. Oncogenic ras provokes premature cell senescence associated with accumulation of p53 and p16INK4a. *Cell*. Elsevier; 1997;88:593–602.
115. Rodriguez-Viciana P, Warne PH, Khwaja A, Marte BM, Pappin D, Das P, et al. Role of phosphoinositide 3-OH kinase in cell transformation and control of the actin cytoskeleton by Ras. *Cell*. 1997;89:457–67.
116. Ramaswamy S, Nakamura N, Vazquez F, Batt DB, Perera S, Roberts TM, et al. Regulation of G1 progression by the PTEN tumor suppressor protein is linked to inhibition of the phosphatidylinositol 3-kinase/Akt pathway. *Proc Natl Acad Sci U S A*. 1999;96:2110–5.
117. Boehm JS, Zhao JJ, Yao J, Kim SY, Firestein R, Dunn IF, et al. Integrative genomic approaches identify IKBKE as a breast cancer oncogene. *Cell*. 2007;129:1065–79.

118. Kita-Matsuo H, Barcova M, Prigozhina N, Salomonis N, Wei K, Jacot JG, et al. Lentiviral vectors and protocols for creation of stable hESC lines for fluorescent tracking and drug resistance selection of cardiomyocytes. *PLoS One*. 2009;4.
119. Patterson GH, Lippincott-Schwartz J. A photoactivatable GFP for selective photolabeling of proteins and cells. *Science* (80-). 2002;297:1873–7.
120. Hoffman DB, Pearson CG, Yen TJ, Howell BJ, Salmon ED. Microtubule-dependent changes in assembly of microtubule motor proteins and mitotic spindle checkpoint proteins at PtK1 kinetochores. *Mol Biol Cell*. 2001;12:1995–2009.
121. Stumpff J, von Dassow G, Wagenbach M, Asbury C, Wordeman L. The Kinesin-8 motor Kif18A suppresses kinetochore movements to control mitotic chromosome alignment. *Dev Cell*. 2008;14:252–62.
122. Logarinho E, Bousbaa H. Kinetochore-Microtubule interactions “in check” by Bub1, Bub3 and BubR1. *Cell Cycle*. 2008;7:1763–8.
123. Welburn JPI, Vleugel M, Liu D, Yates JR, Lampson M a, Fukagawa T, et al. Aurora B phosphorylates spatially distinct targets to differentially regulate the kinetochore-microtubule interface. *Mol Cell*. Elsevier Ltd; 2010;38:383–92.
124. Bailer SM, Siniosoglou S, Podtelejnikov A, Hellwig A, Mann M, Hurt E. Nup116p and Nup100p are interchangeable through a conserved motif which constitutes a docking site for the mRNA transport factor Gle2p. *EMBO J*. 1998;17:1107–19.
125. Larsen N a, Al-Bassam J, Wei RR, Harrison SC. Structural analysis of Bub3 interactions in the mitotic spindle checkpoint. *Proc Natl Acad Sci U S A*. 2007;104:1201–6.
126. Pahl PM, Hodges YK, Meltesen L, Perryman MB, Horwitz KB, Horwitz LD. ZNF207, a ubiquitously expressed zinc finger gene on chromosome 6p21.3. *Genomics*. 1998;53:410–2.
127. Son MJ, Woolard K, Nam DH, Lee J, Fine HA. SSEA-1 Is an enrichment marker for tumor-initiating cells in human glioblastoma. *Cell Stem Cell*. Elsevier Ltd; 2009;4:440–52.
128. Powell S, Szklarczyk D, Trachana K, Roth A, Kuhn M, Muller J, et al. eggNOG v3.0: Orthologous groups covering 1133 organisms at 41 different taxonomic ranges. *Nucleic Acids Res*. 2012;40:284–9.
129. Hoyt MA, Totis L, Roberts BT. *S. cerevisiae* genes required for cell cycle arrest in response to loss of microtubule function. *Cell*. 1991;66:507–17.

130. Ren Y, Seo H-S, Blobel G, Hoelz A. Structural and functional analysis of the interaction between the nucleoporin Nup98 and the mRNA export factor Rae1. *Proc Natl Acad Sci U S A*. 2010;107:10406–11.
131. Pritchard CEJ, Fornerod M, Kasper LH, Van Deursen JMA. RAE1 is a shuttling mRNA export factor that binds to a GLEBS-like NUP98 motif at the nuclear pore complex through multiple domains. *J Cell Biol*. 2000;145:237–53.
132. Howell BJ, Moree B, Farrar EM, Stewart S, Fang G, Salmon ED. Spindle checkpoint protein dynamics at kinetochores in living cells. *Curr Biol*. 2004;15:953–64.
133. Jablonski S a., Chan GKT, Cooke C a., Earnshaw WC, Yen TJ. The hBUB1 and hBUBR1 kinases sequentially assemble onto kinetochores during prophase with hBUBR1 concentrating at the kinetochore plates in mitosis. *Chromosoma*. 1998;107:386–96.
134. Taylor SS, McKeon F. Kinetochore localization of murine Bub1 is required for normal mitotic timing and checkpoint response to spindle damage. *Cell*. 1997;89:727–35.
135. Kiyomitsu T, Obuse C, Yanagida M. Human Blinkin/AF15q14 is required for chromosome alignment and the mitotic checkpoint through direct interaction with Bub1 and BubR1. *Dev Cell*. 2007;13:663–76.
136. London N, Ceto S, Ranish J, Biggins S. Phosphoregulation of Spc105 by Mps1 and PP1 regulates Bub1 localization to kinetochores. *Curr Biol*. 2012;22:900–6.
137. Primorac I, Weir JR, Chiroli E, Gross F, Hoffmann I, van Gerwen S, et al. Bub3 reads phosphorylated MELT repeats to promote spindle assembly checkpoint signaling. *Elife*. 2013;2:e01030.
138. Yamagishi Y, Yang C-H, Tanno Y, Watanabe Y. MPS1/Mph1 phosphorylates the kinetochore protein KNL1/Spc7 to recruit SAC components. *Nat Cell Biol*. Nature Publishing Group; 2012;14:746–52.
139. Vanoosthuysen V. Bub3p facilitates spindle checkpoint silencing in fission yeast. *Mol Biol Cell*. 2009;20:5096–105.
140. Logarinho E, Resende T, Bousbaa H. The human spindle assembly checkpoint protein Bub3 is required for the establishment of efficient kinetochore–microtubule attachments. 2008;19:1798–813.
141. Meraldi P, Draviam VM, Sorger PK. Timing and checkpoints in the regulation of mitotic progression. *Dev Cell*. 2004;7:45–60.

142. Kawashima SA, Tsukahara T, Langeegger M, Hauf S, Kitajima TS, Watanabe Y. Shugoshin enables tension-generating attachment of kinetochores by loading Aurora to centromeres. *Genes Dev.* 2007;21:420–35.
143. Tsukahara T, Tanno Y, Watanabe Y. Phosphorylation of the CPC by Cdk1 promotes chromosome bi-orientation. *Nature.* Nature Publishing Group; 2010;467:719–23.
144. Benanti JA, Galloway DA. The normal response to RAS: Senescence or transformation? *Cell Cycle.* 2004;3:715–7.
145. Kalitsis P, Earle E, Fowler KJ, Choo KH. Bub3 gene disruption in mice reveals essential mitotic spindle checkpoint function during early embryogenesis. *Genes Dev.* 2000;14:2277–82.
146. Perera D, Tilston V, Hopwood JA, Barchi M, Boot-Handford RP, Taylor SS. Bub1 maintains centromeric cohesion by activation of the spindle checkpoint. *Dev Cell.* 2007;13:566–79.
147. Klebig C, Korinth D, Meraldi P. Bub1 regulates chromosome segregation in a kinetochore-independent manner. *J Cell Biol.* 2009;185:841–58.
148. Liu ST, Rattner JB, Jablonski SA, Yen TJ. Mapping the assembly pathways that specify formation of the trilaminar kinetochore plates in human cells. *J Cell Biol.* 2006;175:41–53.
149. Shepperd LA, Meadows JC, Sochaj AM, Lancaster TC, Zou J, Buttrick GJ, et al. Phosphodependent recruitment of Bub1 and Bub3 to Spc7/KNL1 by Mph1 kinase maintains the spindle checkpoint. *Curr Biol.* Elsevier; 2012;22:891–9.
150. Jiang Y, Li X, Yang W, Hawke DH, Zheng Y, Xia Y, et al. PKM2 regulates chromosome segregation and mitosis progression of tumor Cells. *Mol Cell.* Elsevier Inc.; 2013;1–13.
151. Slee RB, Grimes BR, Bansal R, Gore J, Blackburn C, Brown L, et al. Selective inhibition of pancreatic ductal adenocarcinoma cell growth by the mitotic MPS1 kinase inhibitor NMS-P715. *Mol Cancer Ther.* 2014;13:307–15.
152. Jemaà M, Galluzzi L, Kepp O, Senovilla L, Brands M, Boemer U, et al. Characterization of novel MPS1 inhibitors with preclinical anticancer activity. *Cell Death Differ.* 2013;20:1532–45.
153. Tannous BA, Kerami M, Van Der Stoop PM, Kwiatkowski N, Wang J, Zhou W, et al. Effects of the selective MPS1 inhibitor MPS1-IN-3 on glioblastoma sensitivity to antimitotic drugs. *J Natl Cancer Inst.* 2013;105:1322–31.

154. Chen J, Xie J, Jiang Z, Wang B, Wang Y, Hu X. Shikonin and its analogs inhibit cancer cell glycolysis by targeting tumor pyruvate kinase-M2. *Oncogene*. 2011;30:4297–306.
155. Pezuk JA, Brassesco MS, Morales AG, de Oliveira JC, de Paula Queiroz RG, Machado HR, et al. Polo-like kinase 1 inhibition causes decreased proliferation by cell cycle arrest, leading to cell death in glioblastoma. *Cancer Gene Ther*. Nature Publishing Group; 2013;20:499–506.
156. Shi JQ, Lasky K, Shinde V, Stringer B, Qian MG, Liao D, et al. MLN0905, a Small-Molecule PLK1 Inhibitor, Induces Antitumor Responses in Human Models of Diffuse Large B-cell Lymphoma. *Mol Cancer Ther*. 2012;11:2045–53.
157. De Oliveira JC, Pezuk JA, Brassesco MS, Morales AG, de Paula Queiroz RG, Scrideli CA, et al. PLK1 expression and BI2536 effects in childhood acute lymphoblastic leukemia. *Pediatr Blood Cancer*. 2014;61:1227–31.
158. Danovi D, Folarin A, Gogolok S, Ender C, Elbatsh AMO, Engström PG, et al. A high-content small molecule screen identifies sensitivity of glioblastoma stem cells to inhibition of polo-like kinase 1. *PLoS One*. 2013;8:e77053.
159. Maertens J, Lubbert M, Fiedler W, Fouillard L, Turlure P, Bug G, et al. Phase I/II study of Volasertib (BI6727), an intravenous polo-like kinase (PLK) inhibitor, in patients with acute myeloid leukemia (AML): Results from the randomized phase II part for Volasertib in combination with low-dose Cytarabine (LDAC) versus LDAC mo. *Blood Annu Meet Abstr*. 2012. page 411.
160. Talapatra SK, Anthony NG, Mackay SP, Kozielski F. Mitotic kinesin Eg5 overcomes inhibition to the phase I/II clinical candidate SB743921 by an allosteric resistance mechanism. *J Med Chem*. 2013;56:6317–29.
161. Cheung CHA, Coumar MS, Hsieh H-P, Chang J-Y. Aurora kinase inhibitors in preclinical and clinical testing. *Expert Opin Investig Drugs*. 2009;18:379–98.